

April 2007

Development of a Pulsatile Flow Generator and Analysis of Wave Propagation in Blood Vessels for Implementation in the Early Detection of Arterial Disease

Jayr Manjikian
Worcester Polytechnic Institute

Ritul Gupta
Worcester Polytechnic Institute

Trisha A. Josephs
Worcester Polytechnic Institute

Walter C. Uchendu
Worcester Polytechnic Institute

Follow this and additional works at: <https://digitalcommons.wpi.edu/mqp-all>

Repository Citation

Manjikian, J., Gupta, R., Josephs, T. A., & Uchendu, W. C. (2007). *Development of a Pulsatile Flow Generator and Analysis of Wave Propagation in Blood Vessels for Implementation in the Early Detection of Arterial Disease*. Retrieved from <https://digitalcommons.wpi.edu/mqp-all/2635>

This Unrestricted is brought to you for free and open access by the Major Qualifying Projects at Digital WPI. It has been accepted for inclusion in Major Qualifying Projects (All Years) by an authorized administrator of Digital WPI. For more information, please contact digitalwpi@wpi.edu.

Project Number: BJS-AW05

**Development of a Pulsatile Flow Generator and Analysis of Wave
Propagation in Blood Vessels for Implementation in the Early Detection of
Arterial Disease**

A Major Qualifying Project Report
submitted to the Faculty of
WORCESTER POLYTECHNIC INSTITUTE
in partial fulfillment of the requirements for the
Degree of Bachelor of Science

by

Ritul Gupta

Trisha A. Josephs

Jayr Manjikian

Walter C. Uchendu

Date: April 26, 2007

Approved:

Professor Brian James Savilonis

I. Table of Contents

II. Authorship Page.....	6
III. Acknowledgments	7
IV. Abstract.....	8
V. Table of Figures	9
VI. Table of Tables	10
1. Introduction	11
2. Literature Review	13
2.1. Circulatory System	13
2.1.1. Blood.....	13
2.1.1.1. Viscoelasticity.....	14
2.1.1.2. Clinical Significance	15
2.1.2. Arteries.....	16
2.1.2.1. Anatomy	16
2.1.2.2. Arterial Properties.....	16
2.1.2.3. Mechanical Properties.....	17
2.1.2.4. Impedance	17
2.1.2.5. Compliance.....	18
2.2. Arterial Disease States	19
2.3. Stenotic Hemodynamics	23
2.4. Pulse Wave Velocity.....	24
2.5. Prosthetic Models.....	27
2.5.1. Clinical Materials.....	27
2.5.2. Latex	28
2.5.3. Comparison of Prosthetic/Latex/Human Arteries	29
2.6. Mechanical Flow Systems.....	30
2.6.1. Pulsatile Flow Generators	30
2.6.2. Cam-follower	30
2.6.3. Slider Crank.....	31
2.6.4. Comparison of Flow Systems	33
2.7. Motion Control.....	33
2.7.1. DC Motors.....	33

2.7.1.1.	DC Stepper Motor	34
2.7.1.2.	DC Brushless Motor	34
2.7.2.	Motion Controllers	35
2.7.2.1.	ION Digital Drive	35
2.7.3.	Servo Loop Tuning	37
2.7.4.	Proportional Integral Differential Controller (PID)	38
2.8.	Pressure Measurement	39
2.8.1.	Indirect Blood Pressure Measurement	39
2.8.2.	Direct Blood Pressure Measurement	40
2.9.	Wave Analysis	40
2.9.1.	Fourier Transform	40
2.9.2.	Fast Fourier Transform	41
2.9.3.	Short Fourier Tranforms	41
3.	Project Approach	42
3.1.	Objectives	42
3.2.	Aims	42
3.3.	Assumptions	42
4.	Design Approach	44
4.1.	Design Iteration 1	44
4.1.1.	Slider Crank System	45
4.1.2.	Pressure and Flow System	45
4.1.3.	Recirculation	46
4.1.4.	Arterial Stiffness Models	46
4.1.5.	Arterial Stenotic Models	46
4.2.	Final Design	47
4.2.1.	Motion Controlled Cardiovascular System	50
4.2.2.	Arterial Stiffness Models	51
4.2.3.	Arterial Stenotic Models	53
4.3.	Design Validation	54
4.3.1.	Arterial Models	54
4.3.1.1.	Compliance Testing Systems	54
4.3.1.2.	Final System	55
5.	Methodology	56
5.1.	Blood Substitute Preparation	56

5.1.1. Viscosity Testing.....	56
5.2. Latex Arterial Model Development.....	58
5.2.1. Stiffness Model.....	58
5.2.2. Stenosis Model.....	59
5.3. Arterial Testing.....	59
5.3.1. Radial Compliance Testing.....	59
5.3.2. Tensile Testing.....	60
5.3.3. Pulse Wave Velocity Analysis.....	60
5.4. Pulsatile Flow Generator System Calibration.....	61
5.4.1. Pulse Wave Development & Calibration.....	62
6. Results.....	64
6.1. Piston Slider Crank Analysis.....	64
Table 10: Kinematic Analysis.....	64
6.2. Arterial Testing.....	65
6.2.1. Radial Compliance Testing.....	65
6.2.2. Tensile Testing.....	68
6.2.3. Pulse Wave Velocity Analysis.....	68
6.3. Pulsatile Flow Pressure Waveform Analysis.....	70
7. Analysis and Discussion.....	71
7.1. Arterial Testing.....	71
7.2. Harmonic Statistical Analysis.....	71
8. Conclusions.....	76
VII. Recommendations.....	77
VIII. References.....	78
IX. Nomenclature.....	82
X. Appendices.....	83
Appendix A: Piston Slider-Crank Kinematic Analysis.....	83
Appendix B: Pulsatile Flow Pressure Waveforms.....	84
Appendix C: Pressure Waveform Fast Fourier Analysis.....	94
Appendix D: ION Digital Drive.....	106
Appendix E: Piston CAD Drawing.....	108
Appendix F: Connecting Rod CAD Drawing.....	109
Appendix G: DC Motor Specifications.....	110
Appendix H: Pressure Transducer Specifications.....	111

Appendix I: Expense Report..... 112

II. Authorship Page

1. Introduction (TJ, WU)
- 2.1. Circulatory System (RG, WU, TJ, JM)
- 2.2. Arterial Disease States (WU, TJ)
- 2.3. Stenotic Hemodynamics (WU)
- 2.4. Pulse Wave Velocity (JM)
- 2.5. Prosthetic Models (TJ, WU)
- 2.6. Mechanical Flow Systems (JM)
- 2.7. Motion Control (WU)
- 2.8. Pressure Measurement (WU)
- 2.9. Wave Analysis (TJ)
3. Project Approach (WU)
4. Design Approach (WU, JM)
- 5.1. Blood Substitute Preparation (WU)
- 5.2. Latex Arterial Model Development (RG)
- 5.3. Arterial Testing (JM)
- 5.4. Pulsatile Flow Generator System Calibration (WU)
- 6.1. Results – Arterial Testing (JM, WU)
- 6.2. Results – Pulsatile Flow Pressure Waveforms (WU, TJ)
7. Analysis and Discussion (Group)
8. Conclusion (Group)

III. Acknowledgments

We would like to extend our gratitude and great appreciation to the following people and organizations. Their assistance both intellectually and material played a vital role in the development and successful completion of this project.

Prof. Brian J Savilonis
Prof. Kristen Billiar
Neil Whitehouse
Mike O'Donnell

Performance Motion Devices, Inc. (PMD), Lincoln, MA
Zeus, Inc., Orangeburg, SC

IV. Abstract

The objective of this project was to design a pulsatile flow generator for the analysis of wave propagation in blood vessels for implementation in the early detection of arterial disease. Latex iliac artery models, varying in arterial compliance and degrees of stenosis, were studied ex vivo utilizing the system at 1 Hz (60bpm) to validate the systems physiological functional capabilities. Validation methods proved successful as the physiological models produced waveform variances with changes in arterial wall mechanical properties and morphology.

V. Table of Figures

- Figure 1: The PQRST wave
- Figure 2: Viscoelasticity and shear rate relationship.
- Figure 3: Arterial Anatomy
- Figure 4: Compliance curve for an artery and vein
- Figure 5: Initial Stages of Atherosclerosis
- Figure 6: Fatty Streak Formation
- Figure 7: Advanced Atherosclerotic Lesion
- Figure 8: Unstable Plaque
- Figure 9: Doppler time & velocity spectral for normal and stenosed blood vessels
- Figure 10: Flow through a Stenotic Region
- Figure 11: Balances of forces in an arterial wall
- Figure 12: Cam-Follower System
- Figure 13: Slider- Crank Mechanism
- Figure 14: Kinematic equations
- Figure 15: DC Motor Motion
- Figure 16: Pulsatile Flow Generator Motion Control System
- Figure 17: ION Digital Drive
- Figure 18: ION Digital Drive Schematic
- Figure 19: PID Analysis
- Figure 20: PID Voltage Control Schematic
- Figure 21: Design Iteration One
- Figure 22: Base for Flow Generator
- Figure 23: Occlusion Insert Development
- Figure 24: Pulsatile Flow Generator CAD Front View
- Figure 25: Pulsatile Flow Generator CAD Angle View
- Figure 26: Pulsatile Flow Generator Front View
- Figure 27: Pulsatile Flow Generator Angle View
- Figure 28: Pulsatile Flow Generator Motion Control System
- Figure 29: Cardiac Cycle Replication
- Figure 30: Arterial Compliance Models
- Figure 31: Arterial Stenosis CAD Models
- Figure 32: Compliance Testing System CAD Model
- Figure 33: Pulse Wave Velocity vs. Mean Blood Pressure
- Figure 34: Phase Initialization Parameters
- Figure 35: Current Loop Parameters
- Figure 36: Waveform Morphology Code
- Figure 37: Arterial Model Elastic Modulus Analysis

VI. Table of Tables

Table 1:	Arterial Wall Thickness
Table 2:	Vein Wall Thickness
Table 3:	Modulus of Physiological Human Arteries
Table 4:	Tensile Properties of Physiological Human Arteries
Table 5:	Mechanical and Physical properties of Proposed Biomaterials
Table 6:	Proposed Polymer Biomaterials - Comparison of Characteristics
Table 7:	Comparison of Mechanical Properties of Arteries, Latex models and PTFE.
Table 8:	Design Iteration One
Table 9:	Density and Viscosity of Aqueous Glycerine Solutions
Table 10:	Kinematic Analysis
Table 11:	Radial Compliance Analysis
Table 12:	Compliance Analysis using dr/dP
Table 13:	Pulse Wave Velocity Analysis
Table 14:	Frequency & Harmonic Analysis for Stiffness & Occlusion Models
Table 15:	Stiffness Harmonic 1 vs. 2
Table 16:	Stiffness Harmonic 1 vs. 3
Table 17:	Stiffness Harmonic 1 vs. 4
Table 18:	Stiffness Harmonic 1 vs. 5
Table 19:	Occlusion Harmonic 1 vs. 2
Table 20:	Occlusion Harmonic 1 vs. 3
Table 21:	Occlusion Harmonic 1 vs. 4
Table 22:	Occlusion Harmonic 1 vs. 5
Table 23:	Control Sample vs. Occluded Samples t-test Analysis

1. Introduction

The American Heart Association has reported that 36.3% of deaths in the United States of America were caused by cardiovascular diseases. Cardiovascular diseases include high blood pressure, coronary heart disease, myocardial infarction, stroke, stenosis, and atherosclerosis. High blood pressure is considered the silent killer because there are no symptoms and the only way to check is to take your blood pressure. However if your blood pressure is not controlled it can lead to stroke, heart attack or heart failure. High blood pressure or hypertension is when systolic pressure is over or equal to 140 mmHg or diastolic pressure is equal or greater than 90 mmHg. Some methods of regulating hypertension include diet and exercise.

Coronary heart disease, the leader of deaths in America begins with the onset of atherosclerosis. Atherosclerosis occurs when fatty streaks form plaque; in the case of coronary heart disease the artery walls build up with atheromatous plaques. Blood clotting can occur once the atheromatous plaques rupture, impeding blood flow. Prevention of this disease involves the proper introduction of diet control and regular cardio exercise into ones lifestyle.

Myocardial infarction happens when there is an interruption of blood supply to part of the heart. There is an increased risk for myocardial infarction in smokers, coronary heart disease patients, stroke victims, and those suffering from abnormalities in their heart rhythms. Symptoms include shortness of breath, chest pain, and palpitations. Immediate treatment consists of oxygen, aspirin, and pain relief. Long term treatment includes anticoagulants, dilation of flow or a bypass surgery (American Heart Association, 2007).

The most important aspect of the development and progression of cardiovascular diseases and in the case of our experimentation, arterial disease, is the role of hemodynamics. Hemodynamics consists of the properties and flow of blood; these properties are pressure flow and resistance of circulated blood. Common hemodynamic measurements include cardiac output, stroke index, blood pressure, cardiac index and heart rate (International Hemodynamic Society, 2000). Arterial disease is the end result of the thickening or reduction in elasticity of the inner arterial wall. The internal mechanical forces acting on the inner arterial wall are the arterial pressure and shear stress. The wall shear stress is characterized as the tangential drag force experienced by the inner arterial wall caused by the pulsatile fluid flow of blood. Arterial wall shear stress has been credited with being the initial variable in the development of arterial disease with abnormal and irregularly experienced arterial wall shear stresses bringing about the development of arterial disease.

The development of lesions and the formation of plaque along the lining of the inner arterial wall will be apparent within an artery exposed to abnormal levels of wall shear stress. Damage to the arterial wall in this manner elicits a continued response by the body's immune system resulting in the accumulation of fibrin, calcium, cholesterol, proteins, and other biological particles within the blood at the site of arterial damage. The accumulation of biological particles in this manner will eventually restrict pulsatile blood flow through the artery, minimizes the amount of oxygen to the surrounding tissues and causing further restriction and stress on surrounding regions of the cardiovascular system.

Advancements in detecting plaque build up and blockages of arteries are critical for atherosclerosis. Therefore being able to detect when an artery begins to have harden and thicken beyond normal aging is ideal. This idealism would decrease the number of incidents that occur with arterial disease. Currently recognition of atherosclerosis does not happen until the progression of the disease is sever.

This project aims to both design and manufacture a pulsatile flow generator for the analysis of wave propagation in blood vessels for implementation in the early detection of arterial disease. This design should replicate pulse waves (pulsatile flow) within a physiological and should operate at a rate of 60 bpm or 1Hz. The system should also allow researchers to change the waveform morphology to correspond to different locations of the arterial tree.

As the paper progresses, the group aims to provide an outlook into scope and methods of our project through the Literature Review, Project Approach, Design Approach, Results, Analysis and Discussion and finally the conclusion. All vital and pertinent information for a proper understanding of the project, such as the arterial disease states and their hemodynamic effects on the blood flow through the system, will be detailed in our Literature Review section. The Project approach will detail our aims and objectives, as well as, explaining the consumptions that were made through the course of the project. At this point the paper will transition into the Design aspects of the project and ending with a thorough analysis of our results.

2. Literature Review

2.1. Circulatory System

The circulatory system is composed of the heart, capillaries, capillary beds, veins, arteries, arteriole, venule and blood. A rhythmic beat is made by the heart; the beginning of this beat happens when there is an action potential in the sino-atrial node, this stimulation spreads to the atrio-ventricular node, which propagates the bundle of His. As a result, the heart produces what is more commonly known as a PQRST wave, a depiction of the atrial depolarization (P), the ventricular depolarization (QRS) and the phase of rapid repolarization of the ventricles (T).

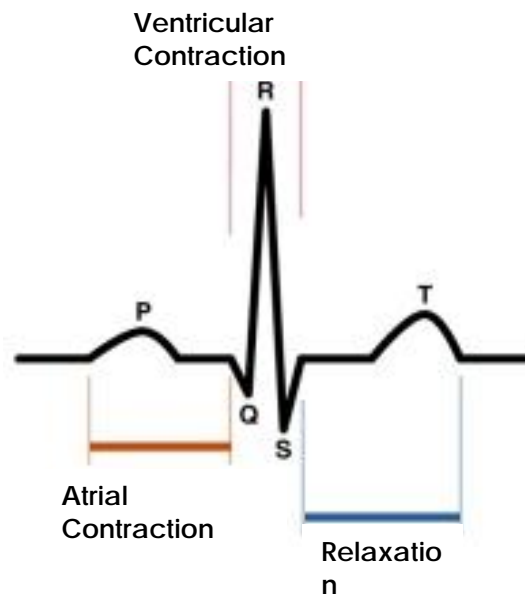


Figure 1: The PQRST wave

Once blood leaves the heart it flows into the arteries, then from the arteries into the arterioles and then in the capillaries. As blood returns back to the heart via the veins it travels through the capillaries into the venules and lastly it ends up in the veins. The function of the arteries is to circulate oxygenated blood to the organs, whereas the veins carry deoxygenated blood back to the heart to get oxygenated again.

2.1.1. Blood

Blood is a unique tissue in the body that has fluid properties that accounts from nearly 8% of body weight. Often known as the “River of Life” in ancient times, a healthy adult male has blood volumes of 5-6L while healthy females have 4-5L of blood. In the body, blood serves as a “vehicle” for the transportation of nearly every biological molecule. The general path of flow for blood is from the heart to the body, back to heart, to lungs and back to heart to be sent through the body again. Blood is a viscoelastic fluid that is composed of cellular and fluid components, that is, blood is composed of plasma and cells. The cells provide the elastic component of viscoelasticity and are also responsible for providing oxygen to the various tissues in the body.

Plasma on the other hand provides viscosity component of viscoelasticity and carries all biological molecules, as well as provide an ideal environment to host blood cells

Blood performs many regulatory functions in the body. Blood helps maintain an appropriate body temperature by absorbing and distributing heat throughout the body. To prevent drastic body temperature fluctuations, blood is directed towards the skin surface to encourage heat loss or away from the surface to prevent heat loss. Blood also consists of large quantities of salts and blood proteins. Since proteins are sensitive to pH, a significant change could permanently damage the protein, thereby inducing massive damage to the native tissue. Therefore, buffers in the blood help maintain a very narrow range of pH. To perform this function, Carbon di-oxide (CO₂) and other molecules are regularly bound or released to maintain a pH between 7.35 and 7.45. This allows the body to utilize osmosis and control fluid loss to surrounding tissue in order to maintain adequate fluid volume and water content in the circulatory system.

Blood is a sticky and opaque fluid that changes from scarlet (oxygenated) to dark red (deoxygenated). It also has a higher density than water. At a temperature of 37 degrees C, water has a density of 993.4 kg/m³ while blood has a density of approximately 1060kg/m³. Normally, blood is approximately 5 times more viscous than water. It also has a slightly higher temperature than body temperature.

2.1.1.1. Viscoelasticity

Viscoelasticity is an important property that is characteristic of most physiological tissues and fluids. Viscoelasticity is described as the ability of a material to show both viscous and elastic properties. Blood is also a viscoelastic material and is dependent on both viscosity and elasticity for proper flow through the body. For blood flow, the viscosity effects are generally attributed to plasma while the elastic properties are attributed to the blood cells, mainly red blood cells. Viscosity is generally related to the energy dissipated during flow, primarily due to deformation and sliding of RBCs and RBC aggregates. Elasticity refers to the energy stored during flow due to the deformation of RBC's. In the body, viscoelasticity reflects a cumulative effect of many parameters such as viscosity, blood cell deformability, aggregation, etc.

Why is viscoelasticity important? Blood flows in a pulsatile manner. As the heart beats, the viscoelastic properties of blood determine how the energy is stored or dissipated in the fluid. This is because RBC's naturally tend to aggregate and stack together in a space efficient manner. These stacks must be reduced in order blood to flow freely. Therefore, once the energy is applied, the energy is stored into the cells due to elastic deformation and re-orientation of cell and cell microstructure, respectively. As the blood flows through the body, it requires continuous input of energy, which is dissipated through viscous forces such as friction. Therefore, since the blood exhibits both viscous and elastic properties, it is considered a viscoelastic fluid.

Viscoelasticity profile of blood can be divided into three parts between low shear, medium shear, and high shear. Studies have shown that blood viscoelasticity is highly dependent on the rate of shear stress being applied. The three regions are as follow:

- Region 1: Low shear rate: at low shear, the RBC's are undisturbed and form aggregates, as mentioned previously, in a space efficient manner. In this region, viscoelasticity is dominated by red blood cell aggregates.
- Region 2: Mid-shear rate: at medium shear rates, the aggregates start to break down and the cells become increasingly disaggregated with increasing shear rates. The cells become deformed and somewhat oriented in the direction of the flow. In this region, the aggregates have increasingly lowered affect on the viscoelasticity of the fluid, and increased effect due to the deformability of the cells.
- Region 3: High Shear rate: At high shear rates, the cells are completely aligned in the direction of the flow, and viscoelasticity is influenced primarily by the ability of the cells to deform. A visual representation of the three rates can be observed in Figure 1.

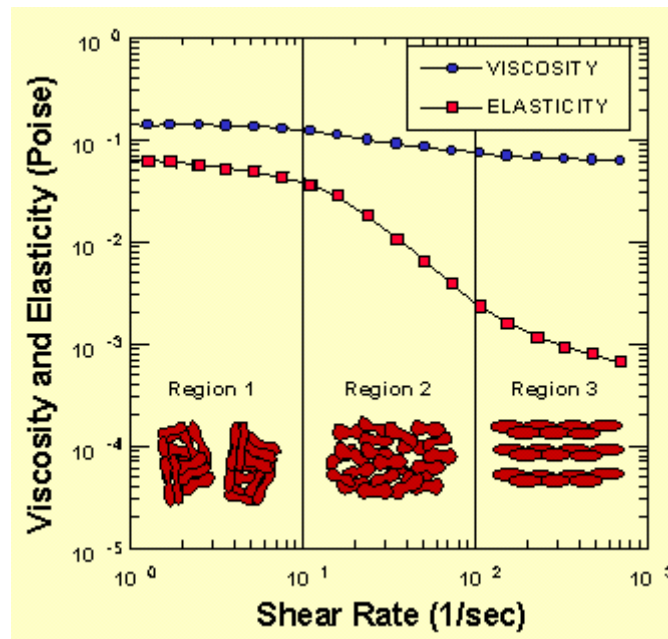


Figure 2: Viscoelasticity and shear rate relationship.

2.1.1.2. Clinical Significance

Blood rheology plays an extremely vital role in the development and progression of atherosclerosis and arterial disease. Literature details how specific regions along the arterial tree are more apt to the development of atherosclerotic plaque, fatty streaks, (Caro et al., 1971; Friedman et al., 1981) as well as, how the hemodynamics of these particular regions are not only controlled by the mechanical properties of the arterial but also by the rheological properties of the blood flowing in the aforementioned regions.

The development of atherosclerosis has been attributed to many of the components of blood hemodynamics, which includes disturbed flow patterns (Hughes and How, 1995; Staalsen et al., 1995), low shear stress (Dobrin et al., 1989; White et al., 1993; Delfino et al., 1997), low and oscillating shear (Bassiouny et al., 1992; Taylor et al., 1998, 1999), temporal variation of the shear stress (Ojha, 1994),

spatial wall shear stress gradient (Kleinstreuer et al., 1996; Lei et al., 1997), and wall tension (Schwartz et al., 1992; Hofer et al., 1996). (Chen et al., 2005)

2.1.2. Arteries

2.1.2.1. Anatomy

Arteries transport blood from the heart to the organs in the body. The anatomy of the artery is broken down into the lumen, tunica interna, tunica media, and the tunica externa. The lumen is the hollow center of the artery, which blood flows through. The inner most layer of the artery is the tunica interna and it is the closest to the lumen; consisting of endothelium, a basement membrane, and internal elastic lamina containing a simple squamous epithelium lining. The complete cardiovascular system has a continuous layer on the inner surface of endothelial cells. This endothelial lining of the blood vessel is usually the only layer to come into contact with the blood.

The middle layer, generally the thickest layer, is the tunica media; the circularly arrangements around the lumen are elastic fibers and smooth muscle fibers. It is the abundant elastic fibers that cause arteries to have a high compliance. This high compliance means that the walls stretch or expand easily to the reaction of small pressure increases without tearing. The tunica externa is the outermost layer made up of elastic and collagen fibers.

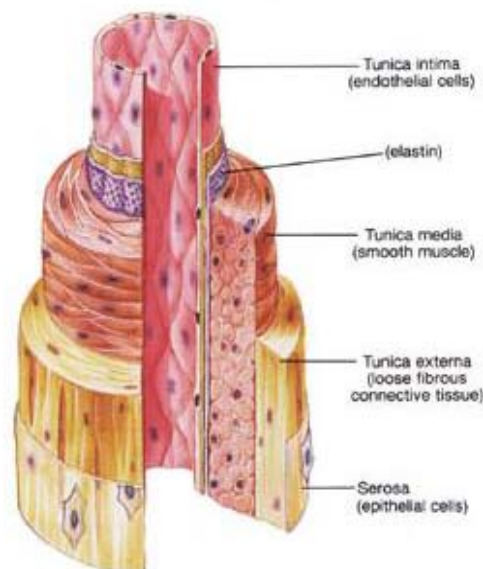


Figure 3: Arterial Anatomy (Fox, 1998)

2.1.2.2. Arterial Properties

The artery is considered a 3-dimensional structure comprised of parts which exhibit non-linear behavior, unequal physical properties along different axes or anisotropic behavior, and let us not forget viscoelastic behavior. Given the properties of anisotropic components varying with direction of applied stress and the properties of the viscoelastic components varying with time in

response to an applied stress or strain, these component behaviors and their respective mechanical properties allow us to make a general assessment of the properties of the artery. (Hayashi 1993) This assessment is one which concludes that an artery is simply a viscoelastic material. Due to its complex nature, it is quite difficult to simply define an arteries properties by one single descriptor.

2.1.2.3. Mechanical Properties

Arterial mechanical properties describe the characteristics that make up the tissue. The major mechanical properties include wall thickness, Young’s modulus, compliance, pulse wave velocity and radius. Below are tables which compare arterial and vein wall thicknesses.

	Artery	Arteriole	Capillary
Diameter	25 mm	30μ	8μ
Wall thickness	2 mm	20μ	1μ

Table 1: Arterial Wall Thickness (McDonald, 1974).

	Large vein	Venule-small vein
Diameter	5 mm	20μ
Wall thickness	0.5 mm	2μ

Table 2: Vein Wall Thickness (McDonald, 1974).

For the arterial wall the range of Young’s modulus is $2 - 8 \times 10^6 \text{ dyn/cm}^2$, which can be converted to 200 - 800 kPa.^[7] Young’s modulus is a proportion between the strain and the stress, stated by Hooke’s Law. Here E is Young’s modulus, σ is the stress, and ϵ is the strain.

$$E = \frac{\sigma}{\epsilon} \quad \text{Equation 1}$$

Wall thickness and Young’s modulus usually remain constant in each specific artery assuming that the artery is healthy. If the artery is diseased, then these properties can change. Compliance and pulse wave velocity are two of the properties, which can change as the artery undergoes changes such as stiffening

2.1.2.4. Impedance

The human body, specifically blood is made up of many unique and independent parts which all have effects on how the total function of the body works. One of the main effects these parts have is impedance or resistance.

Impedance is basically the resistance caused by any object. With respect to human blood, the impedance on the flow of blood can be considered any property or phenomenon which can hinder or alter the normal blood flow through the cardiovascular system. Some examples of this include, the viscosity of the blood itself, the plasma and cells contained in blood and some of the branching points of the arteries.

Since the viscosity of blood is a key factor in how it flows, any change in viscosity, due to whatever reason, can cause an increased or decreased resistance. This change in impedance would alter how the blood flows and alter the amount of pressure contained within the vessel. The plasma and cells contained within the blood act in a similar manner but the impedimental effects of them are much less significant than that of viscosity.

2.1.2.5. Compliance

Before occlusion occurs, there is a critical stage in the development and progression of arterial disease. This vital stage in the disease process is the development and formation of plaque lining the inner arterial wall brought about by the prevalence of lesions along various points of the inner arterial wall. This initial thickening and reduction in elasticity, due to the formation of plaque changes the haemodynamics through the artery considerably, altering the structure and function of the inner arterial wall and the prevalence of disease (Fung, 1993).

“A particular characteristic of the flow in stenotic vessels is the appearance of transitional/turbulent flow patterns, which in general are considered pathological in normal blood circulation. Although for mild stenosis the degree of stenosis is usually defined as a percentage diameter reduction the flow is likely to remain laminar, in moderate to severe stenosis conditions transitional and turbulent flow patterns appear in the post-stenotic area. Early in vivo velocity measurements point to a highly complex flow field with laminar, transitional and turbulent flow regimes coexisting in different spatial locations at various instants in time.” The wall shear stress is proportional to the velocity gradient at the wall and the fluid viscosity and is an estimate of the mean wall shear stress in the artery, as detailed in the following equation.

$$\tau_{wall} = \frac{32\mu Q}{\pi D^3} D \quad \text{Equation 2}$$

Due to the complexity of the velocity gradient, in particular, testing and analysis of this characteristic, the group has decided to research the relationship between the change in pressure and the change in the elasticity of the arterial sample in order to determine how a small change in the stiffness of the sample correlates with a change in pressure. We are able to use the change in pressure due to the relationship between the pressure and the inner wall shear stress. One of the major haemodynamic forces acting on the artery is the transmural pressure across the thickness of the arterial wall.

Arterial compliance, the viscoelastic property measuring the elasticity of the arterial wall, usually fluctuates with smooth muscle contraction and relaxation, therefore there can be many different types of curves to present compliance trends. In Figure 2 below, the compliance curves for both an artery and vein are shown. As can be seen, these curves are not linear. This is because the arterial wall tissue is not homogenous and therefore mechanical properties such as viscoelasticity play a major part in its functionality. This is because the arterial wall tissue is not homogenous and therefore mechanical properties such as elasticity end up having a non-linear change. This phenomenon is exactly what the group hopes to isolate and verify within the testing samples. By analyzing the compliance of a sample, the study group can gain a better understanding of what the mechanical properties of the sample are and if they compare to those in actual arteries (Fung,

1993). The compliance recorded can be both static or dynamic. For the purposes of this experiment though, because of lack of testing resources, the group has concentrated more on the static compliance of a vessel.

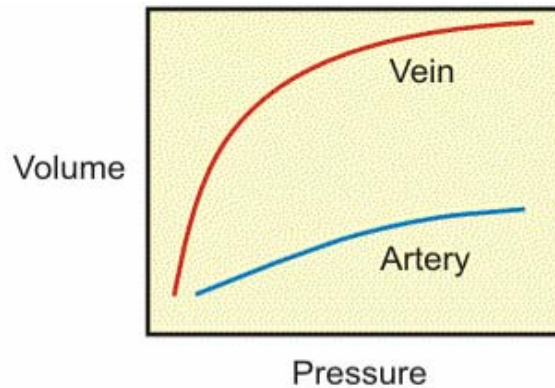


Figure 4: Compliance curve for an artery and vein

The group has decided to design a system which can be used to accurately observe the changes in radius of each sample. The compliance itself will be determined utilizing the following equations:

$$C = \left(\frac{\Delta R}{R_i} \times \frac{100}{P} \times 100 \right) \quad \text{Equation 3}$$

$$C = \left(\frac{\Delta R}{\Delta P} \right) \quad \text{Equation 4}$$

where C is the compliance, ΔR is the step change in radius of the arterial sample, P is the pressure at which the new radius was observed and ΔP is the difference between the original pressure and new pressure (Avolio et. Al, 2002).

These equations would allow for the group to have an understanding of the stiffness of each testing sample. By knowing the stiffness, the group would be able to determine the type of artery being tested i.e. diseased or healthy. The group would also look at pulse wave velocity calculations to confirm the findings of compliance testing.

2.2. Arterial Disease States

There are many disease states that can occur in the arteries such as atherosclerosis and stenosis, just to name a few. Atherosclerosis can be broken down into two components: athermatous and sclerotic tissue. Athermatous is “gruel, a soft and lipid-rich” where as sclerotic tissue is “hard and collagen-rich (Safar et al., 2002).” On an average more than 70% of the plaque volume is from sclerotic tissue, however it is moderately benign since smooth muscle cells secrete collagen therefore stabilizing the plaque. Unlike athermatous, plaque is destabilized, consequently increasing the risk for formation of a thrombus (Safar et al., 2002).

The initial observable changes of the artery due to atherosclerosis takes place in the endothelium of the artery and include the increased endothelial permeability to lipoproteins and other plasma constituents, up-regulation of leukocyte adhesion molecules and the up-regulation of endothelial adhesion molecules into the arterial wall, which is detailed in Figure 3.

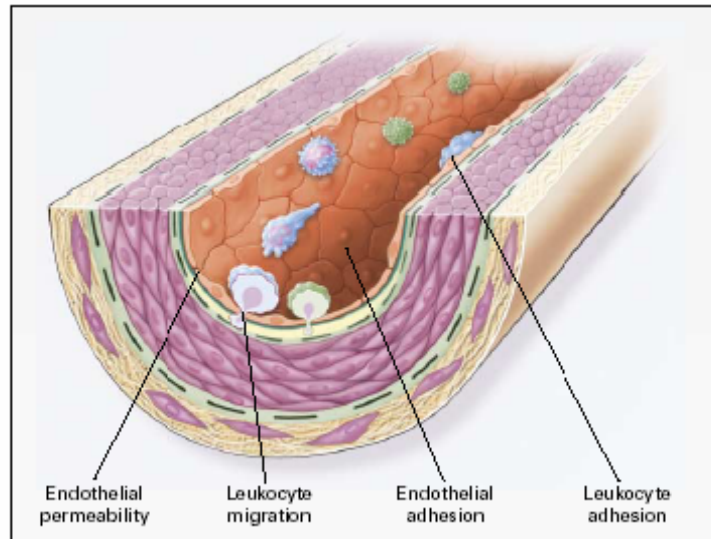


Figure 5: Initial Stages of Atherosclerosis

The observed causes of endothelial dysfunction leading to atherosclerosis include elevated and modified low-density lipoprotein (LDL); free radicals caused by cigarette smoking, hypertension, and diabetes mellitus; disturbed regions of flow; genetic alterations; and/or elevated plasma homocysteine concentrations.

The very next stage in the progression of atherosclerosis is the formation of fatty streaks. This type of lesion formation may be present throughout one's lifetime and is common in infants and young children. These fatty streaks initially consist of foam cells (macrophages containing lipids) together with T lymphocytes. Later, smooth muscle cells also appear in the fatty streak. The steps involved in this process include smooth muscle cell migration, T-cell activation, foam cell formation, and platelet adherence and aggregation. If these responses continue, they can thicken the artery wall. Due to this initial thickening, the artery compensates this by gradual dilation so that up to a point the lumen remains unaltered. This is known as vessel wall remodeling, which is detailed in Figure 4.

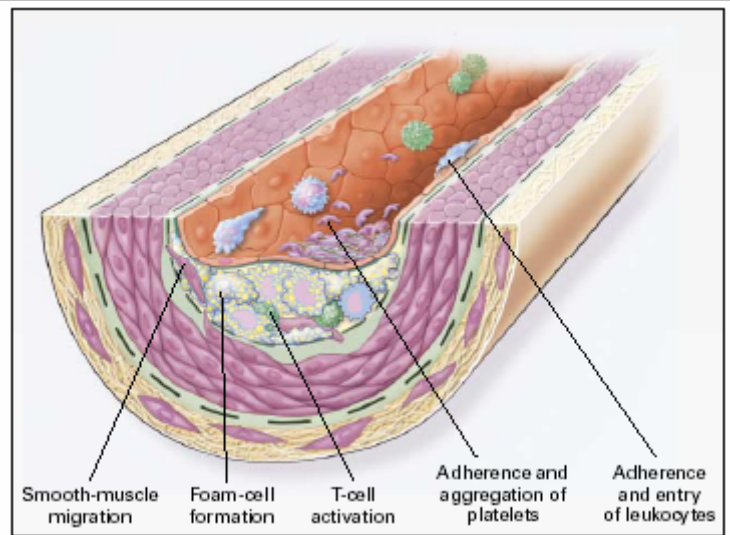


Figure 6: Fatty Streak Formation (image from Ross, R., 1999.)

Now, as the fatty streaks progress and form into intermediate and advanced lesions, they tend to form a fibrous cap or thin layer that separates the lesion from the lumen, which is detailed in Figure 5. This formation represents a type of healing or fibrous response to the injury. The fibrous cap covers a mixture of leukocytes, lipid, and debris, which may form a necrotic core. These lesions expand at their shoulders due to continued leukocyte adhesion and entry. The necrotic core represents the result of apoptosis and necrosis, increased proteolytic activity, and lipid accumulation. At some point the artery can no longer compensate by dilation; the lesion may then intrude into the lumen and alter the flow of blood.

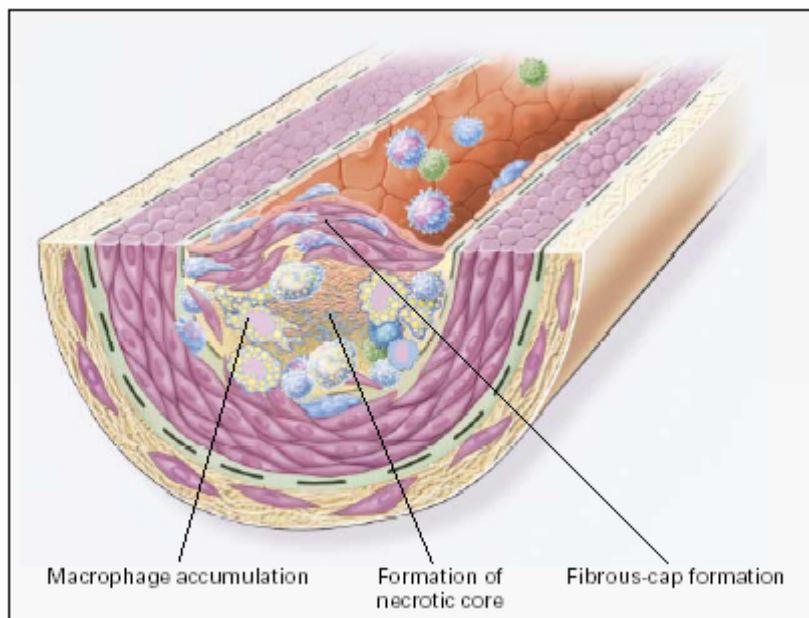


Figure 7: Advanced Atherosclerotic Lesion (image from Ross, R., 1999.)

The rupturing of the fibrous cap or ulceration of the fibrous plaque can rapidly lead to thrombosis, which is detailed in Figure 6, and usually occurs at sites of thinning of the fibrous cap that covers the advanced lesion. Thinning of the fibrous cap is apparently due to the continuing introduction and activation of macrophages, which release matrix metalloproteinase's (MMPs) and other proteolytic enzymes at these sites. These enzymes cause degradation of the matrix, which can lead to hemorrhage from the *vasa vasorum* or from the lumen of the artery and can result in thrombus formation and occlusion of the artery. The adherence and buildup of plaque is to follow this initial formation.

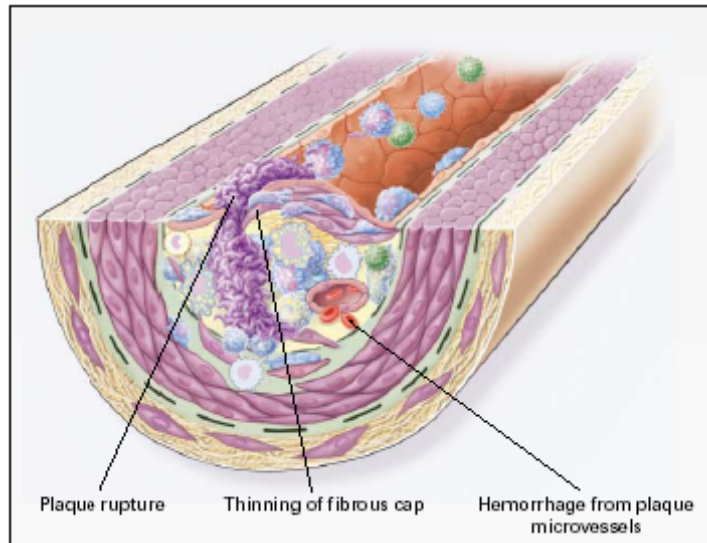


Figure 8: Unstable Plaque

The noticeable appearance for atherosclerosis is when the artery is very narrow or completely blocked, yet some symptoms that occur are “chest pain, pressure, tightness, or heaviness; leg cramps or pain with exercise; weakness on one side of the body; disturbance in speech, vision, or balance; abdominal pain or cramping (Fuster, Valentin, et al., 1999).” Treatments include prevention, lowering the risk by knowing health profile; lowering levels of cholesterol intake as well as triglycerides is prevention for decreasing the risk.

Lastly there are drugs that are used to low the progression of the disease such as antiplatelet agents, fibrinates, and fish oils just to name a few (Recognizing the Symptoms. 1999).

Stenosis is the blockage of an artery which can be caused by plaque build-up, such as that found in atherosclerosis (Recognizing the Symptoms. 1999). Basically stenosis is the diagnosis when there is significant atherosclerosis found within an artery causing severe enough blocked to greatly impede blood flow.

2.3. Stenotic Hemodynamics

As aforementioned, stenosis is characterized by a narrowing and protrusion of the arterial wall consisting of a converging and diverging morphology. Bernoulli's equation applies within the converging region of the stenosed artery but Poiseuille's law best describes the stenosed region of the artery. However, neither law governs the diverging region of the stenosed artery in which flow is turbulent and subject to viscous losses due its separation as it enters the region.

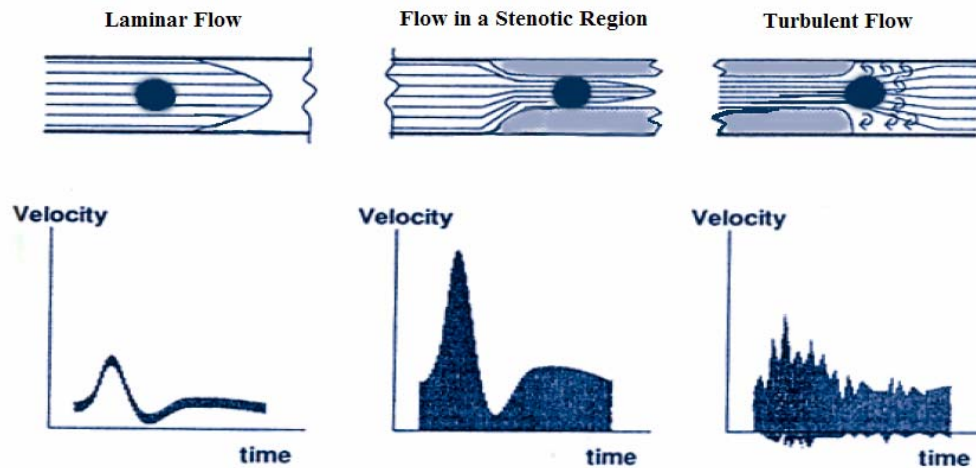


Figure 9: Doppler time & velocity spectral for normal and stenosed blood vessels (Smith, 1991)

The above figure characterizes the stenotic hemodynamics detailed above. One can clearly see the flow through a relatively average sized blood vessel starts off as laminar flow and as it enters the stenotic region, that same quantity of blood is forced through the narrowed region increasing the velocity. However as the flow of blood exits the stenotic region and flows into a region of increased area, the flow becomes turbulent as the velocity decreases suddenly.

The protrusion of the arterial wall will also result in the fall in pressure distal to the stenosed region of the artery due to the increased resistance leading to the increase in loss of pressure along the entire length of the stenosed arterial region. (Young et al, 1973) This pressure loss, ΔP , when treated through semi-empirical relations, can be directly related to the flow, Q , with the following relationship,

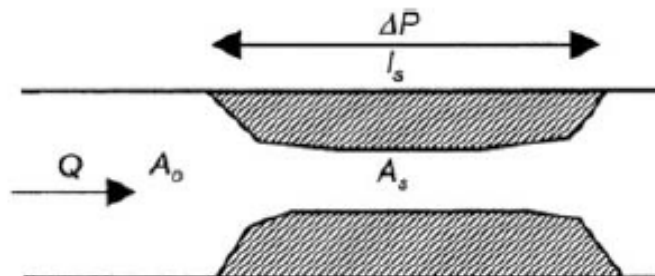


Figure 10: Flow through a Stenotic Region

$$\Delta P = \frac{8\pi \cdot \eta \cdot l_s}{A_s^2} \cdot Q + \frac{K_t \cdot \rho}{2A_0^2} \cdot [A_0 / A_s - 1]^2 \cdot Q^2$$

Equation 5



$$\Delta P =: a_1 Q + a_2 Q^2$$

Equation 6

where A_0 = cross-sectional area of the unobstructed lumen, A_s = the area of the stenosed lumen, ρ = the fluid density, η = the fluid viscosity, l_s = the length over which the pressure drop is measured and K_t which is an experimentally determined coefficient heavily dependent on the geometry of the stenotic region.

The first term in the relationship represents the viscous losses, while the second term in the relationship, derived from the mechanics of flow in an expansive tube, represents the loss of pressure distal to the stenotic region. (Newman et al, 1979)

This empirical formula for the ΔP across the stenotic region accurately depicts how flow, Q , and arterial area exist as quadratic terms detailing the hemodynamic activity of stenotic resistance increasing proportionally with flow.

2.4. Pulse Wave Velocity

When a heartbeat occurs, before the blood flow actually reaches a certain point in an artery, a pulse wave reaches that point. At any point where there is a branching of the artery, the wave is usually deflected back at a certain speed and goes back to its original starting point just before the aortic valve and dissipates in lieu of a new pulse wave created by the next heart beat. As an artery becomes stiffer, this pulse wave increases in velocity therefore the velocity after deflection also increases leading to the wave possibly reaching the aortic valve before it closes. This could lead to an unsafe increase in blood pressure. Basically, with age, the artery stiffens due to a wide array of issues and when this occurs, the pulse wave velocity number increases. The stiffer a vessel is, the higher its pulse-wave velocity would be (Fung, 1993).

Pulse wave velocity studies are usually performed *in vivo* but for the purposes of this study a mathematical equation was used to calculate the pulse wave velocity using an experimental elastic modulus. Since the samples used do not recreate a branching point, pulse wave velocity was used as a way of confirming the health range of the arterial samples created. The pulse wave velocity would basically allow the group to understand, along with the compliance, the mechanical properties of the sample with relation to the study.

If one considers the sample used as a isolated, cylindrical elastic tube and neglects the viscoelasticity of the material itself, then it can be assumed that flow inside the tube is basically one-dimensional with a longitudinal velocity component $u(x,t)$ as a function of the axial

coordinate x and the time component t . Because of these assumptions two equations can be used as the starting point to derive the final equation (Macdonald, 1974).

The equation of continuity

$$\frac{\partial A}{\partial t} + \frac{\partial}{\partial x}(uA) = 0 \quad \text{Equation 7}$$

and the equation of motion:

$$\frac{\partial u}{\partial t} + u \frac{\partial u}{\partial x} + \frac{1}{\rho} \frac{\partial p_i}{\partial x} = 0 \quad \text{Equation 8}$$

From these two equations some other assumptions can be made such as that because cross sectional area A is dependent on the transmural pressure,

$$p_i - p_e = P(A) \quad \text{Equation 9}$$

then it can be assume that the mass of the tube is ignored as well. Since the mass is ignored, the differential equations seen above can be converted into or replaced by algebraic equations leaving a basic equation of

$$C = \sqrt{\frac{A}{\rho} \frac{dP}{dA}} \quad \text{Equation 10}$$

This however is not where the derivation would stop for the purposes of this study (Macdonald 106). Because the group will be assuming its model to be an elastic tube, the derivation must be altered to include the Young's Modulus, E . As seen in Figure 7 below, since there needs to be a balance of forces on the arterial wall, then new factors must be taken into account such as the circumferential strain and the wall thickness, h .

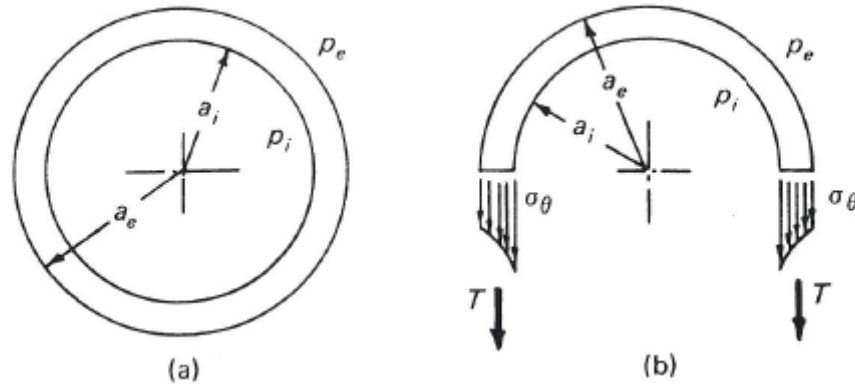


Figure 11: Balances of forces in an arterial wall

Circumferential strain is denoted as.

$$da_i/a_i \quad \text{Equation 11}$$

When this number is multiplied by both the Young's modulus, E, and the thickness, h, the equations would look like such.

$$\frac{Ehdai}{ai} = ai(dpi) \quad \text{Equation 12}$$

This equations is set equal to the product of the radius at a certain point, a_i , and the change in pressure dp_i

$$C = \sqrt{\frac{Eh}{2\rho ai}} \quad \text{Equation 13}$$

Therefore, the pulse wave velocity equation would be

$$C = \sqrt{\frac{Eh}{2\rho ai}} \quad \text{Equation 14}$$

but since the group did not assume that the model being used would be a thin-walled vessel, the equation must include the strain on the mid wall, therefore the final equations used would be

$$c = \sqrt{\frac{Eh}{2\rho(R + h/2)}}$$

Equation 15

where E, stands for the elastic modulus of the sample, R stands for the radius of the sample, h, stands for the wall thickness of the sample, ρ stands for density of blood and C stands for the pulse wave velocity. As this number increases, the stiffness of the artery does as well (Macdonald, 1974).

2.5. Prosthetic Models

With the advent of biomedical engineering the rise of biocompatible material, some focus in the industry has shifted towards finding the correct type of material which could correctly mimic the mechanical properties of the human body. In order to gain an understanding of the type of materials available that are clinically used for arterial treatment, the group felt it necessary to research all known materials used clinically.

2.5.1. Clinical Materials

The ideal Arterial Blood Vessel Biomaterial Substitute should closely resemble the properties of natural physiological blood vessels as detailed in Tables 3 and 4.

Modulus of Human Arteries	
<u>Arterial Segment</u>	<u>E (GPa)</u>
Thoracic Aorta	.4 - 1.0
Abdominal Aorta	.4 - 1.5
Iliac Artery	.8 - 4.0
Femoral Artery	1.2 - 4.0
Carotid Artery	.3 - .8

Table 3: Modulus of Physiological Human Arteries (Ratner, 2004)

Tensile Properties of Human Arteries		
<u>Age (yrs)</u>	<u>Tensile Strength (g/mm²)</u>	<u>Elongation (%)</u>
10 – 19	137 – 143	96.6 – 101.4
20 – 39	104.7 – 123.3	76.4 – 79.6
40 – 59	99.3 – 108.7	64.5 – 71.5
60 - 79	99.3 – 108.7	. - .

Table 4: Tensile Properties of Physiological Human Arteries (Ratner, 2004)

Upon further review of the literature and commercial availability, etc., the group has condensed the polymer class of biomaterials to those most suitable to our application and testing. The mechanical and physical properties of those biomaterials can be found in Table 5.

Material	Tensile Modulus (GPa)	Tensile Strength (MPa)	Elongation (%)	T _g (°C)	T _m (°C)	Water Absorption (%)	Water Contact Angle (°)
PET	2.8-4.1	59-72	50-300	69-82	265-270	0.1-0.2	73-78
PTFE	0.4	14-35	200-400	-10	327	0	110
PE	0.1-0.3	4-16	90-800	-20	95-115	.009	93-95
Polyurethane	.07	31-41	600-800	(-)53 – (-)67	120-150	.02	63-69

Table 5: Mechanical and Physical properties of Proposed Biomaterials (Ratner, 2004)

These characteristics have been detailed in Table 6.

Biomaterial	Advantages	Disadvantages
Poly(ethyleneterephthalate) – PET –	<ul style="list-style-type: none"> ○ Chemically Inert 	<ul style="list-style-type: none"> ○ Subject to hydrolysis ○ Low MW contaminants
Polytetrafluoroethylene – PTFE –	<ul style="list-style-type: none"> ○ Resistance to chemical degradation ○ Hydrophobicity ○ Low friction 	<ul style="list-style-type: none"> ○ Low wear resistance ○ Does not display typical thermoplastic flow behavior
Poly(ether urethane urea)	<ul style="list-style-type: none"> ○ High flex life ○ Range of mechanical properties 	<ul style="list-style-type: none"> ○ Uncertain molecular structure- property relationships ○ Surface radically different from bulk (high mobility of "soft segments") ○ Low MW contaminants Subject to hydrolysis, oxidation, and calcification

Table 6: Proposed Polymer Biomaterials Comparison of Characteristics

2.5.2. Latex

Latex models of arterial vessels have been used previously in medical research. A research team in the United Kingdom found a way to manufacture latex tubing that had similar characteristics of human arteries. The artery in which this group mimicked was the superficial femoral artery. A 7×10^{-3} m rod was for painting on the layers of latex. The procedure which was used comprised of painting thin layers onto the rod using a fine brush and letting it dry for 30 minutes before applying another layer. Once the latex was taken off the rod it was allowed to dry for 24 hours.

The various testing that was done to compare the latex models to that of human arteries were compliance, pulse wave velocity, and Young's modulus. The results of the experimentation were that compliance ranged between 337.5×10^{-12} to $900 \times 10^{-12} \text{ m}^3 \text{ Pa}^{-1} \text{ m}^{-1}$ which covers in vivo ranges that have been observed; Young's modulus was measured to be $0.61 \times 10^6 \text{ Pa}$ which compares to published data by Duck in 1990, human arteries range between 0.3×10^6 and $5.5 \times 10^6 \text{ Pa}$; lastly the pulse wave velocity ranged from 6-9 m/s which was 5-15% lower than the predicted value. The end conclusion was that latex models were similar to that of human arteries except for the increased compliance at higher pressures (Walker et. al., 1999).

Another group of researchers at Brunel University have used latex tubes to model arterial waves. The wave of particular significance to the group was the wave from the heart to the feet which is about 2 m. The lengths of the latex tubes were 2 m, the diameter range was 4 -16 mm, the wall thickness range was 0.1 - 0.2 mm, wave speed was 3.5 - 7.1 m/s, and the compliance was $0.024 - 4.55 \times 10^{-8} \text{ m}^2 \text{ Pa}^{-1}$. The outcome was that bigger pulse pressure was observed in the smaller tubes in comparison to the larger ones; there were also greater wave intensities in the smaller tubes than the larger tubes (Feng et. al., 2006).

A different group in the United Kingdom used latex modeling to look at the waveforms after an aneurysm by monitoring intrasac pressure (ISP). Here they found that intrasac pressure had significant drop relative to arterial blood pressure (Chaudhuri et. al., 2006).

From the literature what is observed is comparative data when using latex for arterial modeling, therefore encouraging the use of latex for our experimental analysis.

2.5.3. Comparison of Prosthetic/Latex/Human Arteries

It is pertinent for experimentation to find a material that is very similar to that of human arterial mechanics when making a physiological model. Arteries have a Young's Modulus of $3.21 \times 10^5 \text{ Pa}$, where latex arterial models are $0.61 \times 10^6 \text{ Pa}$ and PTFE is $0.4 \times 10^9 \text{ Pa}$. Compliance and Young's modulus values can be seen in the table below (Feng et. al., 2006). These values were taken from a study where latex models were also used, but the morphology of their models were quite different than the ones that would be used by the group. Differences in wall thickness and radius would lead to different compliance values. The group would create latex models that would be compliant enough to fall within a physiological range. These values show that although PTFE would be a better substitute, latex can still serve as a good model.

Material	Young's Modulus	Wave Speed	Compliance
Artery	$3.21 \times 10^5 \pm 2.11 \times 10^5 \text{ Pa}$ [3]	4 – 20 m/s [1]	$68 \times 10^{-12} \text{ m}^3 \text{ Pa}^{-1} \text{ m}^{-1}$ [2]
Latex Model	$0.61 \times 10^6 \text{ Pa}$	6 - 9 m/s	$337.5 \times 10^{-12} - 900 \times 10^{-12} \text{ m}^3 \text{ Pa}^{-1} \text{ m}^{-1}$ [2]
PTFE	0.4 GPa		1.6 % diameter change/mmHg $\times 10^{-2}$ [4]

Table 7: Comparison of Mechanical Properties of Arteries, Latex models and PTFE.

Another reason why latex should be used in comparison to PTFE is cost. Latex by the gallon is \$39.95 where different types of models can be made; unlike PTFE which is about \$4 per foot but with this type of testing custom models are needed and that is more expensive.

2.6. Mechanical Flow Systems

2.6.1. Pulsatile Flow Generators

In order for blood flow to be mimicked, a system must be used which can recreate the pumping action of the heart. Studies usually yield two different ways of creating this pumping action; a slider-crank system or a cam-follower system. They are both systems in which a piston and flywheel are incorporated with each system having its own advantages and disadvantages.

2.6.2. Cam-follower

The cam-follower system is a pumping system in which the timing and force put on the piston is actually controlled not only by the motor, but also by the shape of the cam itself. As seen in Figure 7 below, the flywheel or cam is not in a circular shape. Rather its shape has been determined using physical analysis taking into account the amount of force needed on the piston along with the displacement of the piston with time. The cam can actually be produced using different types of software which exist such as DynaCam. This software program allows one to create the cam one would need in order to produce the type of flow wave desired.

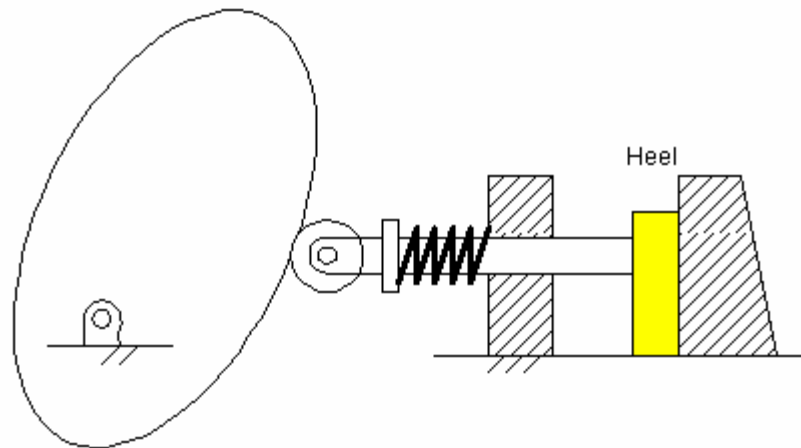


Figure 12: Cam-Follower System

Its shape for the most part is an oval shape with different types of small bends or concaves in order to mimic the action of the heart as much as possible. Its oval shape with the bends and concaves allows for the “break” between pumps to occur and since the human heart does have the split second pause between pumps, this system is thought to be very close to how the heart pumps blood. Also the amount of revolutions of the cam can be controlled by the motor power and rpm.

Although the cam follower system seems to be a very good way to mimic the human heart and how it pumps blood throughout the body, it does have its disadvantages. One problem is friction which can occur between the follower and the cam surface. Since the follower follows the path of the cam, eventually friction can occur causing a slight altering of the path. When this occurs, the wave created by the contour can be altered as well. This system must follow very strict precision constraints otherwise it will not produce the results needed. The friction can especially be a problem at high speeds because the cam follower may not move as fluidly as needed at high speeds in order to attain a good pumping action. Even though many use lubrication such as ester based oils to keep the friction low, overtime this hesitation can still occur (Makoto et. al., 2005).

Another problem that can occur with the cam-follower system is that wear on the cam caused by the follower can redistribute the pressure placed on the cam. Basically you start to get a cam contour which is no longer smooth but rather bumpy causing an inaccurate flow wave to be produced. (Anders et. al., 1996)

A third problem with the cam-follower system is that the cam-follower system assumes a constant camshaft speed. At high speeds though, all cam-follower systems exhibit some camshaft speed fluctuation, which can lead to follower inaccuracies and distortions.^[16] Since every cam-follower system is theoretically different though, the “high-speeds” which can cause this fluctuation may be lower in different models. Therefore, with the cam-follower system effectiveness testing must be performed in order to accurately observe that max speed at which the system still runs properly.

2.6.3. Slider Crank

The second type of pulsatile flow generating system is the slider-crank system. This system is similar to the engine of most cars. It differs from the cam-follower system in that the piston is directly connected to the cam or flywheel via a connecting rod. Therefore the cam itself does not have an oval shape but rather a circular shape.

The slider-crank system offers advantages in that some of the frictional problems with the cam-follower system are solved. Since the piston is directly connected to flywheel, the only concern about friction would be in the tube where the piston pumps, but this can be easily overcome using a good long lasting lubricant and does not present as much of a frictional issue as does the cam-follower system.

A second advantage is that the slider-crank system allows for the control of the flow to come from control over the motor rather than from the contour of the cam. This allows the researcher to be a bit more precise as long as the motor can be controlled properly.

The slider-crank system is one which the kinematics plays a major role. As seen in Figure 8 below, there are many unknowns such as angles and lengths which must be calculated in order to get a good working system that has no hesitations or pauses.

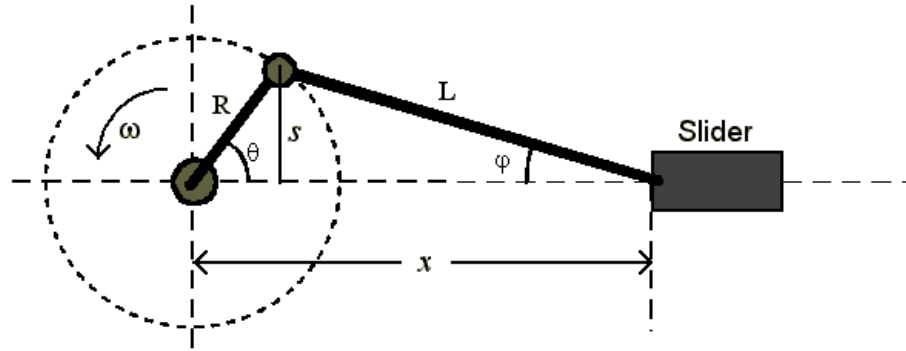


Figure 13: Slider- Crank Mechanism

By performing simple kinematic analyses on the whole system using the equations seen in Figure 9 below, the vital unknowns such as omega, and the length of the connecting rod, L, can be calculated. The analysis for this project can be seen below in Table 7.

$$\cos(\phi) = \sqrt{1 - \left(\frac{r}{L} \sin \theta\right)^2}$$

$$x = \left[r + \frac{r^2}{4L} \right] - r \left[\cos \theta + \frac{r}{4L} \cos(2\theta) \right]$$

$$\dot{x} = rw \left[\sin \theta + \frac{r}{2L} \sin(2\theta) \right]$$

$$\ddot{x} = rw^2 \left[\cos \theta + \frac{r}{L} \cos(2\theta) \right]$$

$$F_{\text{Pressure}} = P \times A$$

$$F_{\text{Net}} = F_{\text{Pressure}} - F_{\text{Inertia}}$$

$$F_{\text{Inertia}} = M \times a$$

$$F_{\text{Total}} = F_{\text{Net}} \cos(\phi)$$

$$T = I \times \alpha = F_{\text{Total}} \times d$$

Figure 14: Kinematic equations

There are also some disadvantages of the slider-crank system though. The piston head and the connecting rod must be at a perfect positioning in order for there to be enough clearance for the connecting rod to move up and down as it is turned by the flywheel. This can be overcome as long as the physical calculations seen above are done correctly. The calculations take into account that enough space is needed so that the connecting rod does not come into contact with the wall of the piston head, thereby causing a hesitation or pause in the fluid movement of the system (Corbo et al. 1999).

A second problem is that since the slider-crank is in constant motion, the flow wave it would produce would be just a normal sine wave. Unfortunately this result would not tell the research group anything as the human body does not produce a normal sine wave. To overcome this problem, the slider-crank system must be controlled through the motor. To control the motor, a motion controlling device must be included in the system in order to direct the motor to produce the right type of wave needed. By including this motion controlling device, the now modified slider-crank system offers even more potential as a full-time multi-use pulsatile flow generator. Basically, with this controlling device, any type of wave can be created by the motor/system by just altering the settings.

2.6.4. Comparison of Flow Systems

In order for the group to come to a reasonable decision about which type of pulsatile flow generator to use. The group felt it was important to look at both the cam-follower system and the slider-crank system and compare/contrast the two systems to see which would best fit the type of testing the group would be performing.

Both the cam-follower and the slider-crank have their advantages which were stated previously. The cam-follower is a simple system where the contour of the cam controls the wave profile which is produced by the entire system. The important aspect when creating the cam is to take into account the trough which serves as the slight pause between the pulses. The height and length of the concave will determine how long that pause is and also determine how much of a curvature the cam has on its side. This means that the length and height of that concave determines the amount of force the cam places on piston which would force the blood substitute through the system. The physical specifications of the cam can be created using various software such as DynaCam.

The slider-crank also has its advantages as stated previously. The difference with the slider-crank is that the control of the flow is not in the cam but with the motor. The physical calculations of the slider-crank rely much more on kinematical analysis. The kinematical analysis performed by the group on the slider-crank design can be seen above. It is not as easy to have a slider-crank produce the wave profile desired but if controlled correctly it can produce a much more accurate wave profile for a longer period of time.

Both also have some drawbacks. The biggest drawback with the cam-follower is consistency and longevity. A cam-follower is a simpler setup but with possible friction between the roller and the cam and also vibration which may occur from the cyclical motion of the oval shaped cam can be detrimental to a wave profile. A slider-crank has problems as well. The ability to control the system and be able to produce the desired wave is not an easy task and basically calls on a group to use some kind of motor control in order to harness the ability of the slider-crank system and be able to produce the desired wave.

Considering both the negatives and positives of the cam-follower and slider-crank systems, the group has chosen to incorporate a slider-crank system for their pulsatile flow generator. The group feels that the slider-crank will provide the group with a much more accurate wave profile for a longer period of time than the cam-follower system. Also since the physics have been completed the group feels that by using a motion controlling device to control the motor, the group will be able to harness the abilities of the slider-crank system and be able to produce the desired wave in order to commence proper testing.

2.7. Motion Control

2.7.1. DC Motors

DC electric motors are comprised of a coil, which when powered generates a magnetic field around the armature. The left end of the armature is pushed towards the right away from the left

magnet resulting in a clockwise rotation. The armature continues to rotate in this manner until it reaches a horizontal alignment, at which the commutator reverses the current through the coil, thus reversing the magnetic field. As this process continues, circular motion is created.

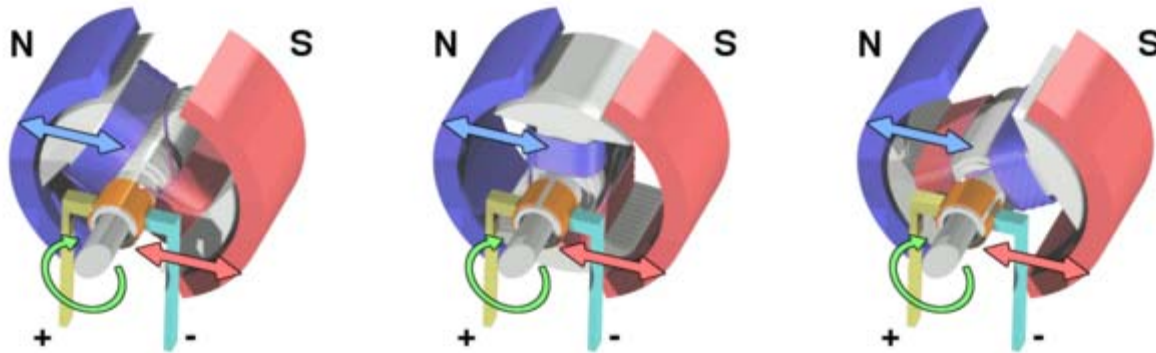


Figure 15: DC Motor Motion

The speed of the motor depends on the flow of current and voltage to the motor coils, as well as, the motor braking torque. The speed is directly proportional to the voltage and the torque to the current. Varying the current or voltage will vary the speed of the motor. Constant current makes the motor produce a constant rotational motion, while varying current changes the rotational velocity of the motion. DC motors feature the capability of adjusting the speed smoothly to zero following acceleration in the opposite direction, in addition to responding quickly to control signals, primarily resulting from the DC motors high torque to inertia ration.

2.7.1.1. DC Stepper Motor

DC Stepper Motors provide a number of advantages including but not limited to feedback signal compatibility and acceleration. Stepper motors can easily bring a load to acceleration. The DC stepper motor is comprised of one electromagnetic pole and a rotating arm with a constant north or south pole, with the outer poles charging from off to on and vice versa. These motors allow for continuous rotational motion but in steps. Stepper motors experience high torque at very low speeds, while at the same time being subject to decreasing torque at high speeds.

2.7.1.2. DC Brushless Motor

DC brushless motors, despite their exceptional qualities, are not comparable to its counterpart in the motion control arena. Brushless motors are comprised by a wound stator surrounding a permanent magnet rotor. The inverse of typical motors, especially given that its windings are commutated electronically rather than by the more common commutator and brushes like its counterpart. DC brushless motors offer benefits not only with price but also with energy, maintenance, as well as, the ability to operate at higher speeds than its counterpart. Its high efficiency and favorable attributes make it a common choice for motion control systems and applications.

2.7.2. Motion Controllers

2.7.2.1. ION Digital Drive

Differential Encoders allow for the detection of rotary positions by means of a code-wheel attached to a dual shaft motor. The differential encoder employed in the development of our pulsatile flow generator is a transmissive optical encoder with a 1000 Index channel. (Figure 1) The Encoder consists of a lensed LED source and a monolithic detector IC enclosed in a small polymer package. The encoder uses a phased array detector technology in order to provide digital quadrature differential outputs on all resolutions. The encoder attachment can be seen below.

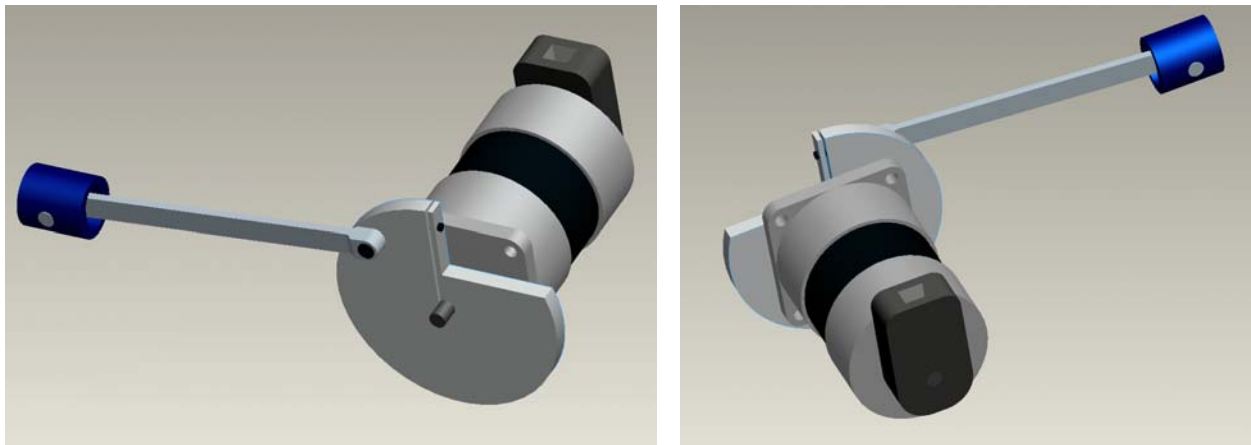


Figure 16: Pulsatile Flow Generator Motion Control System

The group utilized a motion control device which will allowed us to establish servo control of our motor in order to achieve a higher resolution, smoother motion, and a lower holding torque. These parameters were achievable through the connection of the motion control device to the Differential Encoder on our DC Brushless motor.

The Performance Motion Devices (PMD) ION Digital Drive is a complete single-axis motion controller with integrated power, as well as a network communications port, providing advanced motion control features in a compact and manageable form factor. With the addition of the ION Digital Drive, the group was able to take advantage of many of its features, such as encoder position feedback, position servo compensation, its brushless DC motor commutation, as well as, the ION's digital current/torque control.

One of the most important features of the ION Drive was the protection of its high power drive stage from overcurrent, undervoltage, overvoltage, over temperature and short circuit faults, affording us the safety of operating our DC brushless motor and the prevention of some adverse interaction resulting from a spike in the current or drop in the voltage from our power supply. The ION Drive acted as a last line of safety defense for all other components in our system with the aforementioned safety features, as well as, dedicated Enable input and Fault output safety interlocks.

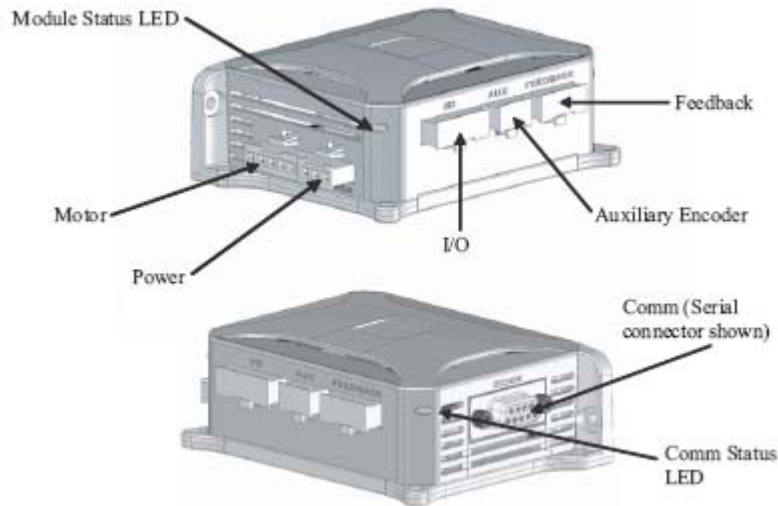


Figure 17: ION Digital Drive

The very heart and soul of the ION Digital Drive is the Magellan Motion Processor (Figure 2), which allowed the ION to deliver the following motion control functions to us even given the dated PC system we were working with:

- Serial host communications over RS232
- Trajectory generation, including trapezoidal and S-curve point-to-point profiling, velocity contouring, as well as, electronic gearing modes
- Advanced PID position loop with integration limit, derivative sample time, velocity and acceleration feedforward output bias, dual biquad filters, and support for dual encoder feedback if needed
- Two encoder input channels capable of up to 10 Mcounts per second
- Sinusoidal and six-step (Hall) brushless DC commutation modes
- Digital current loop with choice of standard A/B or Field Oriented Control (FOC) for our brushless DC motor
- Single phase current loop
- High-efficiency MOSFET power stages for our three-phase brushless DC motor.
- 15 A RMS peak current capability with I²t current foldback limiting
- Choice of 20 kHz or 40 kHz PWM frequencies to support a broad range of motor inductance.
- Single supply operation (An onboard DC/DC converter supplies all internal circuitry and also provides 5V for encoders and other external I/O components)
- Differential or single-ended encoder input buffers for all encoder channels
- Signal conditioning buffers and analog filters on all I/O signals

The basic premise is to utilize the motion control device to generate the flow waveform we are in need of.

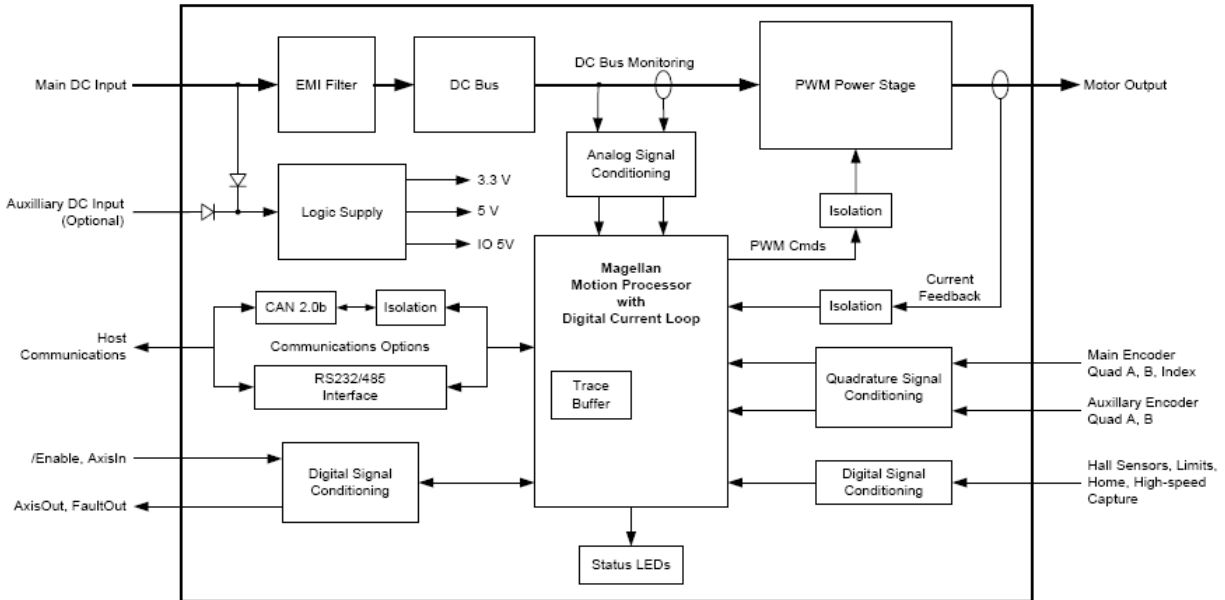


Figure 18: ION Digital Drive Schematic

2.7.3. Servo Loop Tuning

Servo Loop Tuning is basically the process of adjusting servo system parameters in order to achieve an output signal that closely resembles the input signal. This becomes extremely important when trying to output a specific pulsatile pressure waveform given that both the motor and piston slider crank assembly introduce inertia into the system, which forces the servo amplifier to accelerate and decelerate to overcome while following the input signal as closely as possible. Thus, a balance between the need for a high response rate (high gains) and stable operation (low gains) must be achieved.

Servo motion control is represented by two classes. The first class involves command tracking, addressing how well the output signal (actual motion) closely follows the input signal (commanded motion). The most commonly used commands in typical rotary motion are the position, velocity, torque and acceleration commands. The Feedforward control is the part of the controller that deals with these commands, acting as the internal commands working to make sure that the input commands are followed without error.

The second class exists to address the disturbance rejection characteristic of the system, with disturbances resulting from torque disturbances on the Brushless DC motor shaft, as well as, incorrectly estimated motor parameters utilized in the feedforward control. In order to rectify and prevent these issues a Proportional Integral and Derivative (P.I.D.) position loop control is utilized. The disturbance rejection control in contrast to the feedforward control, which estimates the needed internal parameters for a “0” following error, reacts to any unknown disturbances and estimation errors and attempts to rectify or prevent them. A complete servo system is one in which both of these controls are combined providing a substantial level of high performance.

2.7.4. Proportional Integral Differential Controller (PID)

The Proportional Integral Differential Controller is an alternative to the typical on-off control method of motors and motion. PID involves the establishment of a set point and measurement in order to determine the “error” as detailed below:

$$\{\text{error} = (\text{set point}) - (\text{measurement})\}$$

The Set point is the commanded value and the measurement is what the actual value is. The error would then be the difference between the set point and actual value.

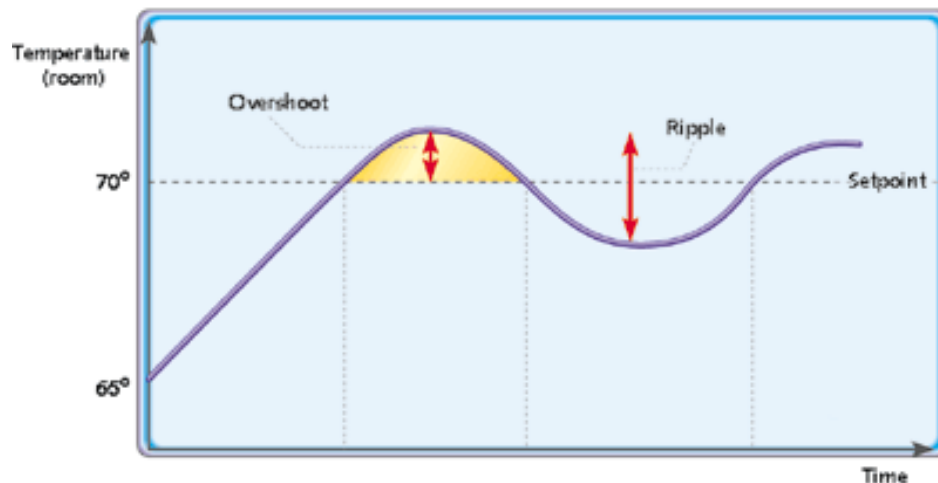


Figure 19: PID Analysis

As aforementioned, a typically servo controller consists of a trajectory and P.I.D. controller, with the trajectory controller generating position set points and the P.I.D. controller functioning on the position error calculated and generating a torque command to the DC Brushless motor. The P.I.D. controller consists of 3 gains that are adjusted and which act on the position error, K_p , K_i , and K_d .

PID Control Loop Parameters

Proportional Gain (K_p) - Proportional gain is the system stiffness. It determines the contribution of restoring force directly proportional to the position error. Restoring force is comparable to a spring in a mechanical system. A high proportional gain gives a stiff responsive system but can cause instability from overshooting and oscillation.

Derivative Gain (K_d) - Derivative gain is the damping effects on the system. It determines the contribution of restoring force proportional to the rate of change (derivative) of position error. This force is much like viscous damping in a damped spring and mass mechanical system—a shock absorber, for example. Increasing derivative gain reduces oscillation at the commanded position, or it rings because of high acceleration.

Integral Gain (Ki) - Integral gain is the static torque load on the system. It determines the contribution of restoring force that increases with time, ensuring that the static position error in the servo loop is forced to 0. This restoring force works against constant torque loads to help achieve zero position error when an axis is stopped. Integral gain improves positional accuracy. High static torque loads need integral gains to minimize position error when stopped. (Understanding Servo Tune – Tutorial - National Instruments)

Derivative and/or integral terms are added to proportional controllers to improve qualitative properties of a particular response. The PID motor voltage control schematic is detailed in the figure below.

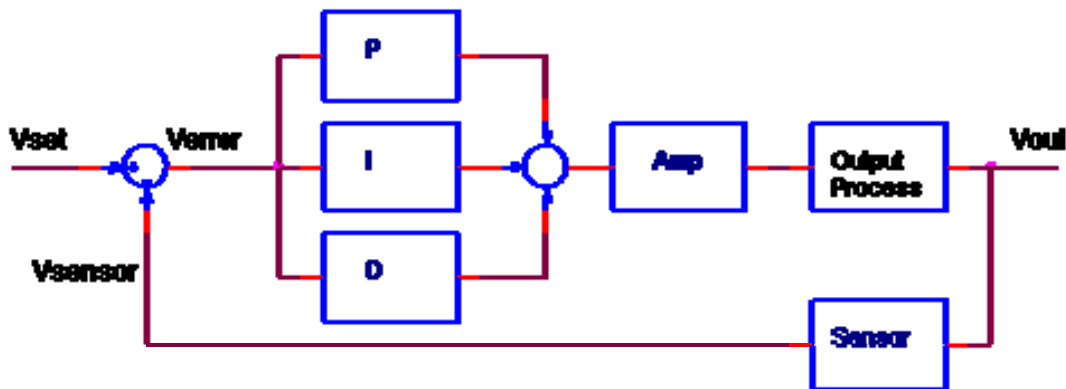


Figure 20: PID Voltage Control Schematic

2.8. Pressure Measurement

One's ability to measure the systolic and diastolic blood pressure accurately, as well as, the other parameters closely related to the blood pressure such as the heart rate and blood flow parameters is of great significance when conducting arterial studies.

2.8.1. Indirect Blood Pressure Measurement

The most common non-invasive (indirect) blood pressure methodology utilizes a cuff technique. This methodology consists of the placement of a cuff proximally on the subject to occlude flow. The cuff pressure is measured by determining the cuff pressure where corresponding changes in blood flow are observed during the occlusion and release of the cuff from the subject. The blood pressure sensor located distal to the cuff on the subject will measure the blood pressure being observed. There typically three blood pressure measurement techniques utilized, the volume pressure recording, photoplethysmography and piezoplethysmography. In addition to these techniques, an increasing number of sensors such as but not limited to photoelectric sensors, Doppler sensors and acoustic sensors. Regardless of the sensor being utilized or the technique being employed, one variable remains constant in indirect measurement and that is the requirements of the cuff.

The non-invasive methodology has 4 primary advantages in blood flow studies. Firstly, being non-invasive, they do not require any surgery. Secondly, they can be utilized to obtain

measurements in conscious subjects in blood pressure and flow studies no matter the duration. Thirdly, they are far less expensive than their counterparts. Fourthly, they can be used on a wide array of subjects in order to provide an outlook on hypertensive cues. (Pfeffer et al, 1971)

However, with advantages comes disadvantages, especially with the indirect method of blood pressure measurement. This form of blood pressure measurement suffers from three major drawbacks. The first drawback is the methods ability to only be capable of capturing blood pressure measurements within a restricted time frame or in other words a small number of cardiac cycles, which ultimately results in its lack of truly depicting a subjects average blood pressure. The second drawback is the fact that this technique also introduces significant stresses into the cardio system affecting the blood pressure and resulting in distorted readings of blood pressure and heart rate. Lastly, the accuracy of this methodology has given rise to scrutiny, especially due to the results of comparison from its direct measurement counterpart shows inconsistencies. (Hartford et al, 1996)

2.8.2. Direct Blood Pressure Measurement

The most common invasive (direct) blood pressure methodology utilizes a catheter based technique. Blood pressure is measured by means of invasively situated fluid-filled catheters connected to external transducer which relays the signals to an amplifier and recording device, which in many cases is a software application. This technique is not only subject to widespread use, it is also one of the oldest techniques still utilized. The versatility of this system allows for effective utilization in studies for a prolonged length of time.

This technique offers many advantages over indirect measurement techniques in that it is more accurate and reliable and allows for the assessment of blood pressure variations. In addition, it currently the most accurate technique for measuring the Mean Arterial Pressure (MAP) directly. Adding to its advantages is the fact that the technique is relatively inexpensive, with catheters and transducer running quite low in price. Lastly, the technique allows for novel flow and vasculature studies by researches due to the availability of the arterial vasculature to researchers utilizing the technique.

There are however disadvantages to using this system, which can easily be overcome with solid and thoughtfully designed methodologies. Such disadvantages include the damping of blood pressure signals due to growth on and or clotting of the tip of the catheter. This is a growing concern in catheters utilized in this technique that are larger than PE10, which can also cause under damping and pressure signal distortions. (Mattson, 1998)

2.9. Wave Analysis

2.9.1. Fourier Transform

Fourier transform is an analysis of which relates two hemodynamic variables, in our situation pressure and flow. If pressure and flow were to be analyzed by just division the information would be meaningless because there would be infinite values when looking at diastolic pressure. Therefore what Fourier transform does is convert pressure and flow into a series sine waves. A

harmonic, also called the sine wave, has an amplitude and phase angle; each sine wave in the series has one. The harmonics are linked to the heart rate, the frequency of the heart is equal to the first harmonic, twice the heart rate is the second harmonic, and so forth. As the harmonics are increased the amplitude decreases but the converted information includes more of the actual detail of the pressure wave.

The analysis of Fourier provides information on the time and linear invariant system through the calculation of amplitude ration and the difference of the phase angle per harmonic. The limitation in using Fourier transformation analysis is that the beginning and ending waves should be the same and so should all the waves that are analyzed. Another limitation is for higher harmonics there is more noise in comparison to lower harmonics. Also in order to do a steady state oscillation calculation relationship the two signals must be linear. Lastly the analysis for Fourier is only done in multiples of the heart rate, giving a limitation to the frequency resolution.

2.9.2. Fast Fourier Transform

Fast Fourier Transform provides the same analysis as normal Fourier Transform but in a sped up version. The FFT works through an algorithm created by Cooley and Tukey in 1965 which is a faster way of analyzing complex series by raising the number of points in a series by the power of 2 (Bourke, 1993).

2.9.3. Short Fourier Tranforms

The regular Fourier transform is unable to analyze time from point to point on the graph; however the way of overcoming this is by simultaneously comparing the localized time and frequency domains together which is referred to as Short Time Fourier Transform. By using this tool, there can be a more specific analysis of each point found on a wave (National Instruments, 2007).

3. Project Approach

3.1. Objectives

The objective of this project was to design a pulsatile flow generator for the analysis of wave propagation in blood vessels for implementation in the early detection of arterial disease. This intention required the development of a system which would replicate a pulse wave (pulsatile flow) within a physiological fluid at a rate of 60 bpm or 1Hz while at the same time offering the ability to change the waveform morphology to correspond to different locations of the arterial tree. In order to guarantee that our project satisfied our object it was necessary to develop a validation methodology which would allow us to compare results gained from system to those found in literature. This would need to be accomplished by developing physiological arterial models and examining the harmonics produced from each model ranging from healthy to stenosed regions.

3.2. Aims

The specific aims of our project are as follows:

- To develop a pulsatile flow generator that develops arterial pressure waves
- To replicate arterial pressure waves within a physiological pressure range (60mmHg-120mmHg)
- To generate a pulsatile flow resulting from a frequency of 1Hz or 60 bpm
- To accurately emulate multiple pressure waveforms corresponding to various locations on the arterial tree
- To create and utilize a physiological fluid with a viscosity close to 4.0 cP
- To fabricate and test physiologically viscoelastic arterial models
- To develop arterial models ranging in increasing thickness and stenosis
- To analyze the pressure waveforms produced by the pulsatile flow generator system and our samples
- To examine the FFT produced from each waveform and quantitatively compare our results to those found in literature

3.3. Assumptions

The most critical assumption that was made in our design of the pulsatile flow generator was the scale-up of the latex arterial models that we planned to utilize in the physiological validation of our system. The models were scaled-up up from a lumen size of 6mm to a lumen size of 1 inch. This was primarily due to the inability of our group to procure synthetic materials with an initial lumen size of 6mm in varying degrees of stiffness and diameter.

Scaling of the models in size also required us to scale the system up, especially with respect to the fixation system in order to accommodate the models. Although the system and models were scaled we felt the data we recorded during experimentation was still accurate and significant due to our insistence that our model operate within a physiological realm and that our models represent as closely as possible physiological human arteries. Establishing that our models did

indeed represent human arteries with respect to its viscoelasticity and morphology we concluded that our results should still be able to accurately validate our system. Of course given access to greater resources and time, the models should be scaled back down in order to be used with animal arteries, etc.

Assumptions were also made with respect to the blood substitute the group utilized, as well as, the arterial models we created. Blood is a viscoelastic fluid that is composed of cellular and fluid components with the cells providing the elastic component of viscoelasticity and the fluid providing the viscosity component. The blood substitute that the group used in the validation testing accurately mimicked the viscosity of whole human blood, but did not necessarily mimic the cellular components of blood. Given this issue, we had to assume that although blood rheology has a direct correlation with the development and progression of atherosclerotic plaque, that the effects of the blood rheology would not have a significant impact of the validation testing we were aiming to do on our system. Since we were testing multiple pre-developed models with varying thickness and stenosis to model the progression of atherosclerotic plaque, we felt the makeup of our blood substitute could be considered negligible as long as it maintained the same viscosity as whole blood.

The models also exhibited the same issues with its mechanical properties and composition. As arteries are simply consist of many components including but not limited to elastic, connective tissue, and smooth muscle and our models did not, we had to make an assumption as to the significance of the makeup of our arteries to its mechanical properties. As our models exhibited comparable mechanical properties to arteries in vivo such as their compliance and pulse wave velocity, we felt that we could assume its uniform makeup of just latex as negligible given our objectives with the project.

4. Design Approach

4.1. Design Iteration 1

The first complete pulsatile flow generator designed by the group can be seen in the CAD view below in Figure 10 with a CAD view of the base itself in Figure 11. The system called for the tubing to be mounted to a back wall. This was done in the hoped of reducing any possible vibrations that may occur in the plastic tubing, causing data to be flawed. The only parts of the design not shown in the schematic below are the motor and motion control device which are found behind the flywheel at point A.

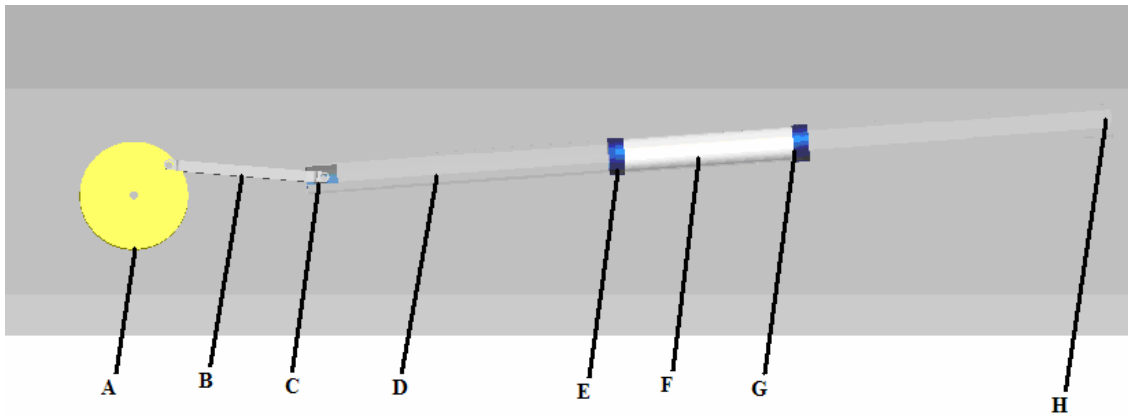


Figure 21: Design Iteration One

A	Flywheel
B	Connecting Rod
C	Piston Head
D	PTFE Hard tubing
E	Clamp and position of 1 st transducer
F	Sample tubing
G	Clamp and position of 2 nd transducer
H	End of tube and position of valve

Table 8: Design Iteration One

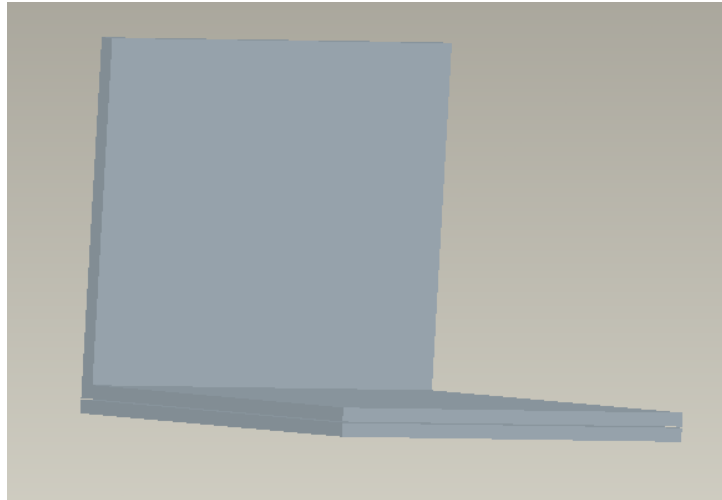


Figure 22: Base for Flow Generator

4.1.1. Slider Crank System

The first iteration of the slider-crank system called for the use of a DC Brushless motor with a peak torque of 25oz-in and a peak current of 3.5A (Anaheim Automation). After some kinematic and force calculations were performed to try to calculate the amount of force needed to push the piston against the 80mmHg of pressure within the tubular system, the group chose to use this motor because it was thought to supply enough power to push the piston.

To control the motor itself in order to produce the desired physiological pressure wave, the group decided upon using the Labview software program. The group felt that by using Labview the group would be able to easily control the motor output.

4.1.2. Pressure and Flow System

The test bed for design iteration one, or the pressure and flow section of the system consisted mostly of opaque PVC tubing. PVC tubing is a commonly used type of plastic tubing which is very strong and will not be effected by the amount of pressure the group was to build up within the system. Also since PVC is a commonly used tubing, the group felt it would have more of an array of sealants to choose from if the use of it became necessary.

The PVC would be connected to the sample using a common plumping fitting. At one end of each fitting the PVC would be locked into place and on the other end, the group's sample would be attached. This aspect of the system can be seen at points D, E, F, and G in Figure 1 above.

The introduction of the blood substitute into the system would be done using a reservoir placed above the entire system. Using a modified painting bucket, the group would rely on gravity to bring the substitute into the system. The bucket used had a five gallon capacity which the group thought would be sufficient for the purposes of the study.

Since the entire system itself would need to be pressurized in order for there to be a proper simulation of human blood pressure, check valves were needed both at the entry point of the fluid and the exit point. These check valves would allow the group to build up the proper amount of pressure within the system. The group chose to place simple two-way ball valves at the entry point of the fluid from the reservoir and the exit point prior to the fluid entering the recirculation reservoir. With system calibration, the group would open and close these two valves to a certain point and build up the pressure within the system. The exit valve, which was found to have to most control over the amount of pressure in the system can be seen in Figure 1 above at point H.

4.1.3. Recirculation

In order to avoid having to manually refill the reservoir every time a test were to be run, the group felt it necessary to devise a recirculation system. This recirculation system would not only allow for more efficient testing, but would also allow the group to keep a constant flow in the system, thereby avoiding any sudden pressure decreases which could flaw the data acquired.

To recirculate the blood substitute, the group chose to fill the introductory reservoir by using a simple drill pump. The drill pump is a small handheld pump which would be attached to any type of power drill. Tubing from one side of the drill pump would be attached to the introductory reservoir and tubing from the other side would be attached to the end of the pulsatile flow system. Although the drill would need to be working at high speeds, the drill pump did provide sufficient head to raise the blood substitute back into the overhead reservoir.

4.1.4. Arterial Stiffness Models

After doing extensive research on what types of materials would be best suited to be used as arterial models the group felt that the two choices had to be either PTFE tubing or ePTFE or expanded PTFE tubing. As seen previously, PTFE and ePTFE have shown some of the best promise for being able to mimic the mechanical properties of arteries. Between these two choices though, based purely on the newest research available, an ePTFE based sample was chosen as the group's initial sample.

4.1.5. Arterial Stenotic Models

To create stenotic arterial models, the group devised a system where small inserts would be created using a commonly used plumbing caulking. Each plastic insert would be cut open using an incision right down the middle of the plastic tubing. Once unrolled, layers of plumbing caulking would be applied to the inner lining at the appropriate measured thickness. This insert would then be pressed into place within the segments of PTFE tubing. The thickness of the caulking layer will be incremented by ~10% per insert until 80% occlusion is reached. The preparation of the model is detailed in the Figure 12 below.

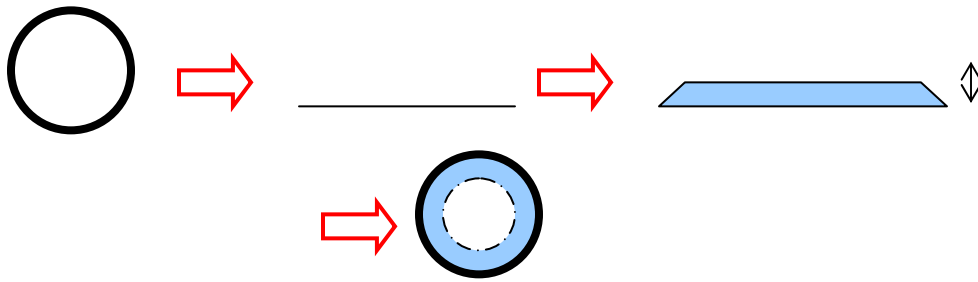


Figure 23: Occlusion Insert Development

4.2. Final Design

As development and manufacturing of our initial design progressed, the group was able to conduct preliminary viability testing of the design as a whole, as well as, the components that comprise the pulsatile flow generator design. It was apparent upon concluding our initial viability testing that many of the components and concepts we had initially developed would need to be further refined in order to accurately represent our project aims and objectives. The particular components of our system that were further refined were the motor that comprised the motion control system, the mounting and structural aspect of our design, tubing, arterial models, and lastly the recirculation system.

Initially, we planned to use a wall mounted structural design. With stability remaining a concern and aim to strive towards, we found that in the long term our wall mounted design would not prove to stand the test of time. In addition, we found that running the system resulting in movement and stability issues as a result of the vibrational effects from the motion control system. In order to overcome our stability issues as well as to guarantee and increase the shelf life of the design, we transitioned from the wall mounted design to a platform mounted design. This design allowed us to mount our system to raised aluminum platforms offering greater stability, as well as, eliminating any vibrational effects and movement due to the motion control system. Lastly, this redesign also afforded to us the capability of adding a retractable base system to our mounting design, comprising of one fixed end holding the motion control system and right end specimen fixation grip and the retractable end that holds the left end specimen fixation grip as well as the start of the recirculation system. This system allows for the testing of samples ranging in size from 4 inches to 24 inches.

In addition to redefining the structural aspect of the design, we also transitioned from the non-transparent PVC tubing to clear Lexan tubing, offering us greater visibility of our system flow. The clear tube allowed us to self regulate the flow of the system given the ability to view how the flow entered and exited the system and if there were any issues at which location in the system did they reside.

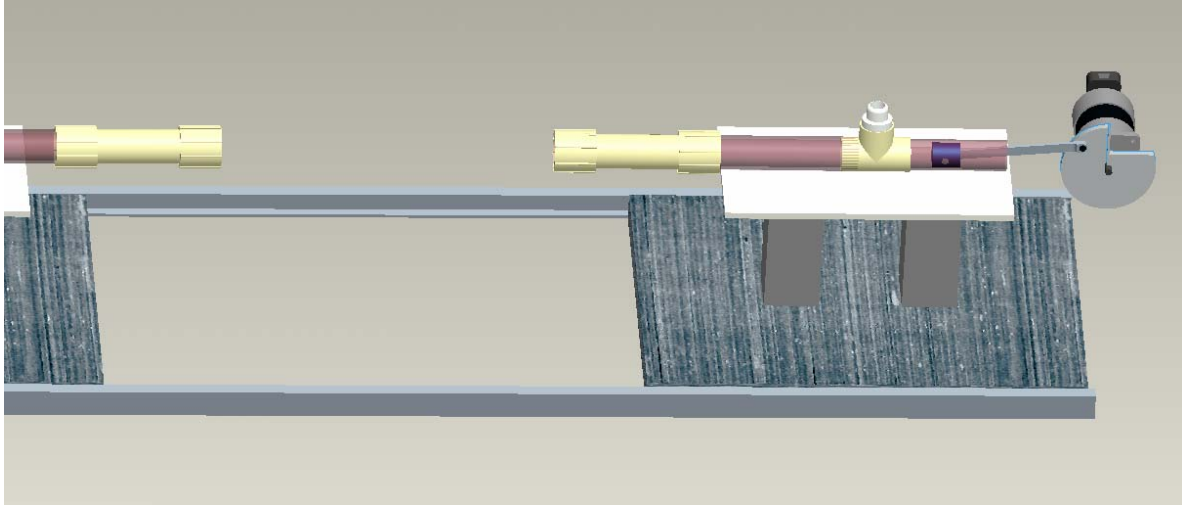


Figure 24: Pulsatile Flow Generator CAD Angle View

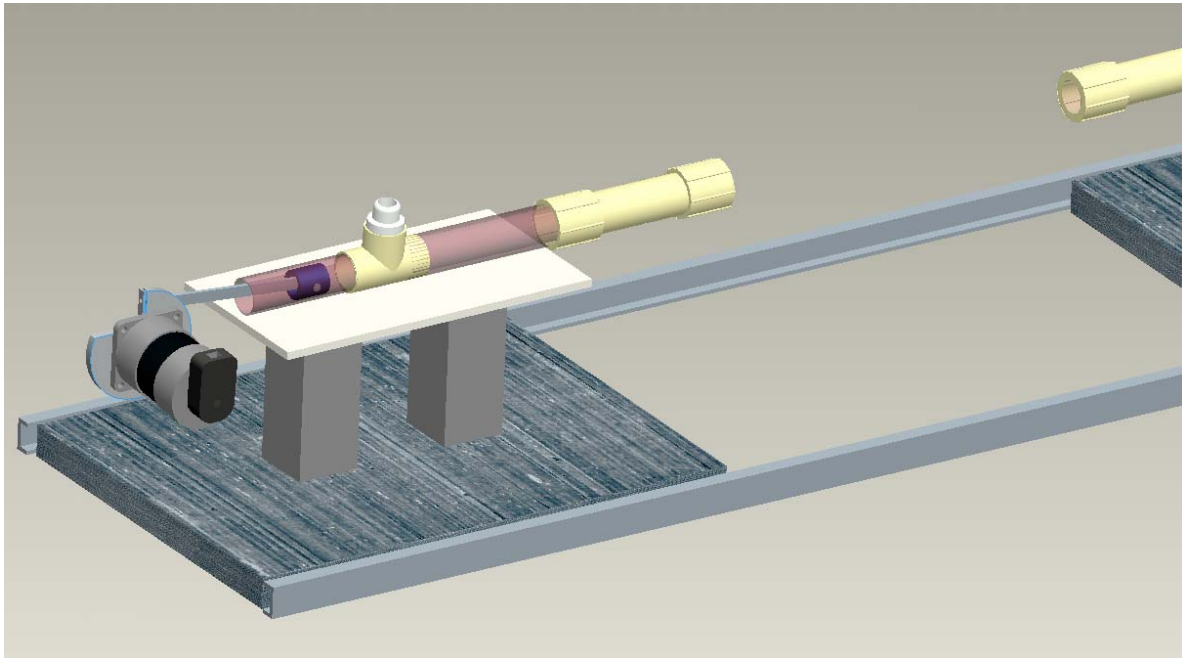


Figure 25: Pulsatile Flow Generator CAD Front View

Due to the inability of the group to procure ePTFE and PTFE samples in the varying thicknesses and inner diameters that we required from Materials Companies such as GORE and Zeus, we were forced to research our other alternatives in more detail. The group went back to some of its original ideas such as the use of liquid latex. After further research into the mechanical properties of latex, the group felt that the properties provided by the latex would suffice in meeting the physiological requirements set forth by the group. Therefore, the group decided that the development of our own latex arterial models would not only be more cost-effective given our limited budget but also would give us greater control and customization with the varying arterial thicknesses. In addition it would allow us to create novel stenotic models that would be more

uniform is composition and more physiological in morphology with respect to our initial plans of using inserts.

The initial recirculation system which comprised of a drill pump system proved to be rather lacking in safety, as well as, stability and was incapable of meeting the total head requirement of 10ft which was need to transport the blood substitute from the 1st resevoir to the 2nd resvoir in the recirculation system. This allowed us to redefine and redesign our recirculation system to a more self regulating system and much easily controlled system. With the addition of a submersible pump that met our total head requirement of 10ft, we were able to situate the pump within our 1st resevoir and have it pump our blood subsitute directly up to the 2nd resevoir offering a more closed and controlled system versus the benchtop mounted drill pump. The final design of our system can be seen in the figure below.

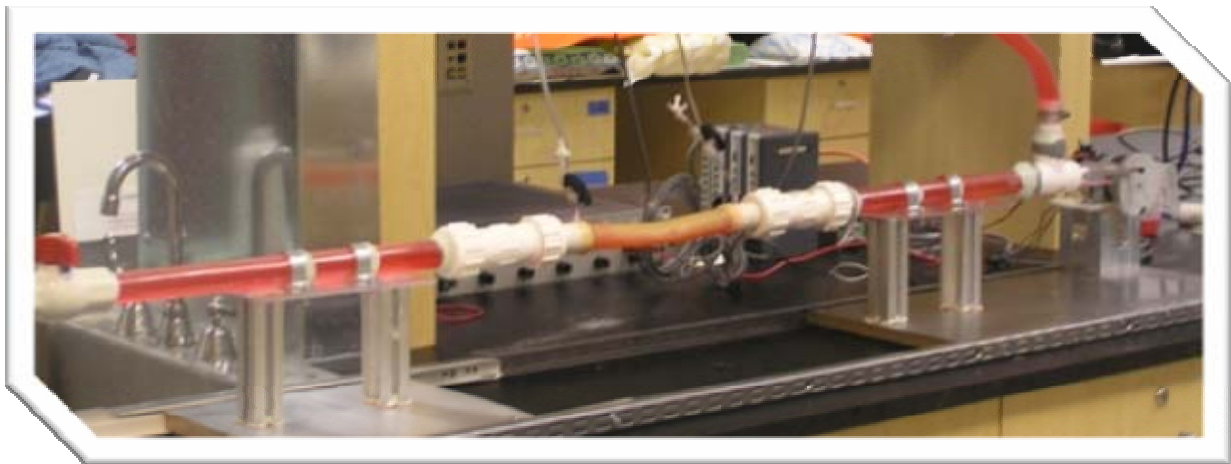


Figure 26: Pulsatile Flow Generator Front View

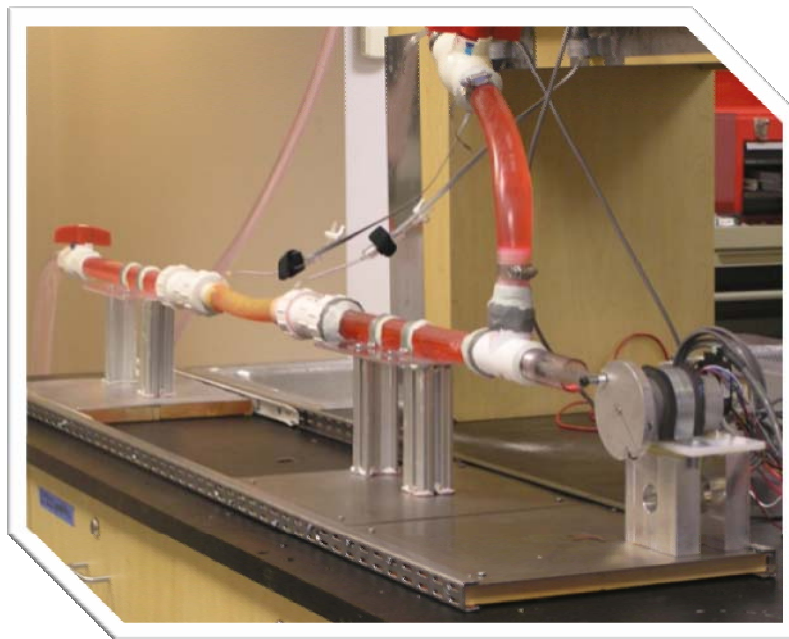


Figure 27: Pulsatile Flow Generator Angle View

4.2.1. Motion Controlled Cardiovascular System

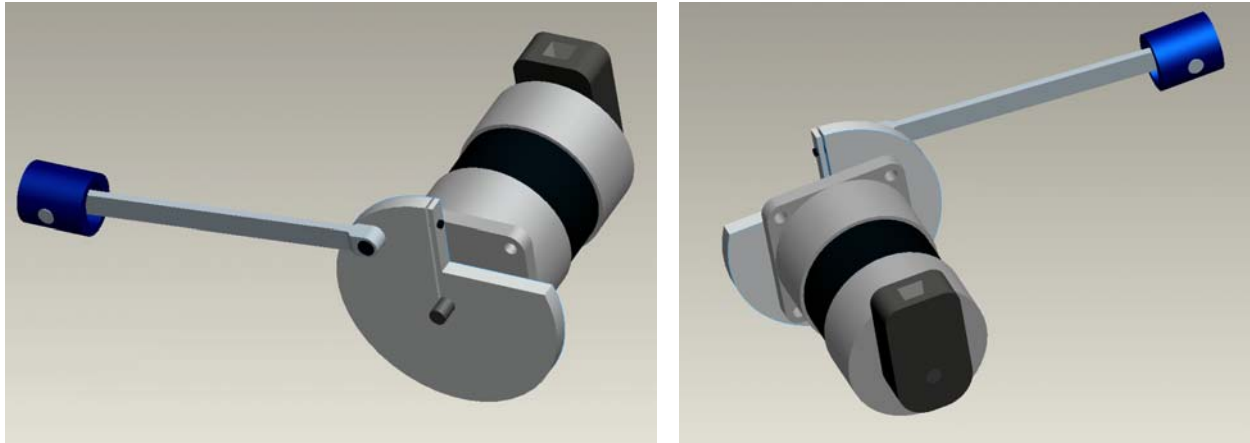


Figure 28: Pulsatile Flow Generator Motion Control System

The governing principle of our design as a whole was the concept of “as physiological as possible”, in that we wanted to guarantee that throughout the entire development process, our system stayed true to the physiological cardiac cycle and blood flow in the human body. We had to validate that our system indeed replicated the basic components of the cardiac cycle, comprised of Early Diastole, Late Diastole, Atrial Diastole, Ventricular Systole. Blood enters the heart through the ventricles during atrial systole and as pressure increases, the blood is forced out of the chambers through the valves and into the circulatory system. Just as the cardiac cycle functions with the inlet and outlet of blood, our system operates in the same manner.

As the motion control system is initiated at the required frequency of 1Hz or 60bpm, the piston moves backwards causing more fluid to enter the fluid chamber from the constant flowing reservoir above. When the piston reaches its desired position it enters the system moving forward at a higher velocity almost at a factor of 10 forcing the fluid into the pulsatile flow system. This fluid motion also acts as an artificial valve as it prevents momentarily the flow of fluid from the reservoir above.

The group has assumed the partial flow of fluid back from the system into the chamber following the system and the fluid flow up into the inlet from the reservoir as the fluid is forced back into the system are negligible. In particular, losses to these two actions are negligible given the minor fluid losses we experience and the fact that it does not disrupt the flow or pressure readings as this increased in velocity volume of fluid flows through the system. The cardiac cycle representation and accurate replication by our piston pulsatile flow generator can be seen detailed in the figure below.

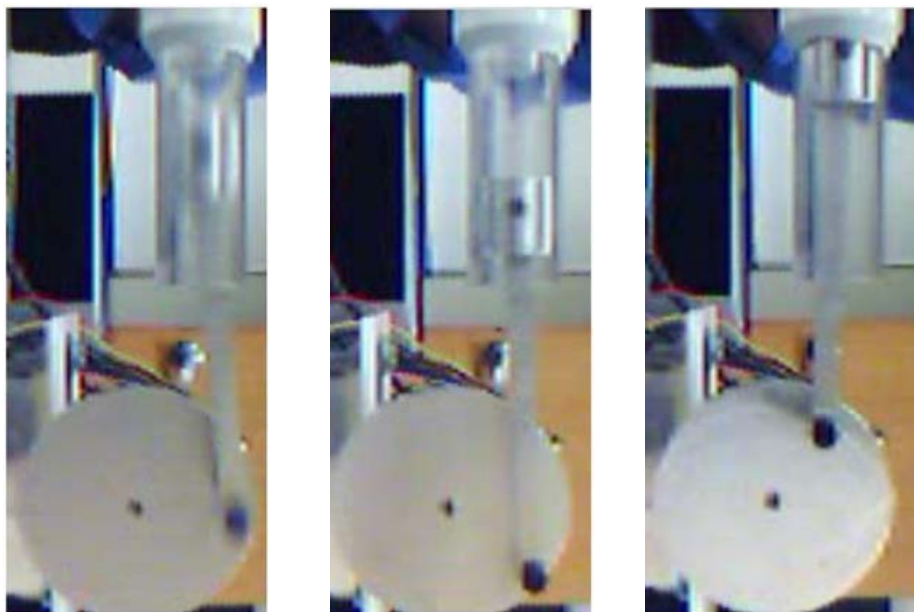
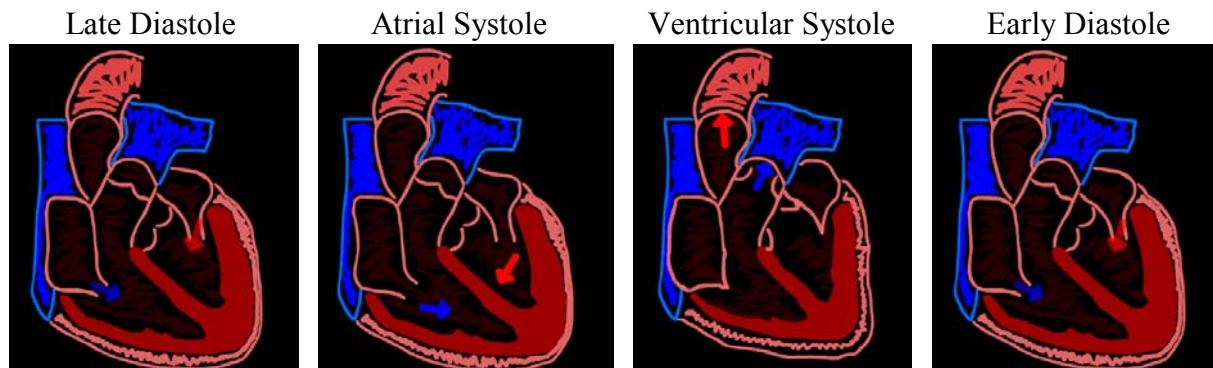
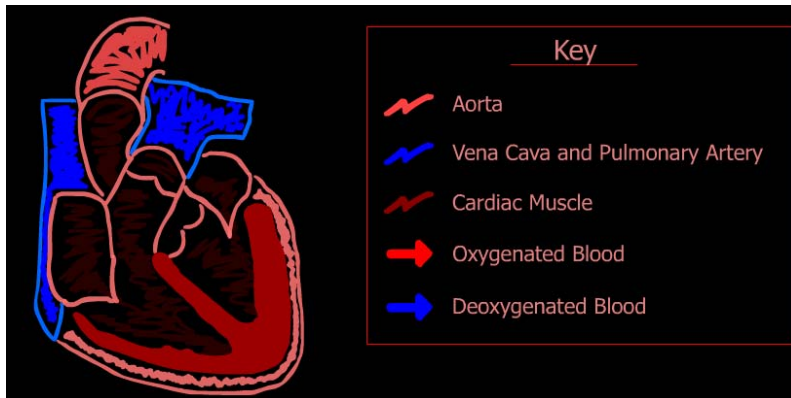


Figure 29: Cardiac Cycle Replication

4.2.2. Arterial Stiffness Models

Latex models with varying wall thicknesses were needed to analyze how changes in stiffness affected the properties of the pulsatile wave. To develop these samples, polyvinyl chloride (PVC) tubes of roughly 15 inches in length and 1 inch inner diameter were loosely attached on

both corners using a clamp. The clamps were then attached to ring stands to hold the PVC horizontally. A permanent marker (Sharpie, twin tip) was then used to mark a corner of the PVC to indicate the starting point.

To create the compliance models, a soft paint brush (12 Royal softgrip S64590) was first dipped in warm water to make the bristles softer. The paint brush was then thoroughly dried using paper towels, and dipped into the liquid latex (Mold Builder by Castin Craft). Using long strokes from one end of the PVC to the other, latex was then evenly brushed over the face. Bands of latex were brushed over to minimize streaking as much as possible. The PVC was then slowly rotated within the slightly loose clamp to expose a new unpainted face of the PVC. The above steps were repeated, where latex was applied, and evenly brushed from one end of the PVC to the other using long strokes. While painting the second face, extra attention was given to the interface of first and second face. The latex was applied closer to the first face, and the two faces were completely blended in order to minimize an uneven interface. These steps were repeated until the first and last faces were properly blended.

Once the application was completed and streaks were minimized, one side of the sample was blow dried using a blow dryer (Vidal Sassoon) until the latex was partially dried. The PVC was then rotated again around its axis to expose a new face. This process continues until all faces of the tube were evenly heated to eliminate any deformations that may occur due to uneven drying.

To determine if the latex was sufficiently dried for the next layer to be painted, one edge of the latex was touched with bare fingers. If the latex felt in any way liquid, drying was continued. A visual means to determine if the latex was wet was by observing the painted layer. If the painted area was still white, it was likely to still be wet. A good indication of sufficiently dried latex is when the latex turns slightly yellow. However, precautions were taken to prevent the latex from completely drying (yellow). This was done in order to ensure that the next layer would evenly bond with the previous layer.

Streaks, though minimized, were common in some of the thicker samples. These samples required a longer time to sufficiently dry, therefore controlling the streakage became more and more difficult as each layer was added.

Each layer was painted with maximum consistency, (that is, amount of latex used) to produce roughly incremental increase in wall thickness of the sample with increasing number of layers. Once the predetermined number of layers is for each sample had been applied (4, 6, 8, 10, and 12 layers), the sample was allowed to dry at room temperature for a period of at least 24 hours.

To remove the sample from the PVC, baby powder (Johnson's) was applied to the outside of the sample to minimize friction. Both the edges of the sample were trimmed to remove the inconsistent areas using a knife or a sharp blade. One side of the trimmed latex was turned inside out, and the sample smoothly slid backwards over the powder. The sample was then turned inside out, and trimmed down a length of roughly 9 inches.

To be able to use these models within the pulsatile flow generator, the edges of each sample had to be mounted on a small PVC pieces. The edges of each sample were slid over the 1-inch inner

diameter PVC tubes and were securely bonded using either a putty (QuickPlastik by Polymeric Systems Inc) or glue (Stik'n Seal by Loctite), and allowed to dry for a period of 12-24 hours. Once dried, roughly 1 mm holes were drilled as close to the latex-PVC interface as possible. 1-mm inner diameter tubing was then inserted through the hole roughly ½ inch deep. The 1mm inner diameter tube would later be attached to the pressure transducers. Common plumber caulking was then applied around the hole on the PVC-tube interface and allowed to dry for another 18-24 hours to prevent possible leakage.

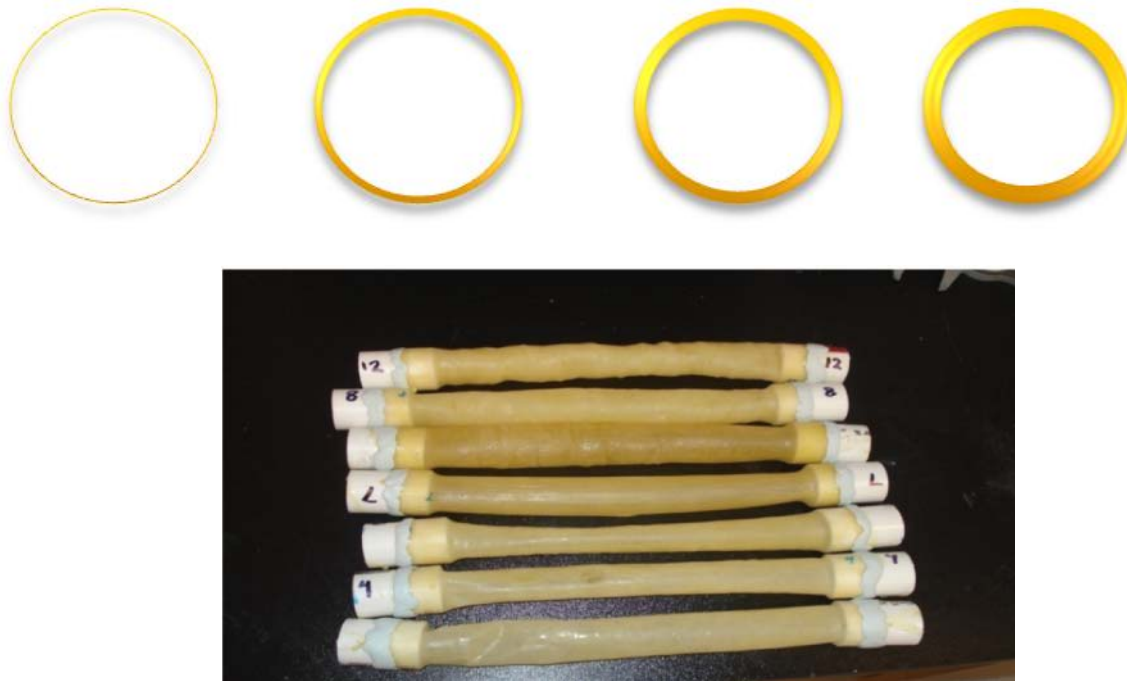


Figure 30: Arterial Compliance Models

4.2.3. Arterial Stenotic Models

To produce the occlusion models, custom designed metal rods were machined. These metal rods each had a point depression about halfway down the rod. It was believed that when painted over with latex and slid off, these samples would have a concave going down into the lumen of the sample, recreating a physiological occlusion.

To extend the metal rods to a sufficient length, two pieces of 2-in long, 1-in outer diameter PVC fittings were tightly secured to the short metal rod using vinyl electrical tape. Initially, the PVC-Occlusion combination was held horizontally using the clamp-ring stand method mentioned above, however, due to the weight of the metal and insufficient strength of the tape, the metal piece began to sag and deform the sample. Therefore, the sample was held vertically on a wooden board, and latex was applied around the base of the PVC. The latex was allowed to dry for a period of 24 hours to secure the sample to the wooden board. Once secured, the occlusion model was evenly painted using the method mentioned above.

Caulking was later inserted into the occlusion and the sample was again allowed to dry for a period of 24 hours. The sample was then bonded to 1-in inner diameter PVC tubing, and drilled using a drill press. 1-mm tube was inserted into the sample, and sealant was again applied to secure the tube to the PVC.

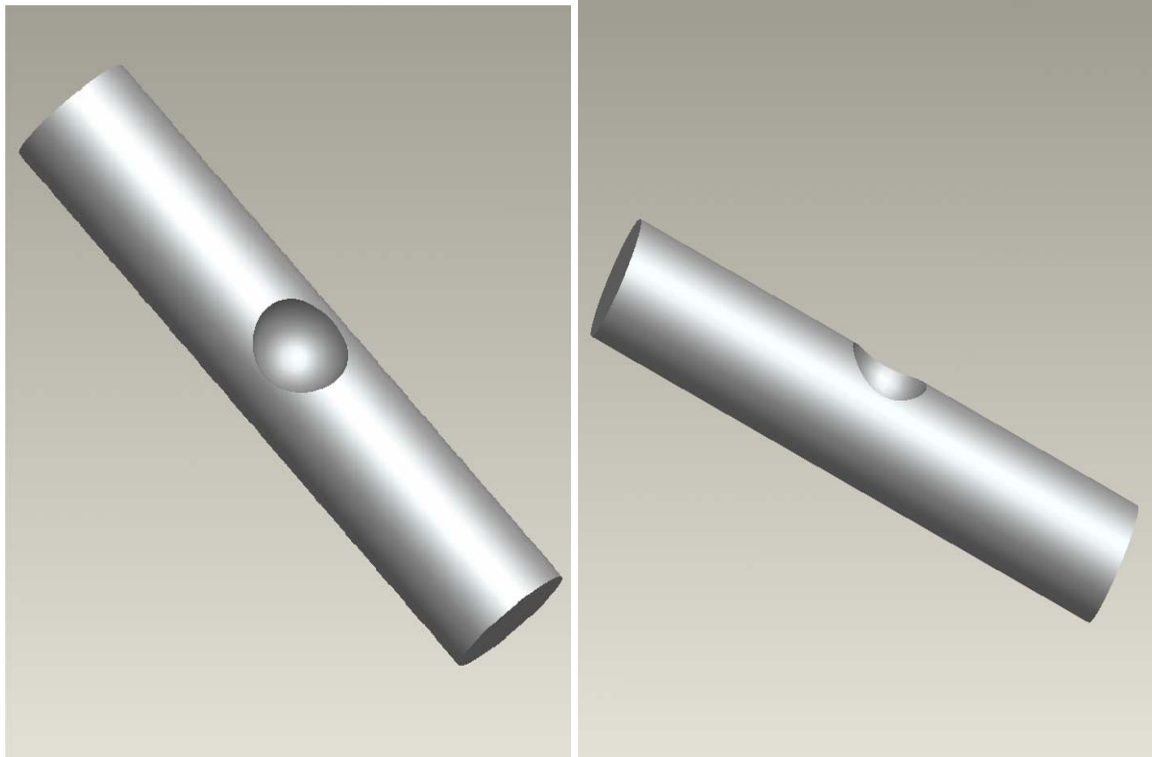


Figure 31: Arterial Stenosis CAD Models

4.3. Design Validation

In order to validate the second design iteration, the group created a few testing methods. Each testign method was used to validate a different part of the system from the entire system itself, down to the models being used for testing.

4.3.1. Arterial Models

For the group to validate that the new latex based arterial stiffness and stenosis models would provide the group with some physiological properties, the group designed and implemented a simple testing system in order to quantify or measure radial compliance and pulse wave velocity. By having an understand of the radial compliance and pulse wave velocity of each sample, the group would better understand exactly how physiologically similar each testing sample was.

4.3.1.1. Compliance Testing Systems

The group chose to research different types of compliance testing systems in order to analyze the radial compliance of each sample and verify their physiological properties. The group studied two specific systems, The 9100 Series Stent/Graft Testing system produced by Enduratech and

the Model SVP216 Vascular Graft and Tube testing system produced by Dynatek Delta. Both these systems provided a very high-tech and accurate way of measuring radial compliance. Also both used very precise measuring tools such as laser monitoring to accurately measure both the strain on the sample and change in pressure (Enduratech and Dyantek Delta, 2000).

Using these types of testing devices would be ideal, but with limited funds to actually hire a company to perform these tests for us and the unavailability of the device at WPI, the group felt that another option would to actually study the design of the devices and devise a way to simplify the device into its most important components.

4.3.1.2. Final System

Since the group did not have access to the best resources available for compliance testing, it felt there was a need to create a type of test, which could be easily made in the and for a low cost. After much research, it was seen that most compliance testing models each contained a way to increase the pressure in the sample and a way to measure what the pressure was using a manometer of some kind (Enduratech, 2000).

Using this simplification of most test systems the group constructed its compliance testing system as seen below in Figure 14. The pump and manometer found at each end of the model was taken from a disassembled sphygmomanometer or a common blood pressure cuff. By sealing the pump and manometer to their respective bases and attaching the samples in between the two bases, the group created a sound, airtight compliance testing model for the purposes of this study.

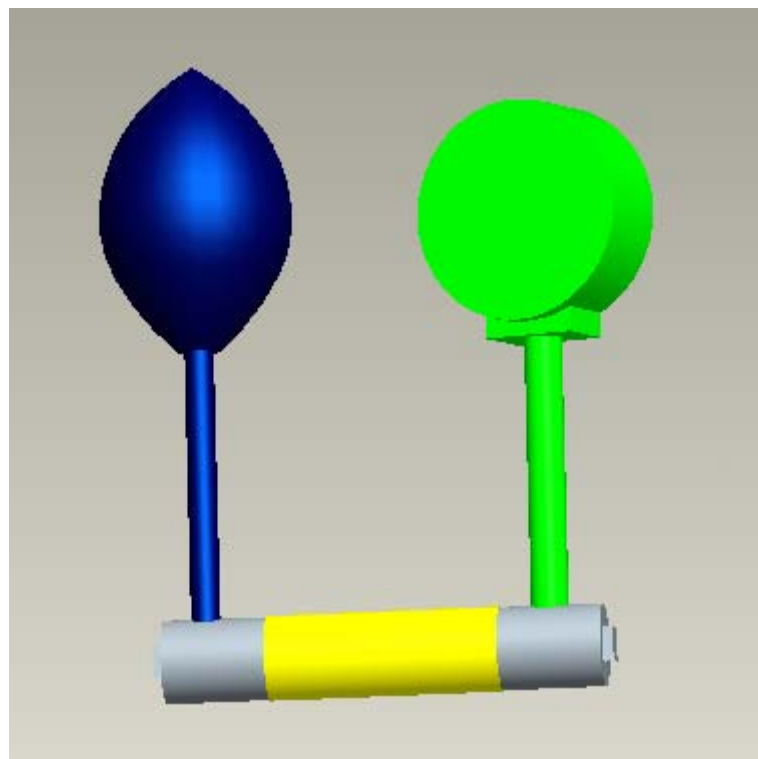


Figure 32: Compliance Testing System CAD Model

5. Methodology

5.1. Blood Substitute Preparation

As mentioned previously, viscoelasticity plays an important role in flow of blood in a physiological setting. That is, the viscous properties of blood due to the plasma and blood cells, respectively, are important towards the flow properties of the blood. It has also been shown that viscosity directly affects the flow pressures and velocity of the blood in the body, where increased viscosity results in increased pressures and lowered velocities. Therefore, to reduce pressure deviations due to incorrect fluid properties, the viscosity of our physiological fluid must closely mimic the viscosity of blood.

Through clinical research, viscosity of whole blood has been measured to be approximately 4 cP (4×10^{-2} poise) (Anand, 2007). Since glycerin is miscible with water and since glycerin has a very high viscosity (15 poise) diluted form of glycerin have most commonly been used as a standard to perform tests where viscosity must be taken into account (Elad, et. al., 2003). Previous studies have used a 40% glycerin and 60% water solution to measure the physiological effects of artificial bloods on various biomedical devices. Since this combination is used in previous studies, it is assumed that the combination has a viscosity that closely resembles the viscosity of whole blood and would be ideal for our experimentations.

The blood substitute was developed utilizing the following procedure:

1. Measure out 8mL of Glycerin (99% Pure ACS Grade)
2. Add the 8L of Glycerin to a 20L carboy
3. Measure out 12L of distilled water
4. Add the 12L of distilled water to the 20L carboy diluting the Glycerin
5. Mix the 40% Glycerin – 60% Water solution

5.1.1. Viscosity Testing

Blood viscosity is typically measured utilizing a viscometer. However, due to our limited resources and previously allocated budget, the group was forced to perform a falling ball viscosity testing methodology on our blood substitute solution. The methodology consisted of drawing a sample of the solution from the 20L carboy and into a 2L Nalgene container.

The sample was then heated up with a common hair dryer until it reached a temperature of 37 °C, which is the temperature at which are documented blood viscosity was measured. Once the sample reached a temperature of 37 °C, it was then poured into a graduated cylinder. A temperature probe was also inserted into the graduated cylinder in order to allow the group a constant observance of the temperature, as well as, to make not of any significant drops in the solution temperature in order to not skew the data.

Strips of tape were fixed to the graduated cylinder to serve as markers for our stopwatch. The first marker was set at a lower point on the graduated cylinder in order to allow the marble to

flow through the fluid for some time and to eliminate some of the acceleration it had built up due to the drop. Once the viscosity testing system was established, the group began to drop uniform marbles with a weight of down the graduated cylinder, starting our timer as it reached the first marker and stopping it as it crossed the second marker. The Δt was then recorded and included in our viscosity testing equation. As we completed this analysis we found that the values for our experimentally found viscosity were extremely off. Upon further research, values for aqueous glycerine solutions were found and our initial assumption of the need to heat our solution to that of blood was incorrect. Since literature did not state whether or not those who used this type of blood substitute did not heat it up we felt it necessary to do so and guarantee that our values were accurate. Thus, we implemented the testing methodology once again but without heating our solution to 37 °C but rather testing at a temperature of 21.6 °C. After performing the viscosity testing, the group observed that it's findings were skewed due to the fact that the proper timing patterns necessary for proper viscosity analysis were unrealistic. The group felt that there was enough evidence in literature to properly validate the use of the 40% aqueous glycerin solution as our blood substitute.

The viscosity, as well as, the density of our solution would fall within the physiological viscosity range of blood is tested at 21.6° C as can be seen in the table below.

Glycerine (%)	Density (g/cm ³)	
	25 °C	30 °C
40	1.09710	1.09475
Glycerine (%)	Viscosity (cP)	
	20 °C	30 °C
40	3.72	2.72

Table 9: Properties of Aqueous Glycerine Solutions (The Dow Chemical Company)

5.2. Latex Arterial Model Development

5.2.1. Stiffness Model

Latex models with varying wall thicknesses were needed to analyze how changes in stiffness affected the properties of the pulsatile wave. To develop these samples, polyvinyl chloride (PVC) tubes of roughly 15 inches in length and 1 inch inner diameter were loosely attached on both corners using a clamp. The clamps were then attached to ring stands to hold the PVC horizontally. A permanent marker (Sharpie, twin tip) was then used to mark a corner of the PVC to indicate the starting point.

To create the compliance models, a soft paint brush (12 Royal softgrip S64590) was first dipped in warm water to make the bristles softer. The paint brush was then thoroughly dried using paper towels, and dipped into the liquid latex (Mold Builder by Castin Craft). Using long strokes from one end of the PVC to the other, latex was then evenly brushed over the face. Bands of latex were brushed over to minimize streaking as much as possible. The PVC was then slowly rotated within the slightly loose clamp to expose a new unpainted face of the PVC. The above steps were repeated, where latex was applied, and evenly brushed from one end of the PVC to the other using long strokes. While painting the second face, extra attention was given to the interface of first and second face. The latex was applied closer to the first face, and the two faces were completely blended in order to minimize an uneven interface. These steps were repeated until the first and last faces were properly blended.

Once the application was completed and streaks were minimized, one side of the sample was blow dried using a blow dryer (Vidal Sassoon) until the latex was partially dried. The PVC was then rotated again around its axis to expose a new face. This process continues until all faces of the tube were evenly heated to eliminate any deformations that may occur due to uneven drying.

To determine if the latex was sufficiently dried for the next layer to be painted, one edge of the latex was touched with bare fingers. If the latex felt in any way liquid, drying was continued. A visual means to determine if the latex was wet was by observing the painted layer. If the painted area was still white, it was likely to still be wet. A good indication of sufficiently dried latex is when the latex turns slightly yellow. However, precautions were taken to prevent the latex from completely drying (yellow). This was done in order to ensure that the next layer would evenly bond with the previous layer.

Streaks, though minimized, were common in some of the thicker samples. These samples required a longer time to sufficiently dry; therefore controlling the development of streaks became more and more difficult as each layer was added.

Each layer was painted with maximum consistency, (that is, amount of latex used) to produce roughly incremental increase in wall thickness of the sample with increasing number of layers. Once the predetermined number of layers is for each sample had been applied (4, 6, 8, 10, and 12 layers), the sample was allowed to dry at room temperature for a period of at least 24 hours.

To remove the sample from the PVC, baby powder (Johnson's) was applied to the outside of the sample to minimize friction. Both the edges of the sample were trimmed to remove the inconsistent areas using a knife or a sharp blade. One side of the trimmed latex was turned inside out, and the sample smoothly slid backwards over the powder. The sample was then turned inside out, and trimmed down a length of roughly 9 inches.

To be able to use these models within the pulsatile flow generator, the edges of each sample had to be mounted on a small PVC pieces. The edges of each sample were slid over the 1-inch inner diameter PVC tubes and were securely bonded using either a putty (QuickPlastik by Polymeric Systems Inc) or glue (Stik'n Seal by Loctite), and allowed to dry for a period of 12-24 hours. Once dried, roughly 1 mm holes were drilled as close to the latex-PVC interface as possible. 1-mm inner diameter tubing was then inserted through the hole roughly ½ inch deep. The 1mm inner diameter tube would later be attached to the pressure transducers. Common plumber caulking was then applied around the hole on the PVC-tube interface and allowed to dry for another 18-24 hours to prevent possible leakage.

5.2.2. Stenosis Model

To produce the occlusion models, custom designed metal rods were machined. These metal rods each had a point depression about halfway down the rod. It was believed that when painted over with latex and slid off, these samples would have a concave going down into the lumen of the sample, recreating a physiological occlusion.

To extend the metal rods to a sufficient length, two pieces of 2-in long, 1-in outer diameter PVC fittings were tightly secured to the short metal rod using vinyl electrical tape. Initially, the PVC-Occlusion combination was held horizontally using the clamp-ring stand method mentioned above, however, due to the weight of the metal and insufficient strength of the tape, the metal piece began to sag and deform the sample. Therefore, the sample was held vertically on a wooden board, and latex was applied around the base of the PVC. The latex was allowed to dry for a period of 24 hours to secure the sample to the wooden board. Once secured, the occlusion model was evenly painted using the method mentioned above.

Caulking was later inserted into the occlusion and the sample was again allowed to dry for a period of 24 hours. The sample was then bonded to 1-in inner diameter PVC tubing, and drilled using a drill press. 1-mm tube was inserted into the sample, and sealant was again applied to secure the tube to the PVC.

5.3. Arterial Testing

Arterial stiffness testing was performed in order for the group to gain an understanding of the mechanical properties of the latex samples used and how those properties compared to the mechanical properties of actual human arteries. Two types of testing and analyses were performed in order to confirm any results observed. These tests included a compliance test and a pulse wave velocity analysis.

5.3.1. Radial Compliance Testing

The first type of test performed in order to analyze the stiffness of the samples was a radial compliance test. This type of testing was done as a preparatory step before each sample could be tested with the flow generator in order for the group to understand exactly what type of sample was being tested. The group felt it was necessary to understand exactly how stiff each sample was and using this information, be able to understand for what age range each sample fell into with regard to arterial health.

Each sample was tested by attaching it between the two bases, verifying that the system was airtight but initiating short pumps and checking for air leaks. Once an airtight system was successfully achieved, each sample was pumped up to a pressure of 80mmHg, 90mmHg, 100mmHg, 110mmHg and 120mmHg. At each pressure point, the new diameter was measured using a caliper. This type of testing was performed on each sample three times, although for some of the thinner models, testing could not reach the later rounds due to plastic deformation of the sample due to high pressure in the system.

5.3.2. Tensile Testing

The second type of analysis performed to observe the amount of stiffness in each sample was a pulse wave velocity analysis. Before a pulse wave velocity analysis could be performed though, a round of tensile testing needed to be performed in order to calculate the elastic modulus of the latex samples used. The elastic modulus was critical value needed to perform the pulse wave velocity analysis using the pulse wave equation. Since there was no change in the chemical composition of the latex during sample production, the group tested two samples, assuming the output curves would be the same for both samples.

As compliance is a measure of wall stiffness, the Tensile Testing method will allow us to analyze the slope of the stress strain curve corresponding to a given pressure. Tensile testing will require the use of the Instron testing machine, which is available to us through the BME Department. The Instron machine can apply either a cyclic or static load. Cyclic loads are normally used to see how fatigue will cause failure in a material. Where as static loading applies a single force until failure. In this experimentation a static loading of max 10lb is being used due to the fact that the group does not wish to analyze the sample until failure, rather just to analyze its curve from elastic until plastic deformation.

5.3.3. Pulse Wave Velocity Analysis

Now that the group had an experimentally measured elastic modulus, pulse wave velocity analysis could be performed. The analysis was performed using the equation

$$c = \sqrt{\frac{Eh}{2\rho(R + h/2)}}$$

Equation 16

from which the pulse wave analysis will be known. This calculation was performed on each sample to be tested. Velocity results were then compared a graph which shows different velocities the age ranges that they correspond to. This graph can be seen in Figure 17 (Fung, 1993).

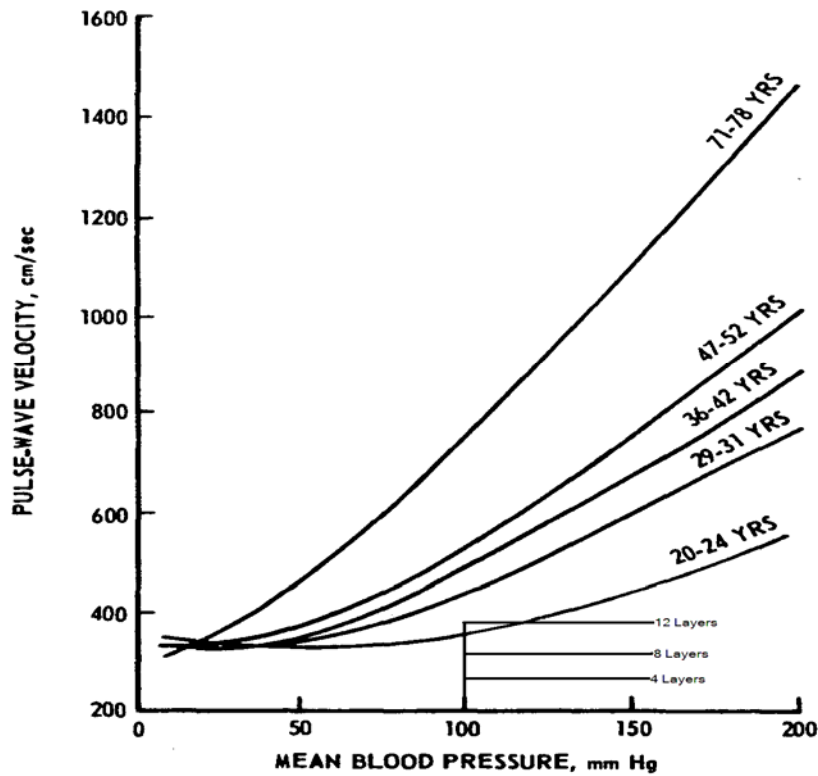


Figure 33: Pulse Wave Velocity vs. Mean Blood Pressure (Fung, Biomechanics)

5.4. Pulsatile Flow Generator System Calibration

It was necessary for us to conduct testing of our arterial samples under physiological conditions. Since the inception of our research project, developing our system as physiological as possible was a big issue and can be seen through the creation of our blood substitute and the development of our physiological arterial samples.

The last parameter for us in order to test under physiological conditions was establishing and maintaining a physiological blood pressure of (75 – 80mmHg). In a controlled experiment, the impedance would have to be created in order to mimic the physiological impedance found in the body. Most prior academic studies at WPI and some within industry used some type of check valve to build up that pressure in the system. In order to achieve this, the group employed the use of two ball valves, one controlling the flow into the system and the other controlling the flow exiting the system. We were able to reach and maintain a physiological pressure of 76mmHg for all testing conducted adhering to the following methodology.

1. Open all valves
2. Turn on the recirculation system and fill up the reservoir
3. Allow the system to circulate until the reservoir has been filled
4. Set the outflow valve to its designated position
5. Allow a column of the solution to fill the tubing
6. Unlock the Piston Motor control and use the piston to raise the fluid column into the reservoir establishing a uniform system pressure
7. Lock and set the piston to its position

5.4.1. Pulse Wave Development & Calibration

In order to calibrate the system, it was necessary to first complete phasing of the motor utilizing the ProMOTION software that was provided to us with the ION Digital Drive. The piston load is disconnected from the motor and Phasing is Initialized.

```
cs PMDOPSetCaptureSource, 0
cs PMDOPSetPhaseCounts, 2000
cs PMDOPSetCommutationMode, 0
cs PMDOPSetPhaseCorrectionMode, 0
cs PMDOPSetPhaseInitializeMode, 1
cs PMDOPSetPhaseInitializeTime, 0
cs PMDOPSetPhasePrescale, 0
```

Figure 34: Phase Initialization Parameters

Motion Control Code was developed using SDIEdit in order to produce the Common Iliac Pressure waveform which we were aiming for. The code consists primarily of the initial P.I.D. parameters and Current Loop values that were estimated using the ProMOTION software.

```
cs PMDOPSetCurrentControlMode, 1
cs2 PMDOPSetFOC, 0, 300
cs2 PMDOPSetFOC, 1, 300
cs2 PMDOPSetFOC, 2, 32767
cs2 PMDOPSetFOC, 256, 300
cs2 PMDOPSetFOC, 257, 300
cs2 PMDOPSetFOC, 258, 32767
cs2 PMDOPSetCurrentLoop, 0, 500
cs2 PMDOPSetCurrentLoop, 1, 500
cs2 PMDOPSetCurrentLoop, 2, 32766
cs2 PMDOPSetCurrentLoop, 256, 500
cs2 PMDOPSetCurrentLoop, 257, 500
cs2 PMDOPSetCurrentLoop, 258, 32766
cs2 PMDOPSetHoldingCurrent, 0, 32767
cs2 PMDOPSetHoldingCurrent, 1, 32767
```

Figure 35: Current Loop Parameters

The last portion of the code is the actual piston control language and is coded as a “while” loop with particular attention to the inlet and outlet velocities which control the development of the amplitude and wavelength of our pressure waveforms in conjunction with the PID parameters.

```

While (x > -1)
  pause 400
  cs PMDOPResetEventStatus, &h0000
  cs PMDOPSetVelocity, 66847
  cs PMDOPSetPosition, 0
  pause 000
  cs PMDOPUpdate, 0
  pause 500
  cs PMDOPResetEventStatus, &h0000
  cs PMDOPSetVelocity, 6684
  cs PMDOPSetPosition, 1000
  pause 000
  cs PMDOPUpdate, 0
  x = x+1
Wend

```

Figure 36: Waveform Morphology Code

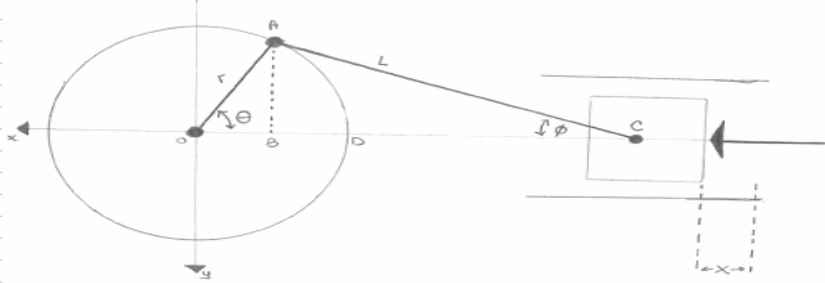
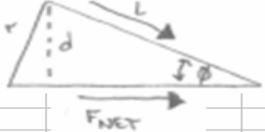
There are two ways of adjusting the P.I.D. gains in order to produce the waveform we are aiming for, utilizing a trial and error methodology or an analytical approach. Given the difficulty in trying to calculate the relative gains that were necessary to produce a waveform close to the common iliac artery pressure waveform and our diminishing timeframe, the group took the route of manually adjusting the gains through trial and error. In order to do so, the system it was necessary for the system to be fully running and outputting pressure readings. The following methodology was followed.

1. Set Ki and Kd to “0”
2. Slowly increase Kp the motor shaft oscillates
3. Increase Kd until the necessary amplitude is observed.
4. Record the value of Kp and Kd
5. Increase/Decrease Kd as necessary

6. Results

6.1. Piston Slider Crank Analysis

Table 10: Kinematic Analysis

Motor Speed (rpm)	ω (rad/s)	r (m)	l (m)	D_{piston} (m)	M_{piston} (kg)	A (m ²)	P (Mpa)	d (m)
120	12.56637061	0.0381	0.127	0.02032	0.03	0.000324293	10700	0.026940768
								
$\cos(\phi) = \sqrt{1 - \left(\frac{r}{L} \sin \theta\right)^2}$ $x = \left[r + \frac{r^2}{4L}\right] - r \left[\cos \theta + \frac{r}{4L} \cos(2\theta)\right]$ $\dot{x} = r\omega \left[\sin \theta + \frac{r}{2L} \sin(2\theta)\right]$ $\ddot{x} = r\omega^2 \left[\cos \theta + \frac{r}{L} \cos(2\theta)\right]$								
$F_{\text{Pressure}} = P \times A$ $F_{\text{Net}} = F_{\text{Pressure}} - F$ $F_{\text{Inertia}} = M \times a$ $F_{\text{Total}} = F_{\text{Net}} \cos(\phi)$ $T = I \times \alpha = F_{\text{Total}} \times d$ 								
F_p	F_i	F_n	F_t	Displacement _{piston} (x)	Velocity _{piston} (x')	Acceleration _{piston} (x'')	Torque (Nm)	Torque (lb·in)
3.469932817	0.165918309	3.30401451	3.2288185	0.014016732	0.410364488	5.530610301	0.086986851	0.769795142
45	0.785398163	0.21375613	12.247324					
15	0.261799388	0.07772395	4.453254					
30	0.523598776	0.07772395	4.453254					
45	0.785398163	0.21375613	12.247324					
60	1.047197551	0.26282298	15.058647					
75	1.308996939	0.29399461	16.844651					
90	1.570796327	0.30469265	17.457603					
105	1.832595715	0.29399461	16.844651					
120	2.094395102	0.26282298	15.058647					
135	2.35619449	0.21375613	12.247324					
150	2.617993878	0.15056827	8.6269266					
165	2.879793266	0.07772395	4.453254					
180	3.141592654	0	0					

6.2. Arterial Testing

6.2.1. Radial Compliance Testing

Once all of the testing was completed, the data collected was used to calculate the radial compliance of each sample. Since three rounds of testing were performed on each sample, an average of the radial compliances of each round was used as the final result. Table 8 below shows the complete data analysis spreadsheet from the radial compliance testing including the average radial compliances. The calculation of these radial compliances were done using the following equation

$$C = \left(\frac{\Delta R}{R_i} \times \frac{100}{P} \times 100 \right) \quad \text{Equation 17}$$

As a secondary compliance analysis, the group also used the same results from the compliance testing and calculated compliances using the following equation as well

$$C = \left(\frac{\Delta R}{\Delta P} \right) \quad \text{Equation 18}$$

The results of which can be seen below in Table 9 below:

**Expansion of Radius Due to Pressure
±0.001**

Round 1

	80mmHg	90mmHg	100mmHg	110mmHg	120mmHg
4 layers	13.99	0.550	0.6005	0.6000	n/a
6 layers	n/a	n/a	n/a	n/a	n/a
8 layers	0.55	0.6000	0.6001	0.6001	0.6505
10 layers	0.501	0.5501	0.5500	0.6001	0.6000
12 layers	0.5505	0.6000	0.6001	0.6500	0.6502

Round 2

	80mmHg	90mmHg	100mmHg	110mmHg	120mmHg
4 layers	n/a	n/a	n/a	n/a	n/a
6 layers	n/a	n/a	n/a	n/a	n/a
8 layers	0.5500	0.6000	0.6001	0.6002	0.6502
10 layers	0.5006	0.5501	0.6000	0.6000	0.6000
12 layers	0.5501	0.6001	0.6001	0.6002	0.6002

Round 3

	80mmHg	90mmHg	100mmHg	110mmHg	120mmHg
4 layers	n/a	n/a	n/a	n/a	n/a
6 layers	n/a	n/a	n/a	n/a	n/a
8 layers	0.5501	0.6001	0.6001	0.6000	0.6504
10 layers	0.5001	0.5500	0.6000	0.6000	0.60045
12 layers	0.5501	0.600475	0.60005	0.650005	0.6000

Average Percent Radial Compliance

	80mmHg	90mmHg	100mmHg	110mmHg	120mmHg
4 layers	12.59	11.18	20.01	18.20	n/a
6 layers	n/a	n/a	n/a	n/a	n/a
8 layers	12.51	22.23	20.02	18.20	25.10
10 layers	0.1395	11.12	16.67	18.18	16.70
12 layers	12.55	22.31	13.34	15.16	13.90

Radial Compliance

80mmHg	90mmHg	100mmHg	110mmHg	120mmHg
%		%		%
12.60	11.17	20.01	18.20	n/a
n/a	n/a	n/a	n/a	n/a
12.5	22.23	20.01	18.20	25.08
0.25	11.12	10.00	18.18	16.67
12.61	22.31	20.02	27.27	25.03

80mmHg	90mmHg	100mmHg	110mmHg	120mmHg
%		%		%
n/a	n/a	n/a	n/a	n/a
n/a	n/a	n/a	n/a	n/a
12.51	22.23	20.02	18.20	25.03
0.15	11.12	20.00	18.18	16.67
12.51	22.30	20.01	18.21	16.69

80mmHg	90mmHg	100mmHg	110mmHg	120mmHg
%		%		%
n/a	n/a	n/a	n/a	n/a
n/a	n/a	n/a	n/a	n/a
12.51	22.23	20.01	18.19	25.07
0.0188	11.11	20.00	18.18	16.74
12.53	22.32	20.01	27.27	16.67

Table 11: Radial Compliance Analysis

Testing Round 1					
	80mmHg	90mmHg	100mmHg	110mmHg	120mmHg
Test Sample	Recorded (r)				
4 layers	1.398	1.398	1.524	1.524.	N/A
6 layers	N/A	N/A	N/A	N/A	N/A
8 layers	1.397	1.524.	1.524.	1.524.	1.652.
10 layers	1.272.	1.397.	1.397	1.524	1.524
12 layers	1.398	1.525	1.524	1.651	1.651

Testing Round 1					
	80mmHg	90mmHg	100mmHg	110mmHg	120mmHg
Test Sample	Δr				
4 layers	0.1279	0.1277	0.2541	0.2542	N/A
6 layers	N/A	N/A	N/A	N/A	N/A
8 layers	0.127	0.254	0.2541	0.2542	0.3828
10 layers	0.0025	0.1272	0.1271	0.2545	0.2547
12 layers	0.1283	0.2551	0.2544	0.3816	0.3813
ΔP	80	90	100	110	120

Testing Round 1					
	80mmHg	90mmHg	100mmHg	110mmHg	120mmHg
Test Sample	Compliance				
4 layers	0.0016	0.00142	0.002541	0.002311	N/A
6 layers	N/A	N/A	N/A	N/A	N/A
8 layers	0.0015	0.0028	0.0025	0.0023	0.0031
10 layers	3.17E-05	0.0014	0.00127	0.0023	0.0021
12 layers	0.0016	0.0028	0.0025	0.0034	0.0031

Testing Round 2					
	80mmHg	90mmHg	100mmHg	110mmHg	120mmHg
Test Sample	Recorded (r)				
4 layers	N/A	N/A	N/A	N/A	N/A
6 layers	N/A	N/A	N/A	N/A	N/A
8 layers	1.3974	1.5244	1.5244	1.5241	1.658
10 layers	1.2714	1.3971	1.5249	1.5245	1.5244
12 layers	1.3977	1.5243	1.5241	1.5248	1.5295

Testing Round 2					
	80mmHg	90mmHg	100mmHg	110mmHg	120mmHg
Test Sample	Compliance				
4 layers	N/A	N/A	N/A	N/A	N/A
6 layers	N/A	N/A	N/A	N/A	N/A
8 layers	0.0015	0.0028	0.0025	0.0023	0.0031
10 layers	1.91E-05	0.0014	0.0025	0.0023	0.0021
12 layers	0.0015	0.0028	0.00254	0.0023	0.0021

Testing Round 2					
	80mmHg	90mmHg	100mmHg	110mmHg	120mmHg
Test Sample	Δr				
4 layers	N/A	N/A	N/A	N/A	N/A
6 layers	N/A	N/A	N/A	N/A	N/A
8 layers	0.1274	0.2544	0.2544	0.2541	0.3118
10 layers	0.0014	0.1271	0.2549	0.2545	0.2544
12 layers	0.1277	0.2553	0.2541	0.2548	0.2545
ΔP	80	90	100	110	120

Testing Round 3					
	80mmHg	90mmHg	100mmHg	110mmHg	120mmHg
Test Sample	Recorded (r)				
4 layers	N/A	N/A	N/A	N/A	N/A
6 layers	N/A	N/A	N/A	N/A	N/A
8 layers	1.3922	1.5243	1.5291	1.5241	1.6521
10 layers	1.2701	1.3972	1.5241	1.5248	1.5253
12 layers	1.3974	1.5207	1.5247	1.6513	1.5243

Testing Round 3					
	80mmHg	90mmHg	100mmHg	110mmHg	120mmHg
Test Sample	Compliance				
4 layers	N/A	N/A	N/A	N/A	N/A
6 layers	N/A	N/A	N/A	N/A	N/A
8 layers	0.0015	0.0028	0.0025	0.002	0.0031
10 layers	2.38E-06	0.0014	0.0025	0.0023	0.0021
12 layers	0.0015	0.0028	0.0025	0.0034	0.0021

Testing Round 3					
	80mmHg	90mmHg	100mmHg	110mmHg	120mmHg
Test Sample	Δr				
4 layers	N/A	N/A	N/A	N/A	N/A
6 layers	N/A	N/A	N/A	N/A	N/A
8 layers	0.1272	0.254113	0.254191	0.254081	0.382041
10 layers	0.0019	0.127032	0.2541	0.2548	0.2543
12 layers	0.1274	0.2507	0.2547	0.3813	0.2543
ΔP	80	90	100	110	120

Average Compliance					
	80mmHg	90mmHg	100mmHg	110mmHg	120mmHg
Test Sample	Compliance				
4 layers	0.0016	0.00142	0.002541	0.002311	N/A
6 layers	N/A	N/A	N/A	N/A	N/A
8 layers	0.0015	0.0028	0.0025	0.0023	0.0031
10 layers	1.77E-05	0.0014	0.0021	0.0023	0.00024
12 layers	0.0014	0.0024	0.0022	0.0030	0.0024

Table 12: Compliance Analysis using dr/dP

6.2.2. Tensile Testing

The results and data points from the tensile testing were recorded and viewed using the Labview software program. The subsequent curve created by the recorded data points were then analyzed by the group using Microsoft Excel. From the time and force data points present, the group calculated the stress and the strain at each data point, thereby producing a stress-strain curve for the sample tested as seen in Figure 18. From this curve, the group calculated the elastic modulus of the latex which was found to be 2434.60.

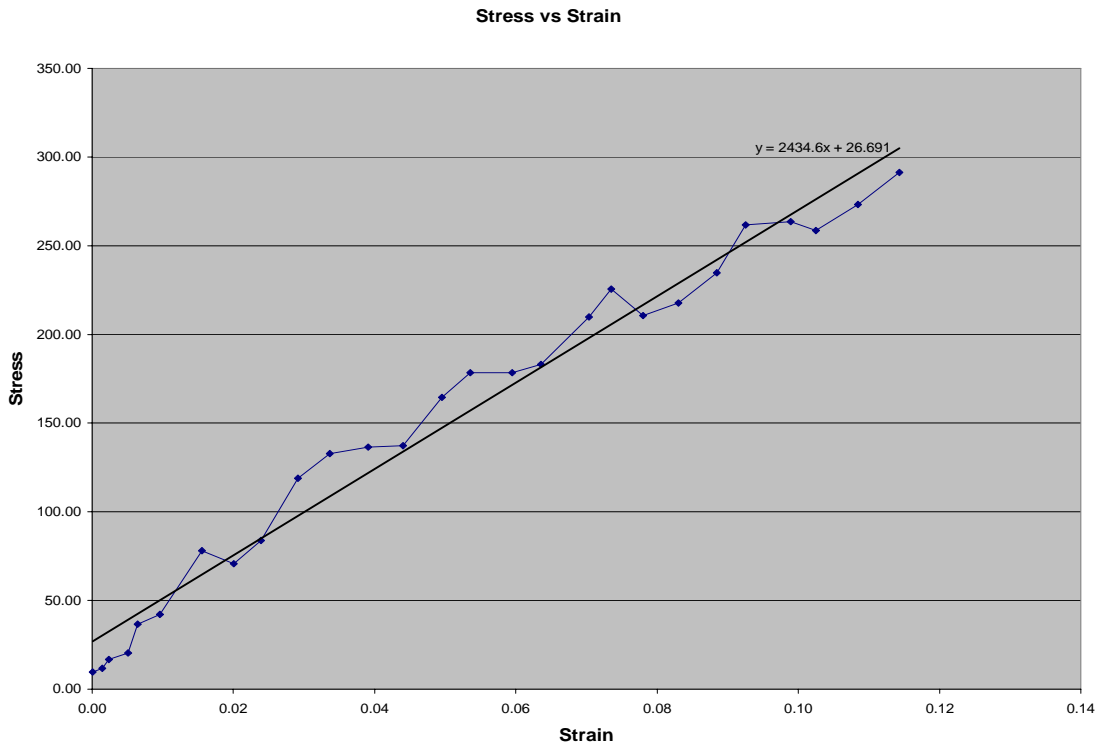


Figure 37: Arterial Model Elastic Modulus Analysis

6.2.3. Pulse Wave Velocity Analysis

Once the Young's Modulus was found, the group calculated the pulse wave velocity of each sample to be tested. The results of the pulse wave velocity calculations can be seen below in Table 10.

Pulse-wave Velocity	Elastic Modulus	Radius	Density of Air	Density of Water	Density of Blood	Thickness
$c = \text{cm/s}$	$E = P = (\text{kg/m}^2\text{s}^2) * 100 = \text{kg/cm}^2\text{s}^2$	$R = \text{cm}$	$\rho = \text{kg/cm}^3$	$\rho = \text{kg/cm}^3$	$\rho = \text{kg/cm}^3$	$h = \text{cm}$
	2.43E+03		1.20E-06	1.00E-03	1.05E-03	

Elastic Modulus	Density of Blood	Pulse Wave Velocity					Thickness	Thickness	Test Sample	Pulse Wave Velocity				
		80mmHg	90mmHg	100mmHg	110mmHg	120mmHg				80mmHg	90mmHg	100mmHg	110mmHg	120mmHg
$E = P = (\text{kg/m}^2\text{s}^2) * 100 = \text{kg/cm}^2\text{s}^2$	$\rho = \text{kg/cm}^3$	R					(h)	(h/2)		c = cm/s				
2.43E+03	1.05E-03	1.40	1.53	1.52	1.61	1.57	0.14	0.07	L12-3	327.43	314.04	314.13	306.10	310.02
2.43E+03	1.05E-03	1.40	1.53	1.52	1.61	1.57	0.14	0.07	L12-1-1	334.26	320.62	320.71	312.52	316.52
2.43E+03	1.05E-03	1.40	1.53	1.52	1.61	1.57	0.11	0.06	L12-2	297.92	285.65	285.73	278.36	281.96
2.43E+03	1.05E-03	1.40	1.53	1.52	1.61	1.57	0.15	0.07	L12-1-2	342.29	328.36	328.45	320.08	324.17
2.43E+03	1.05E-03	1.40	1.53	1.52	1.61	1.57	0.09	0.04	L10-2	268.22	257.09	257.17	250.49	253.75
2.43E+03	1.05E-03	1.27	1.40	1.48	1.52	1.52	0.11	0.05	L10-3	308.04	294.39	286.17	282.31	282.27
2.43E+03	1.05E-03	1.27	1.40	1.48	1.52	1.52	0.09	0.04	L10-3	279.26	266.80	259.30	255.78	255.74
2.43E+03	1.05E-03	1.40	1.52	1.52	1.52	1.65	0.08	0.04	L8-2	259.76	249.00	248.99	248.99	239.42
2.43E+03	1.05E-03	1.40	1.52	1.52	1.52	1.65	0.11	0.06	L8-1	298.61	286.35	286.34	286.34	275.43
2.43E+03	1.05E-03	Need Data	Need Data	Need Data	Need Data	Need Data	0.12	0.06	L7-7	Need Data	Need Data	Need Data	Need Data	Need Data
2.43E+03	1.05E-03	N/A	N/A	N/A	N/A	N/A	0.07	0.04	L6-3	N/A	N/A	N/A	N/A	N/A
2.43E+03	1.05E-03	N/A	N/A	N/A	N/A	N/A	0.06	0.03	L6-2	N/A	N/A	N/A	N/A	N/A
2.43E+03	1.05E-03	N/A	N/A	N/A	N/A	N/A	0.12	0.06	L6-1	N/A	N/A	N/A	N/A	N/A
2.43E+03	1.05E-03	1.40	1.40	1.52	1.52	N/A	0.04	0.02	L4-2	178.60	178.61	171.15	171.14	N/A
2.43E+03	1.05E-03	1.40	1.40	1.52	1.52	N/A	0.07	0.04	L4-3	242.49	242.51	232.48	232.48	N/A
2.43E+03	1.05E-03	1.40	1.40	1.52	1.52	N/A	0.09	0.04	L10-4	265.99	266.01	255.07	255.06	N/A
2.43E+03	1.05E-03	Need Data	Need Data	Need Data	Need Data	Need Data	0.07	0.04	L3-1	Need Data	Need Data	Need Data	Need Data	Need Data

Table 13: Pulse Wave Velocity Analysis

6.3. Pulsatile Flow Pressure Waveform Analysis

Sample	Heart Rate		2nd Harmonic		3rd Harmonic		4th Harmonic		5th Harmonic	
	Hz	Amplitude	Hz	Amplitude	Hz	Amplitude	Hz	Amplitude	Hz	Amplitude
6_3	0.84229	0.94776	1.67236	0.63569	2.51465	0.26545	3.34473	0.18142	4.99268	0.06417
8_2	0.84229	0.87093	1.67236	0.30739	2.51465	0.13662	3.33252	0.11032	4.1748	0.05038
8_3	0.83008	0.84938	1.67236	0.36285	2.50244	0.19675	3.33252	0.16183	4.1626	0.07816
10_2	0.83008	1.08453	1.67236	0.46822	2.50244	0.2265	3.34473	0.15682	4.1748	0.09716
12_1_1	0.83008	1.12919	1.67236	1.07001	2.50244	0.49722	3.33252	0.35988	4.1748	0.21018
12_1_2_2	0.84229	0.80211	1.67236	0.26299	2.50244	0.10705	3.34473	0.06028	4.1748	0.0243
12_3	0.83008	0.84938	1.67236	0.36285	2.50244	0.19675	3.33252	0.16183	4.1626	0.07816
2_socclusion	1.0376	1.25732	2.0752	1.12179	3.11279	0.37831	4.15039	0.25576	5.18799	0.18727
3_socclusion	1.0376	1.15032	2.0752	1.34647	3.11279	0.40528	4.15039	0.41224	5.18799	0.1774
4_socclusion	1.0376	1.15032	2.0752	1.34647	3.11279	0.40528	4.15039	0.31224	5.18799	0.17174
4_socclusion	1.0376	1.26615	2.0752	1.19114	3.125	0.35123	4.1626	0.27581	5.2002	0.19099
6_socclusion	1.0376	1.30622	2.0752	0.82445	3.11279	0.27387	4.15039	0.22507	5.18799	0.14848

Table 14: Frequency & Harmonic Analysis for Stiffness & Occlusion Models

The stiffness model results were comparable for the heart rate magnitudes where the range was 0.80211-1.12919 mmHg. When the harmonics were increased from 2 to 5 the magnitudes of the harmonics decreased. Take 6-3 for example, the first harmonic has a value of 0.94776 mmHg, the second harmonic is 0.63569 mmHg, the third harmonic is 0.26545 mmHg, the fourth harmonic is 0.18142 mmHg, and the fifth harmonic is 0.06417 mmHg. Another trend of the stiffness data is for the thicker layers the second, third, fourth and fifth harmonics are smaller than that of those thinner layers. Sample 8_2 in comparison to 6_3 the second and third harmonic are about half the value that of the 6_3 sample.

The occlusion model results also show comparable magnitudes for the first harmonic ranging from 1.15032-1.30622 mmHg. A trend that is seen in this data set is that the second harmonic has a high value and sometimes surpasses the value of the first, then the third and fourth harmonic drop in magnitude value in comparison to the first two harmonics.

7. Analysis and Discussion

Upon completion of our testing and the successful collection of our pulsatile flow waveform data we were able to compare the variance between our data sets as our arterial models progressed from healthy arterial models to diseased and stenotic arterial models. Utilizing Microsoft Excel and some statistical tests, the group was able to extract meaningful data from the FFT analysis we previously conducted on our pulsatile flow waveforms.

7.1. Arterial Testing

Both compliance and pulse wave velocity analysis showed that the latex arterial models created by the group fell within the compliance levels for a healthy young human being. As seen in Figure 33, the 8 layer arterial sample would fall into the compliance range for a 16-20 year old while the 12 layer would fall within the 20-24 year old range. This validation provided the group with enough evidence that the latex models used provided enough physiological properties to make the pressure wave data collected from each sample relevant.

7.2. Harmonic Statistical Analysis

In order to verify harmonic relevance and determine if any trends can be seen between harmonics of both normal and occluded models, the group performed a series of t-tests comparing not only normal harmonics but also occluded sample harmonics. Since atherosclerosis progresses with increased hypertension, the group theorizes that the amplitude for the occluded sample harmonics should be higher than those of the normal samples due to the changes in morphology.

Each table below represent a paired t-test of unequal variances. The first set of tables is for the Stiffness Models where the second to the fifth harmonic were compared to that of the first. What is seen is that for an alpha of 0.05, which means that after analyzing the data the confidence level that the data is actually different is 90%, is that the second to the fifth harmonics are statistically different for the first. Harmonic one in comparison to harmonic three is $p = 5.27 \times 10^{-6} < t\text{-critical} = 2.228$. When analyzing the statistical data for harmonics one versus two the $p = 0.0116 < t\text{-critical} = 2.36$.

Stiffness Harmonic 1 vs. 2

t-Test: Two-Sample Assuming Unequal Variances

	<i>0.94776</i>	<i>0.63569</i>
Mean	0.93092	0.472385
Variance	0.019279	0.090448
P(T<=t) two-tail	0.011588	
t Critical two-tail	2.364624	

Table 15: Stiffness Harmonic 1 vs. 2

Stiffness Harmonic 1 vs. 3

t-Test: Two-Sample Assuming Unequal Variances

	<i>0.94776</i>	<i>0.26545</i>
Mean	0.93092	0.226815
Variance	0.019279	0.019481
P(T<=t) two-tail	5.27E-06	
t Critical two-tail	2.228139	

Table 16: Stiffness Harmonic 1 vs. 3

Stiffness Harmonic 1 vs. 4

t-Test: Two-Sample Assuming Unequal Variances

	<i>0.94776</i>	<i>0.18142</i>
Mean	0.93092	0.168493
Variance	0.019279	0.01039
P(T<=t) two-tail	1.82E-06	
t Critical two-tail	2.262157	

Table 17: Stiffness Harmonic 1 vs. 4

Stiffness Harmonic 1 vs. 5

t-Test: Two-Sample Assuming Unequal Variances

	<i>0.94776</i>	<i>0.06417</i>
Mean	0.93092	0.089723
Variance	0.019279	0.004132
P(T<=t) two-tail	2.92E-06	
t Critical two-tail	2.364624	

Table 18: Stiffness Harmonic 1 vs. 5

Also seen is that the amplitude for harmonic two is 68.2% of the first harmonic while harmonic three is 24.4% of the first. The magnitude of the fourth harmonic is 18.1% of the first. And lastly the fifth harmonic magnitude is 9.6% of the first harmonic.

Likewise these similar paired t-tests are statistically significant for occluded models. The p-value of occlusion harmonic one verses harmonic two is 0.766 which is less than the t-critical value of 2.776, meaning that the data is statistically different.

Occlusion harmonic 1 vs. 2

t-Test: Two-Sample Assuming Unequal Variances

	<i>1.25732</i>	<i>1.12179</i>
Mean	1.218253	1.177133
Variance	0.006421	0.060644
P(T<=t) two-tail	0.766699	
t Critical two-tail	2.776445	

Table 19: Occlusion harmonic 1 vs. 2

Occlusion harmonic 1 vs. 3

t-Test: Two-Sample Assuming Unequal Variances

	<i>1.25732</i>	<i>0.37831</i>
Mean	1.218253	0.358915
Variance	0.006421	0.003864
P(T<=t) two-tail	2.7E-06	
t Critical two-tail	2.446912	

Table 20: Occlusion harmonic 1 vs. 3

Occlusion Harmonic 1 vs. 4

t-Test: Two-Sample Assuming Unequal Variances

	<i>1.25732</i>	<i>0.25576</i>
Mean	1.218253	0.30634
Variance	0.006421	0.006262
P(T<=t) two-tail	3.53E-06	
t Critical two-tail	2.446912	

Table 21: Occlusion Harmonic 1 vs. 4

Occlusion harmonic 1 vs. 5

t-Test: Two-Sample Assuming Unequal Variances

	<i>1.25732</i>	<i>0.18727</i>
Mean	1.218253	0.172153
Variance	0.006421	0.000314
P(T<=t) two-tail	0.000132	
t Critical two-tail	3.182446	

Table 22: Occlusion harmonic 1 vs. 5

For the occluded models, the group observed is that the second harmonic is 96.6% of the first harmonic magnitude, whereas the third harmonic is 29.5% of the first, which is similar to what is seen in the stiffness models. The fourth harmonic magnitude is found to be 21.0% of the first harmonic and lastly the fifth harmonic in comparison to the first harmonic magnitude is 14.1% of the first harmonic. These statistical analyses show that there are at least 5 clear and statistically different harmonics which can be observed from the FFT analysis meaning that the flow generator is capable of producing pressure waves containing 5 clear harmonics. In most instances though, more than 5 were actually observed.

The next set of data presents t-tests performed to compare the range of harmonics 1-5 of a control sample to harmonics 1-5 of each occlusion sample. The harmonics analyzed were taken from the FFT analysis of the entire data set containing 60 pulse waves. The control sample for the basis of this statistical analysis is sample 8_3. This sample was chosen because of its similarity to a normal healthy artery based on waveform observations and pulse wave velocity analysis.

Unoccluded Sample Harmonic 1-5 vs. Occlusion Models						
t-Test: Paired Two Sample for Means						
	8 3-Control	2/8 in	3/8 in	4/8 in	4/8 in dbl	6/8 in dbl
	<i>Variable 1</i>	<i>Variable 2</i>	<i>Variable 2</i>	<i>Variable 2</i>	<i>Variable 2</i>	<i>Variable 2</i>
Mean	0.330	0.640	0.698	0.677	0.655	0.556
Variance	0.095	0.259	0.266	0.284	0.278	0.248
Observations	5.000	5.000	5.000	5.000	5.000	5.000
Pearson Correlation		0.877	0.746	0.750	0.855	0.969
Hypothesized Mean Difference		0.000	0.000	0.000	0.000	0.000
df		4.000	4.000	4.000	4.000	4.000
t Stat		-2.474	-2.343	-2.135	-2.359	-2.369
P(T<=t) one-tail		0.034	0.040	0.050	0.039	0.038
t Critical one-tail		2.132	2.132	2.132	2.132	2.132
P(T<=t) two-tail		0.069	0.079	0.100	0.078	0.077
t Critical two-tail		2.776	2.776	2.776	2.776	2.776

Table 23: Control Sample vs. Occluded Samples t-test Analysis

In Table 23 the comparison of a control sample to the occlusion samples. shows that there is a statistical difference between the harmonics of the waveforms for both the unoccluded and occluded models. There is also a difference in the means, where the occlusion model is about twice that of the control model. The amplitude values found were taken from the FFT analysis of the entire data set. The group performed this initial test in order to observe whether at this larger scale that any variances can be observed.

The group observed that there is a statistical difference between the occlusion models and the control model with respect to amplitude height as the p-value for each test is much less than the t-critical value. This can be especially seen when comparing occluded samples 2/8 in, 3/8 in and 4/8 in. Since all of these occlusion samples were composed of a one-sided occlusion, with 4/8 being the most occluded, the group's theory that the p-value would probably increase was verified. As can be seen above the p-values for these three samples went from 0.069 for a 2/8 in occlusion model to 0.100 for a 4/8 in occlusion model. Since there is more of an occlusion and a higher amplitude, this increase in p-values is consistent with the groups hypothesis that with more of an occlusion, amplitude would be higer.

The group was not able to observe any other relevant trends within the p-values for each t-test. The group feels that these type of trends would probably need more data point acquisition in order to be relevant.

8. Conclusions

The group was able to conclude from the study that it was successful in developing a pulsatile flow generator which could create physiological arterial pressure waves. The group was successful in replicating pressure waves within a physiological range of 60mmHg – 120mmHg at a frequency of 1Hz or 60 bpm. The motion control device implemented within the system allowed the group the needed variability to emulate pressure waveforms corresponding to various locations on the arterial tree.

The group was also able to conclude that by creating a physiologically similar environment within the system, that the analysis gained from the flow generator would become clinically relevant. With the incorporation and use of a physiologically similar blood substitute and physiologically similar arterial models, the group was able to produce relevant and useful data.

Furthermore, the group was able to conclude that through statistical analysis performed on harmonic amplitude heights, that the pressure waves observed within the occlusion models used were statistically different than the normal stiffness models within a confidence level of 90%. Meaning that the initial testing results were successful in identifying differences between the waveforms observed within a normal arterial model and that of an occlusion model. A trend noticed by the group throughout the analysis was that the mean for the occlusion models was always about twice as much as for the control model meaning that each occlusion model had a higher harmonic amplitude than that of the control.

This along with the difference in p-values tells the group that there is statistical difference between the harmonics for the occlusion models and those for the control for the entire data range. The group was able to observe that with an increase in stenosis, the harmonic amplitudes increased significantly over the first two harmonics and drastically decline onwards. This indicates that the most relevant information for the possible early detection of arterial disease would be contained within the first two harmonics. This could lead to further findings in the hopes of identifying the stage of progression. An example of this can be seen in Table 14 when comparing the harmonics of the control sample with that of the 2/8 or 25% occluded sample. It was seen that there was a doubling of mean for the amplitude values of harmonic 1-5. Also it was seen that there was an increase in amplitude value between the first and second harmonics of the two samples and then a drastic dropoff of ~60%.

The acquisition of this relevant data further validates the group's success in building a fully functional pulsatile flow generator capable of emulating physiological pressure waveforms. The ability of the device to aid in further data acquisition can hopefully someday lead to data which could eventually be used to further analyze pressure waveform variances in the hopes of one day aiding in the early detection of arterial disease.

VII. Recommendations

Although the group feels confident that the findings of the study provide new insight into the possible early detection of arterial disease, there are still ways to improve the study and testing system.

For future iterations of this type of study the group recommends that within the system itself, there should be upgrades in the following areas; pressure transducers and valve control. The group feels that if the data acquired from this type of study were to eventually be used clinically, more precise pressure transducers need to be used, possibly ones that can be imbedded into the tubing system in order to gain a more accurate description of the wave being produced.

Valve control is also an area where there can be improvement. The group used simple ball valves to build up and control the pressure within the system manually. The group recommends that for future iterations, a more advanced valve control system be implemented such as an automated control system where by the openings and closings of the valve could be controlled through a device of some kind and not manually. Also with another type of valve system that can be implemented involves ones which allow for a known incremental increase or decrease in opening space. Instead of relying on human touch to estimate the amount of closure, some kind of marking device would allow for greater efficiency and pressure control.

Another recommendation the group has for future iterations is that testing be completed on a set of physiological arteries, such as those from an animal. Although the latex models served as satisfactory models for this study, the group feels that if the results of this type of study are to ever be used clinically, the testing would need to be completed on animal arteries and eventually human arteries. However this would also mean that the system would have to be scaled down since arteries do not have 1 inch inner diameters. With a higher budget, research teams down the line could scale-down the system, while still using the same motor and motion control system. Upon scaling down the system, a novel fixation system must be developed for practical use with the physiological samples which would fall in a lumen size of about 6mm. This novel fixation system would replace the PVC grip fixation system the group is currently utilizing giving our scaled up models.

The final recommendation the group has for future iterations of this type of project is that more data acquisition should be undertaken. Although the group felt it was successful in observing statistical differences between the harmonics of the occlusion models compared to those of normal models, in order for the data to be more relevant, much more testing needs to be performed. The use of different types of models, or the addition of more data points may allow for further insight into trends that may occur between occlusion and normal arterial models.

VIII. References

- Anand, R. *Use a long saphenous vein patch graft to facilitate microvascular anastomosis when the carotid artery is stenosed*, British Journal of Oral and Maxillofacial Surgery, 45, 2007, 81-82
- Anders, B. Andersson, S. *Simulation of the mild wear in a cam-follower contact with follower rotation*, The Royal Institute of Technology, 1996, 202-210
- Anwaruddin, S., Isaacs S., Nanadram, N.. *Design and Construction of a Pulsatile Flow Generator*, Major Qualifying Project Report-WPI, BJS-AC02, 2003
- Avolio, AP. Chen, SG et. Al. *Effects of aging on changing arterial compliance and left ventricular load in a northern Chinese urban community*, Circulation, 68, 2002, 50-58.
- Bachmann C. & Wilson M., *The Osmotic Swelling Characteristics of Cardiac Valve Prostheses*. Journal of Biomechanical Engineering, 122: 4, August 2000, 453–454.
- Fung, Y.C., *Biomechanics: Mechanical Properties of Living Tissue*, 2nd Edition, New York, Springer Science and Business Media, 1993.
- Bassiouny et al., *Anastomotic intimal hyperplasia: mechanical injury or flow induced*. Journal of Vascular Surgery, 15, 2002, 708–717.
- Blasidell, J. & Richter R.. *Design and Construction of a Pulsatile Flow Generato*, Major Qualifying Project Report-WPI, BJS-PF04, 2005.
- Bourke, P., *DFT (Discrete Fourier Transform) FFT (Fast Fourier Transform)*. June 1993.
- Caro et al., *Atheroma and arterial wall shear: observations, correlation and proposal of a shear dependent mass transfer mechanism for atherogenesis*, Proceedings of the Royal Society of London, B 117, 1971, 109–159.
- Chaudhuri, A., Ansdell, L.E., Grass, A.J., Adiseshiah, M. *Intrasac Pressure Waveforms After Endovascular Aneurysm Repair (EVAR) are a Reliable Marker of Type I Endoleaks, but not Type II or Combines Types: An Experimental Study*, Eur J Vasc Endovasc Surg, 28, 2004, 373-378.
- Corbo, M. A., Stearns, C. F., *Practical Design Against Pump Pulsations*, New York, No Bull Engineering PLLC., 1999.
- Delfino et al., *Residual strain effects on the field in a thick wall finite element model of the human carotid bifurcation.*, Journal of Biomechanics, 30, 777–786.
- Demeulenaere, B., Schutter, J . *Accurate Realization of Follower Motions in High-Speed Cam-Follower Mechanisms.*, PROCEEDINGS OF ISMA, III, 2002, 1107-1116.

Dobrin et al., *Mechanical factors predisposing to intimal hyperplasia and medial thickening in autogenous vein grafts*. *Surgery*, 105, 1999, 393–400.

Duby, Jeffrey., *Design and Construction of a Pulsatile Flow Generator*., Major Qualifying Project Report-WPI, BJS-2004 ME, 2004

Dyantek Delta. *Model SVP216 Vascular Graft and Tube Testing System Manual*., Missouri, 2000.

Elad, D. & Shmuel E.. *Standard handbook of Biomedical Engineering and Design. Chapter 3: Physiological and flow properties of blood*., New York, McGraw Hill, 2003.

Enduratec. *9100 Series Stent/Graft Testing System Manual*, Minnesota, 2000

Feng, J., Long, Q., & Khir, A.W., *Wave dissipation in flexible tubes in the time domain: In vitro model of arterial waves*, *Journal of Biomechanics*, 2006.

Fereshteh-Saniee, F., et al. *An experimental study on the behavior of glass-epoxy composite on low strain rates*, *Journal of Material Processing Technology*, 162-163, 2005, 39-45.

Folkow, B. & Neil, E., *Circulation*., New York, Oxford University Press, 1971.

Fox, S. I., *Concepts of Human Anatomy and Physiology*, 5th E., Brown Publishers, 1998.

Friedman et al., *Correlation between intimal thickness and fluid shear in human arteries*. *Atherosclerosis*, 39, 1981, 425–436.

Fuster, V., et al. *The Vulnerable Atherosclerotic Plaque: Understanding Identification, and Modification*, New York, Futura Publishing Inc., 1999.

Grabowski, S. R., & Torta G., *Principles of Anatomy and Physiology*., 10th ed., Hobokon, John Wiley & Sons, Inc., 2003.

Hartford CG, Marcos EF, Rogers GC. *Noninvasive versus invasive blood pressure measurement in normotensive and hypotensive baboons*. *Lab Anim Sci.*, 46, 1996, 231–233.

Hayashi, K. *Experimental approaches on measuring the mechanical properties and constitutive laws of arterial walls*. *J. Biomech. Eng.*, 115, 1993, 481-488.

Hofer et al., *Numerical study of wall mechanics and fluid dynamics in end-to-side anastomoses and correlation to intimal hyperplasia*. *Journal of Biomechanics*, 29, 1996, 1297–1308.

Hughes & How, *Flow structures at the proximal side-to-end anastomosis: influence of geometry and flow division*., *Journal of Biomechanical Engineering*, 117, 1995, 224–236.

Jie Chen, Xi-Yun Lu, *Numerical investigation of the non-Newtonian pulsatile blood flow in a bifurcation model with a non-planar branch*, Journal of Biomechanics, 39, 2006, 818–832.

Kleinstreuer et al., *Flow input waveform effects on the temporal and spatial wall shear stress gradients in a new femoral graft-artery connector.*, Journal of Biomechanical Engineering, 118, 1996, 506–510.

Lei et al., *Computational design of a bypass graft that minimizes wall shear stress gradients in the region of the distal anastomosis.*, Journal of Vascular Surgery, 25, 1997, 637–646.

Makoto K., *Interactions of Tribology and the Operating Environment: Super low friction of DLC applied to engine cam follower lubricated with ester-containing oil.*, Proceedings of the 32nd Leeds-Lyon Symposium on Tribology, 39:12, 2006, 1682-1685.

Marieb, Elaine N., *Anatomy & Physiology.*, San Francisco, Benjamin Cummings, 2002.

McDonald, D. A., *Blood Flow in Arteries.*, Baltimore, The Williams & Wilkins Company, 1974.

Mohiaddin, RH, Underwood, RS et. Al., *Regional aortic compliance studied by magnetic resonance imaging: the effects of age, training, and coronary artery disease*, British Heart Journal, 62, 2000, 90-96.

Newman DL, Westerhof N, Sipkema P., *Modeling of aortic stenosis.*, J. Biomech., 12, 1979, 229-235.

Ojha, M., *Wall shear stress temporal gradient and anastomotic intimal hyperplasia.*, Circulation Research, 74, 1994, 1227–1231.

Pfeffer JM, Pfeffer MA, Frohlich ED. *Validity of an indirect tail-cuff method for determining systolic arterial pressure in unanesthetized normotensive and spontaneously hypertensive rats*, J Lab Clin Med., 78, 1971, 957–962.

Safar, H, et al. *Aortic Pulse Wave Velocity and Independent Marker of Cardiovascular Risk*, Cardiovascular Research, 95, 2002, 1215-1218.

Schwartz et al., *Myointimal thickening in experimental vein grafts is dependent on wall tension.* Journal of Vascular Surgery, 15, 1992, 176–186.

Smith H-J & J. Zagzebski, *Basic Doppler Physics*, 1991, 55.

Staalsen et al., *The anastomosis angle does change the flow fields at vascular end-to-side anastomoses in vivo.* Journal of Vascular Surgery, 21, 1995, 460–471.

Taylor, C.A., Hughes, T.J.R., Zarins, C.K., *Effect of exercise on hemodynamic conditions in the abdominal aorta.*, Journal of Vascular Surgery, 29, 1999, 1077–1089.

Taylor et al., *Finite element modeling of three-dimensional pulsatile flow in the abdominal aorta: relevance to atherosclerosis.*, *Annals of Biomedical Engineering*, 26, 1998, 975–987.

Walker, R., Smith, R., Sherriff, S., & Wood, R., *Latex vessels with customized compliance for use in arterial flow models*, *Physiol. Meas.*, 20, 1999, 277-286.

White et al., *Hemodynamic patterns in two models of end-to-side vascular graft anastomoses: effects of pulsatility, flow division, Reynolds number, and hood length.*, *Journal of Biomechanical Engineering*, 115, 1993, 104–111.

Young DF, Tsai FY., *Flow characteristics in models of arterial stenoses: I Steady flow.*, *J Biomech*, 6, 1973, 395-410.

Online Resources

Arteries, 2006, North Harris College Biology Department,
<http://science.nhmccd.edu/biol/cardio/artery.htm>

Atherosclerosis Treatment, 2006,
www.diseasesexplained.com/HardeningofTheArteries/atherotreatment.html

Atrial Fibrillation, 2006., www.a-fib.com/EKGsignal.htm

Blood Viscoelasticity: Frequently Asked Questions., 2000, Vilastic Scientific Inc.,
www.vilastic.com/FAQ_Blood.html

Cardiovascular Disease Statistics, American Heart Association., 2007,
www.americanheart.org/presenter.jhtml?identifier=4478

Elastic Constants, 2006,
www.efunda.com/formulae/solid_mechanics/mat_mechanics/elastic_constants_E_nu.cfm

Plasma Viscosity and Blood Viscoelasticity., 2000, Vilastic Scientific Inc.,
www.vilastic.com/tech10.html

Short Time Fourier Transform., National Instruments, 2007,
<http://zone.ni.com/devzone/cda/ph/p/id/235>

Hardening of the Arteries, 2006,
www.diseasesexplained.com/HardeningofTheArteries/symptomsfathero.html

What is Hemodynamics, 2000, International Hemodynamic Society
<http://www.hemodynamicsociety.org/hemodyn.html>

IX. Nomenclature

μ, η	Fluid Viscosity	cP
E	Elastic Modulus	GPa
σ	Stress	GPa
ε	Strain	cm/cm
C	Compliance	cm/s
τ	Shear Stress	kg/cm ³
P	Pressure	mmHg
R	Radius	cm
D	Diameter	cm
Q	Flow Rate	cm ³ /s
A	Area	cm ²
ρ	Fluid Density	kg/cm ³
l	Length	cm
h	Wall Thickness	cm
a_i	Point Radius	cm
c_0	Pulse Wave Velocity	cm/s

X. Appendices

Appendix A: Piston Slider-Crank Kinematic Analysis

Motor Speed (rpm)	ω (rad/s)	r (m)	l (m)	D_{piston} (m)	M_{piston} (kg)	A (m ²)	P (Mpa)	d (m)
120	12.56637061	0.0381	0.127	0.02032	0.03	0.000324293	10700	0.026940768

$\cos(\phi) = \sqrt{1 - \left(\frac{r}{L} \sin \theta\right)^2}$

$x = \left[r + \frac{r^2}{4L}\right] - r \cos \theta + \frac{r}{4L} \cos(2\theta)$

$\dot{x} = r\omega \sin \theta + \frac{r}{2L} \sin(2\theta)$

$\ddot{x} = r\omega^2 \left[\cos \theta + \frac{r}{L} \cos(2\theta)\right]$

$F_{Pressure} = P \times A$

$F_{Net} = F_{Pressure} - F$

$T = I \times \alpha = F_{Total} \times d$

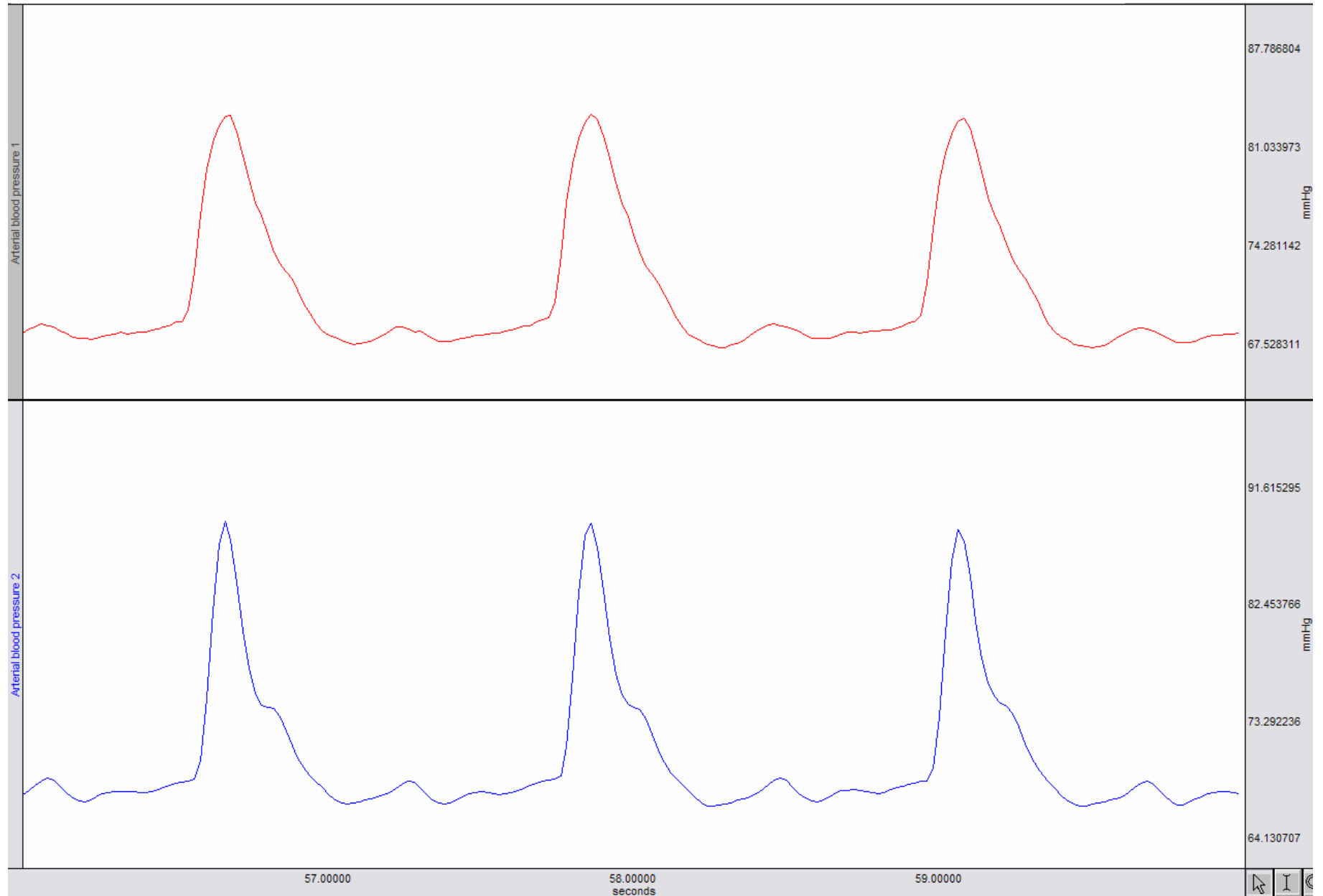
$F_{Kinetic} = M \times a$

$F_{Total} = F_{Net} \cos(\phi)$

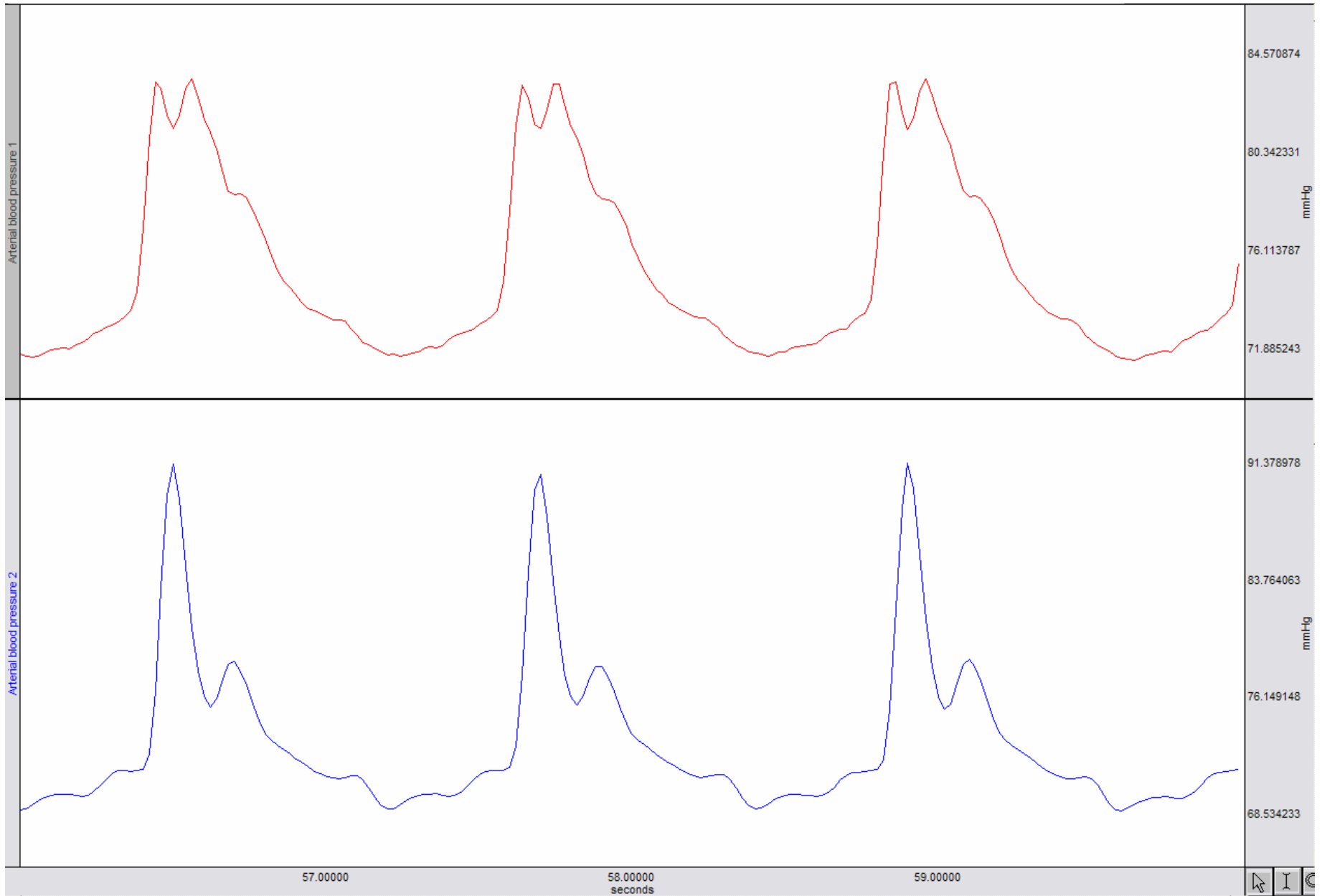
F_p	F_i	F_n	F_t
3.469932817	0.165918309	3.30401451	3.2288185
θ (°)	θ (rad)	ϕ (rad)	ϕ (°)
45	0.785398163	0.21375613	12.247324
15	0.261799388	0.07772395	4.453254
30	0.523598776	0.07772395	4.453254
45	0.785398163	0.21375613	12.247324
60	1.047197551	0.26282298	15.058647
75	1.308996939	0.29399461	16.844651
90	1.570796327	0.30469265	17.457603
105	1.832595715	0.29399461	16.844651
120	2.094395102	0.26282298	15.058647
135	2.35619449	0.21375613	12.247324
150	2.617993878	0.15056827	8.6269266
165	2.879793266	0.07772395	4.453254
180	3.141592654	0	0

Displacement _{piston} (x)	Velocity _{piston} (x')	Acceleration _{piston} (x'')	Torque (Nm)	Torque (lb-in)
0.014016732	0.410364488	5.530610301	0.086986851	0.769795142

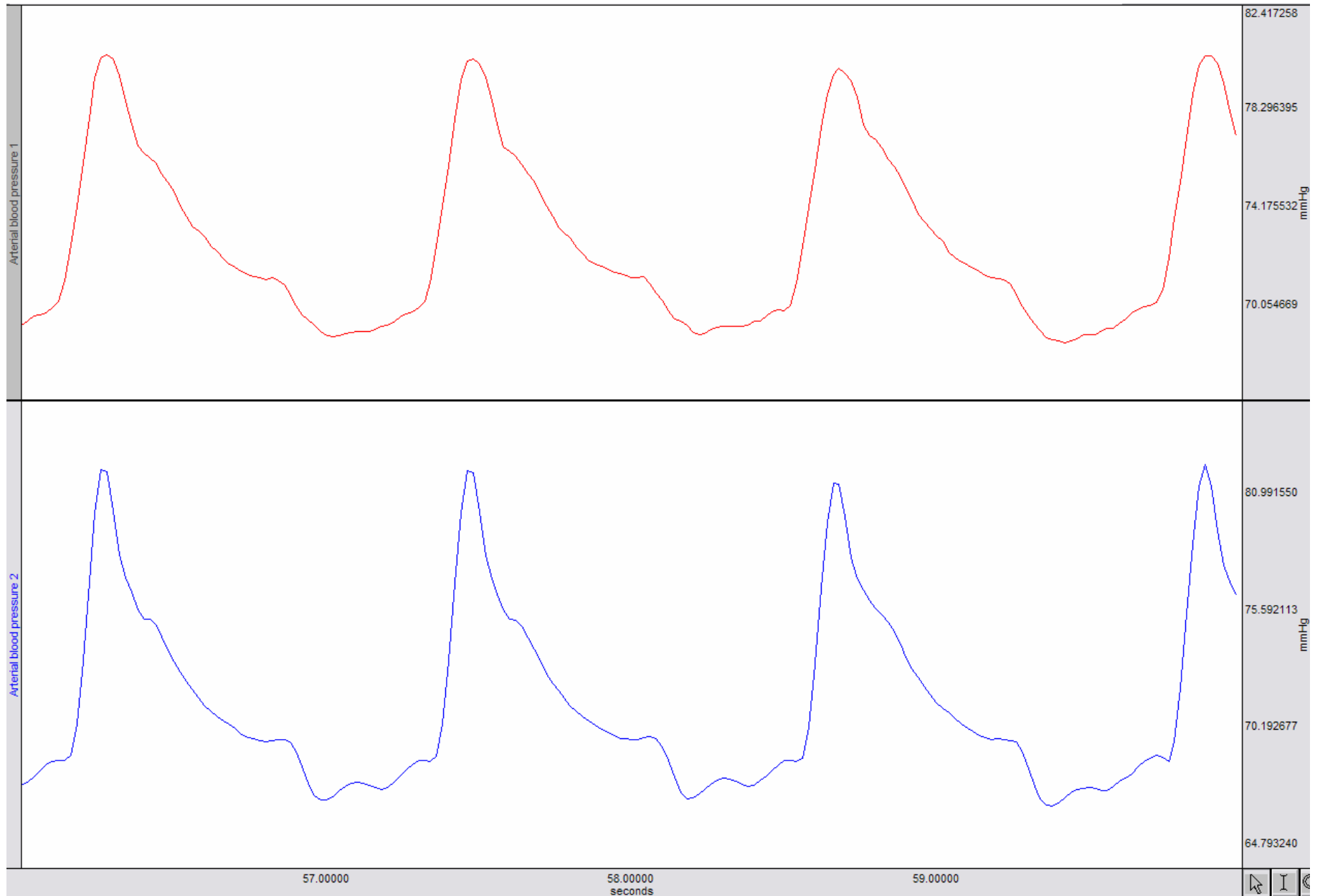
Appendix B: Pulsatile Flow Pressure Waveforms



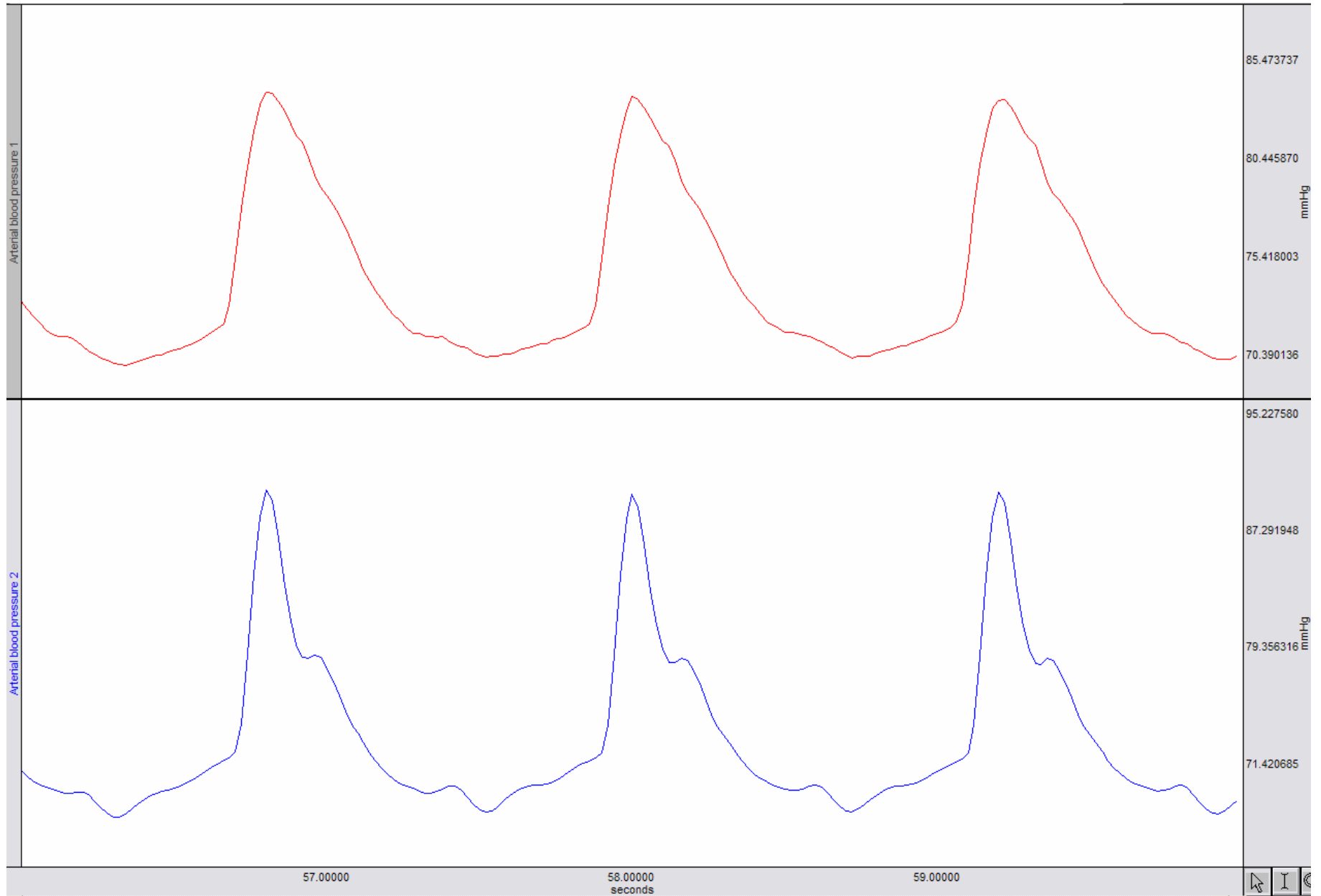
Arterial Model #6_3 – Thickness = .07cm



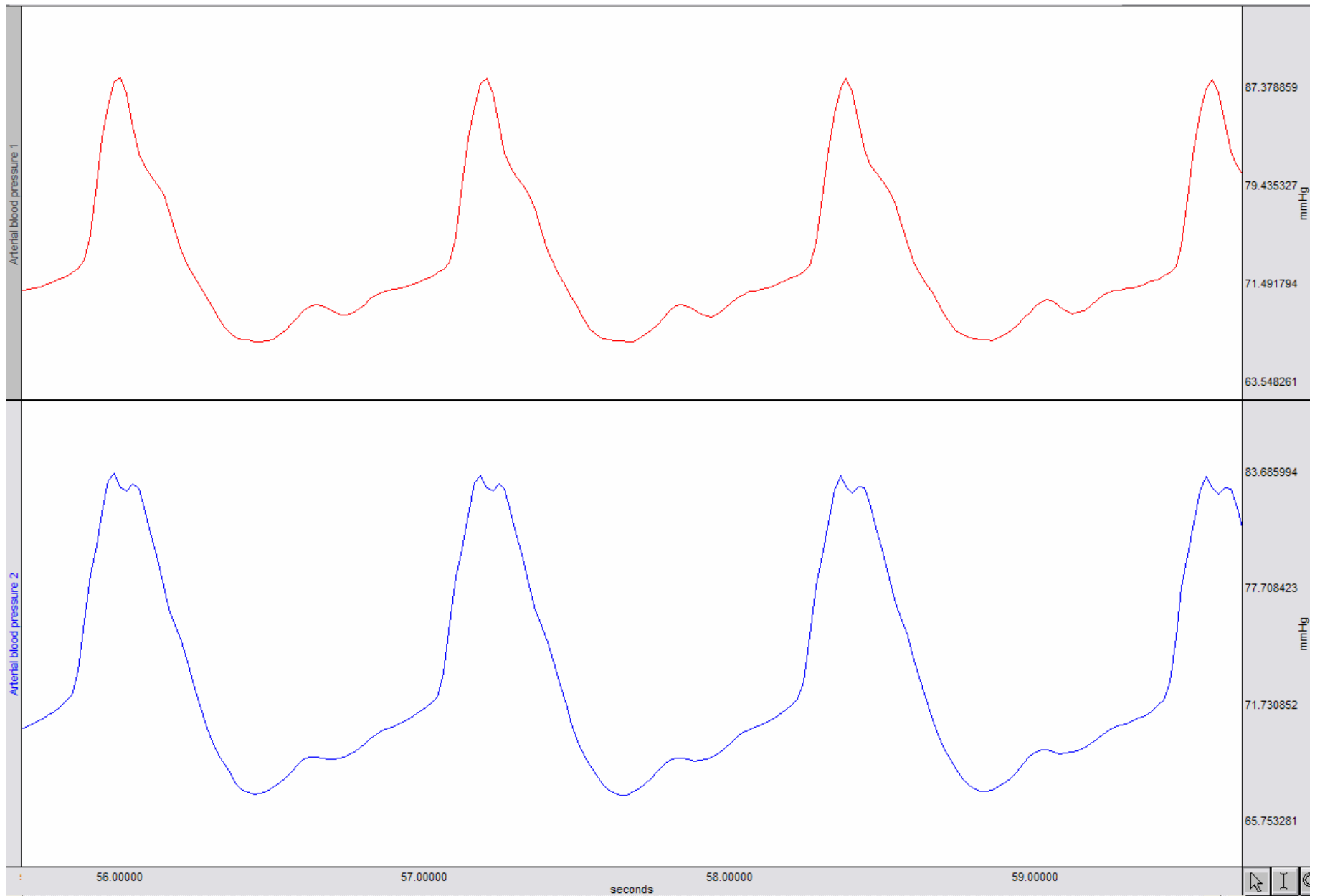
Arterial Model #8_2 – Thickness = .08cm



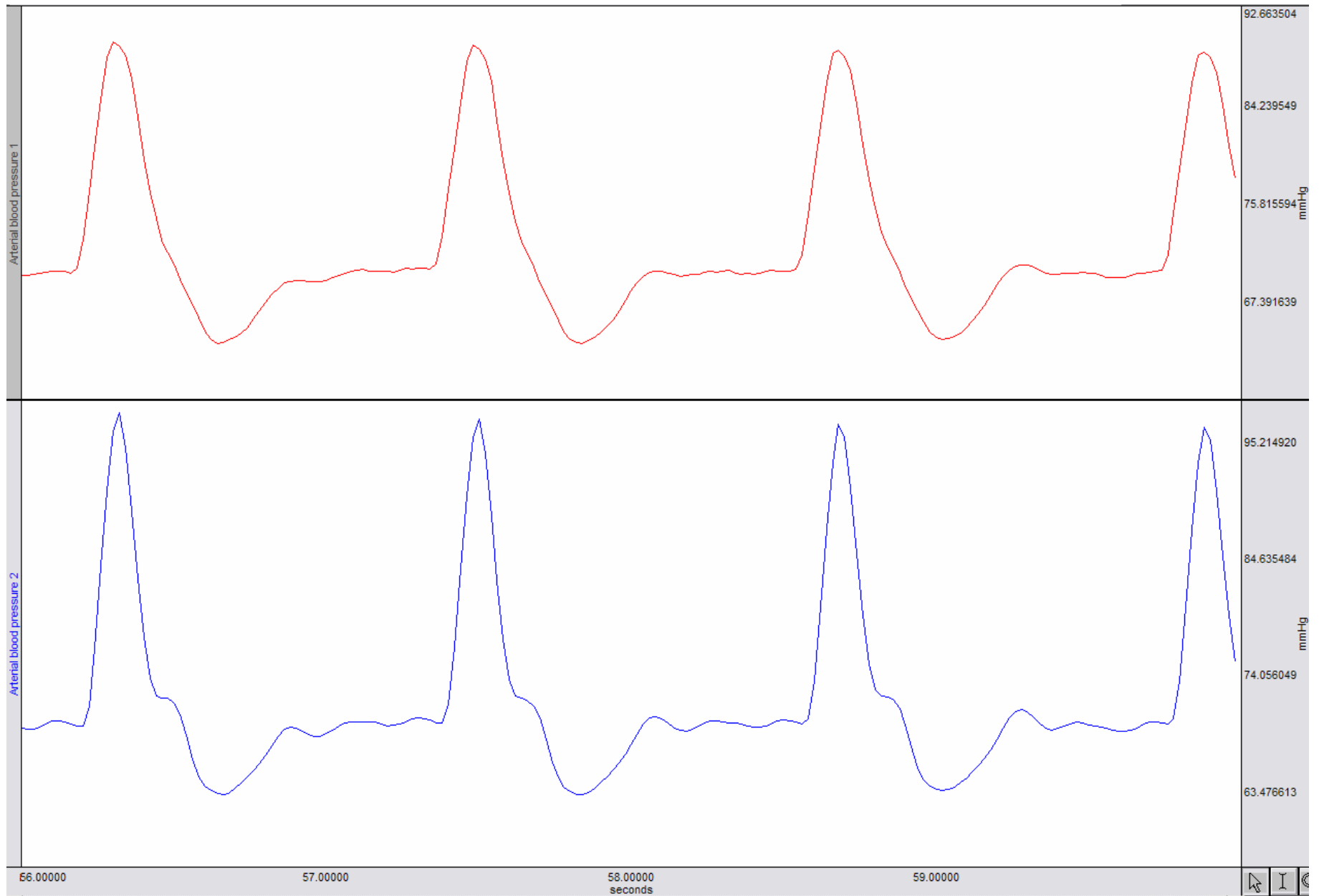
Arterial Model #8_3 – Thickness = .08cm



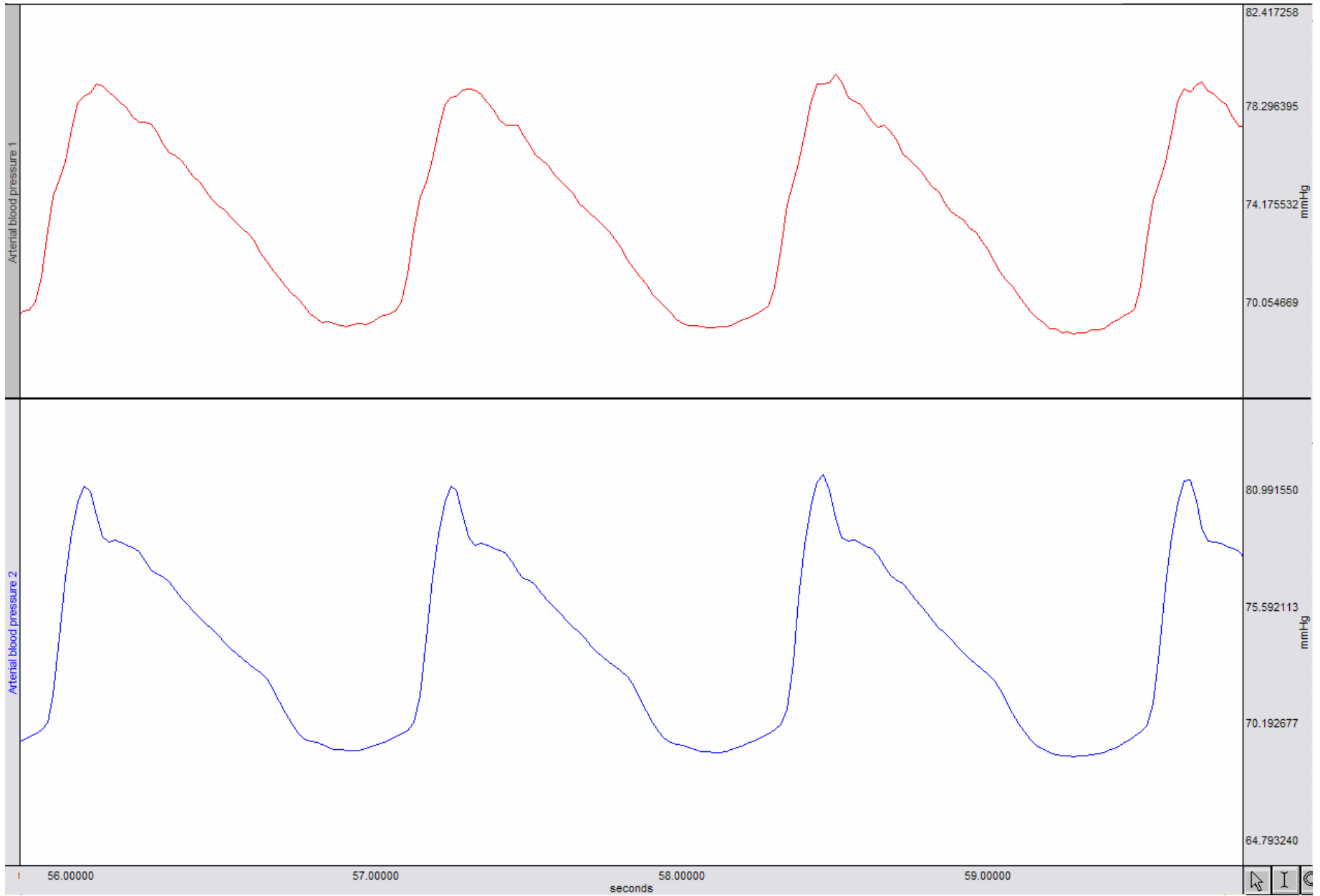
Arterial Model #10_2 – Thickness = .09cm



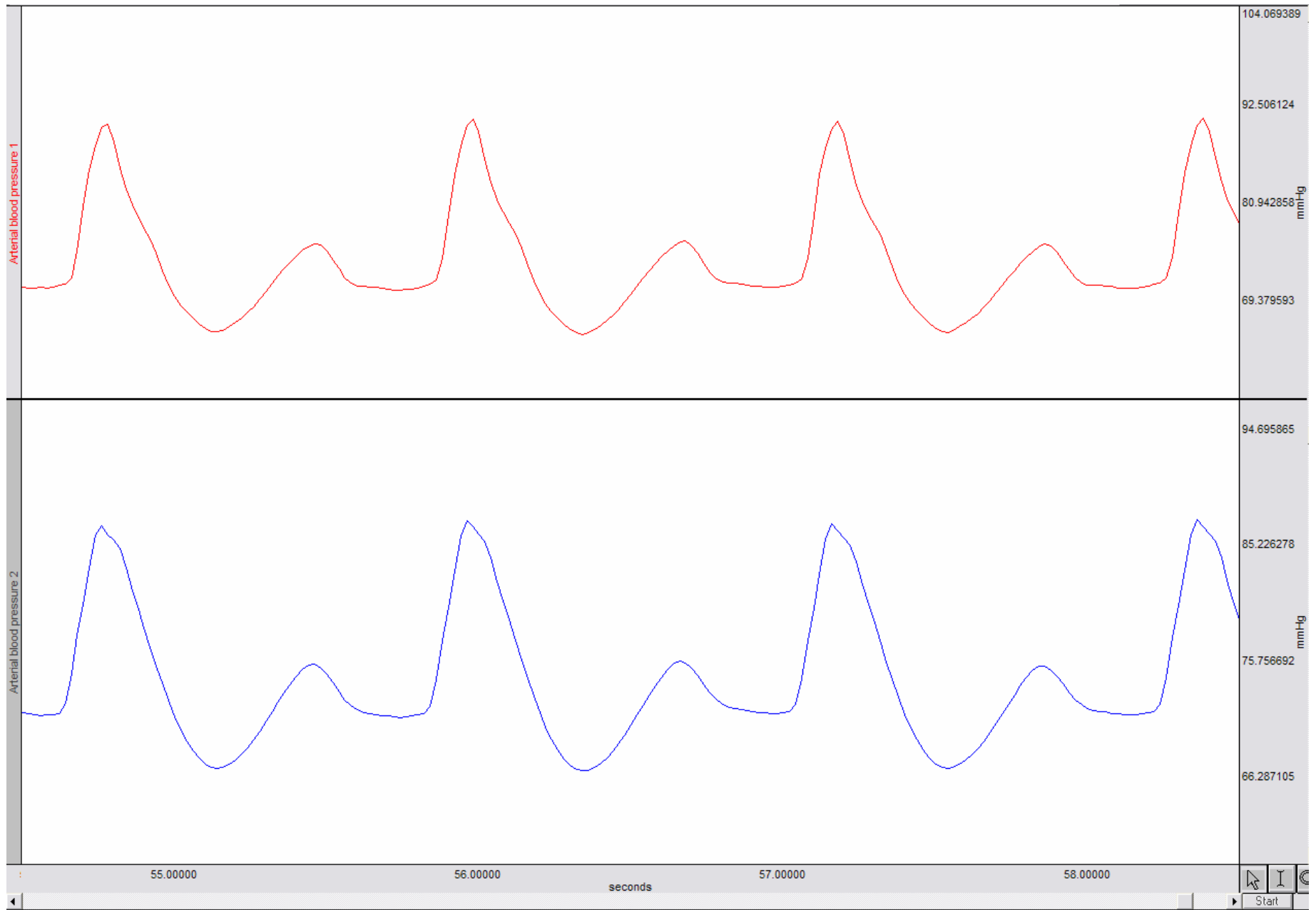
Arterial Model #10_3 – Thickness = .11cm



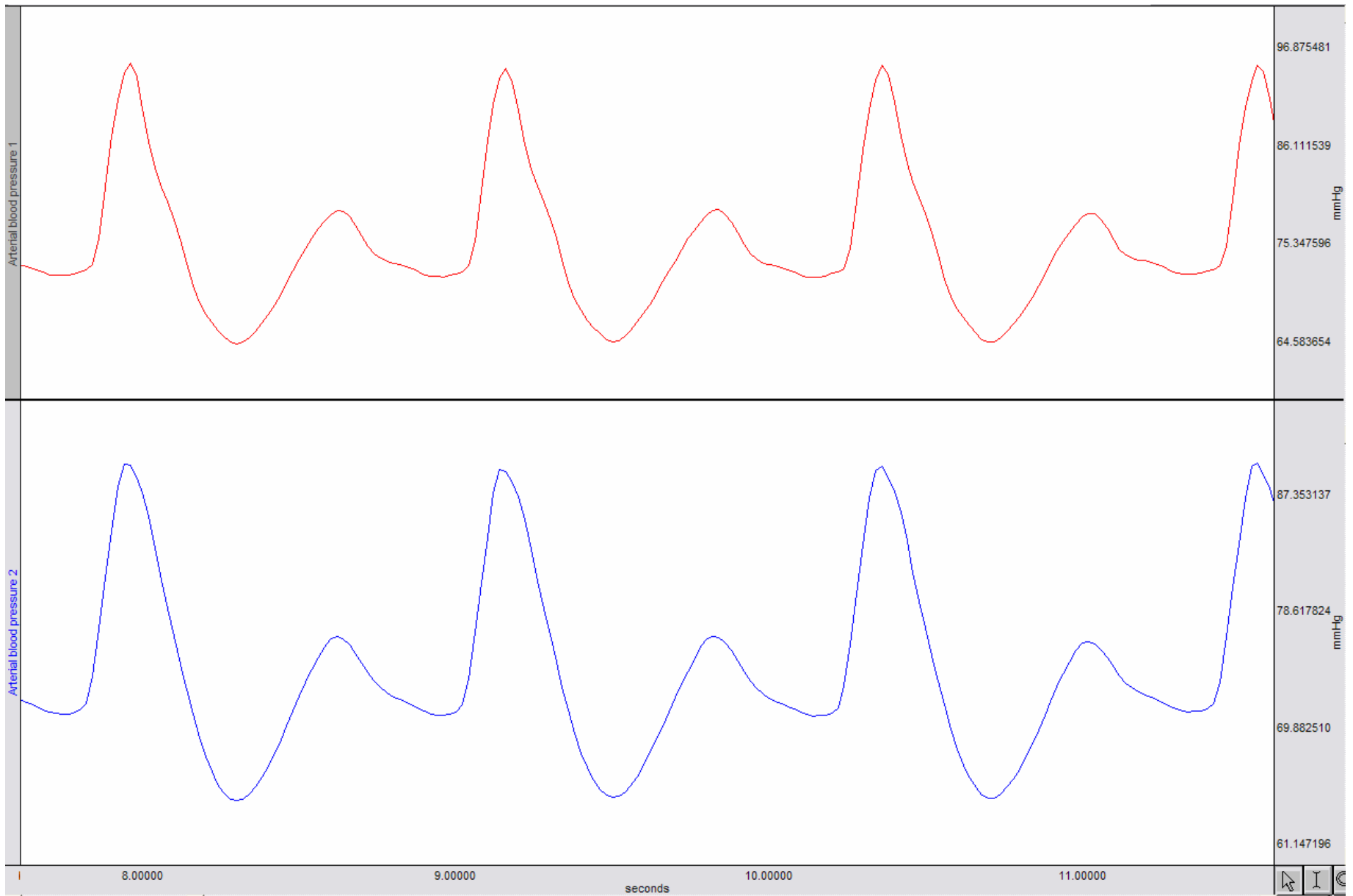
Arterial Model #12_1_1 – Thickness = .14cm



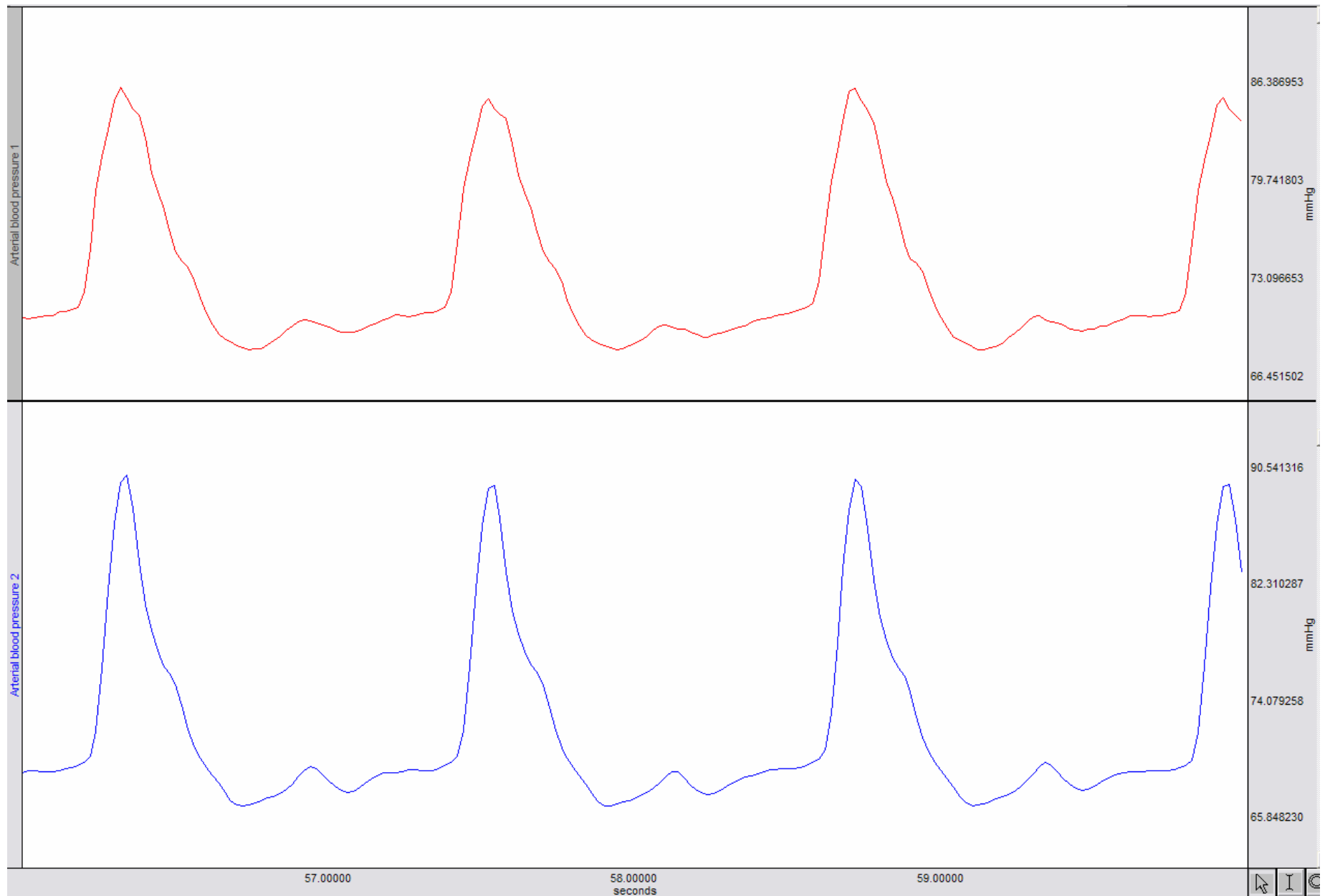
Arterial Model #12_1_2 – Thickness = .15cm



Arterial Model #3_8ths Occlusion

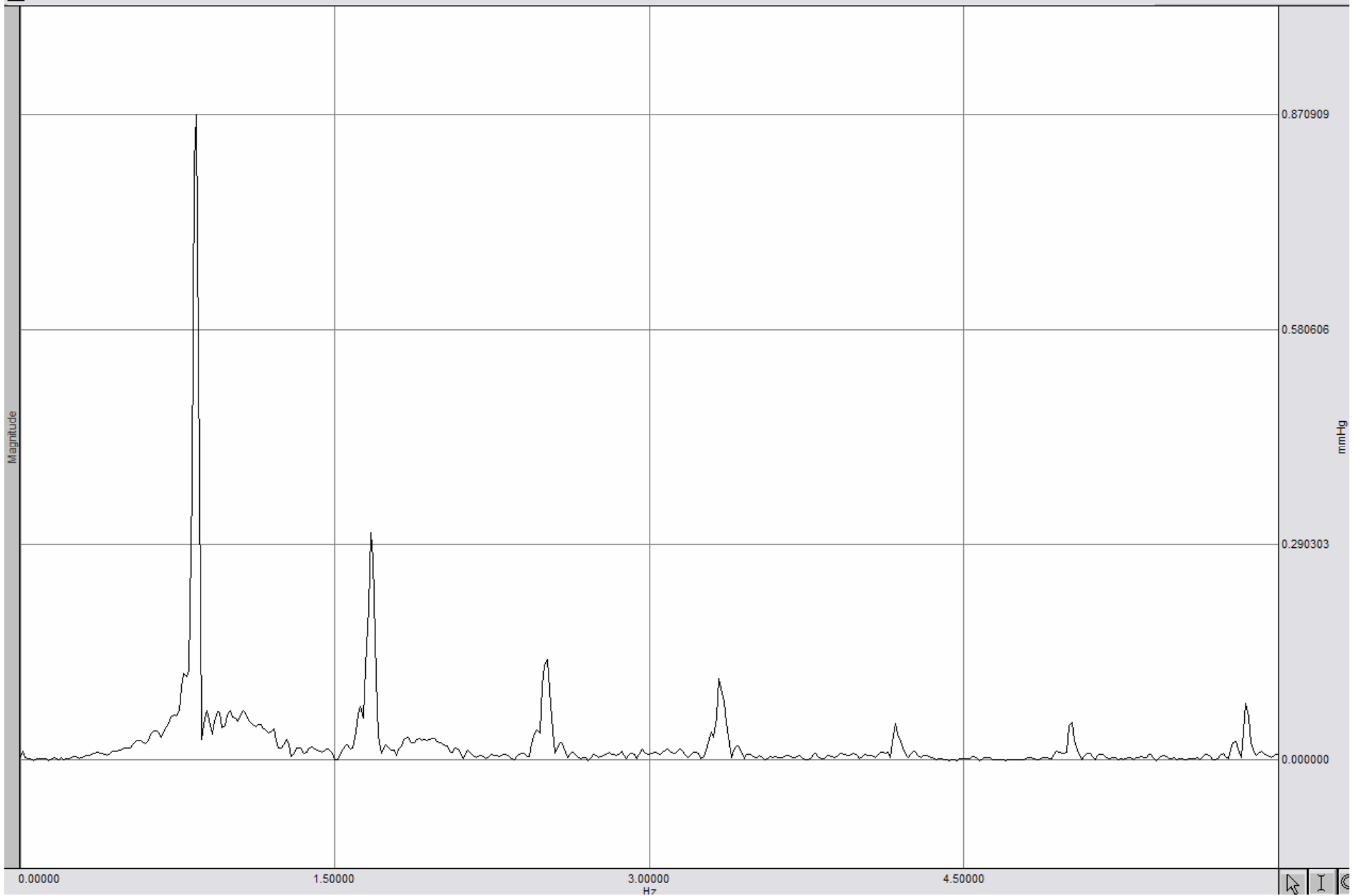


Arterial Model #4_8ths Double Occlusion

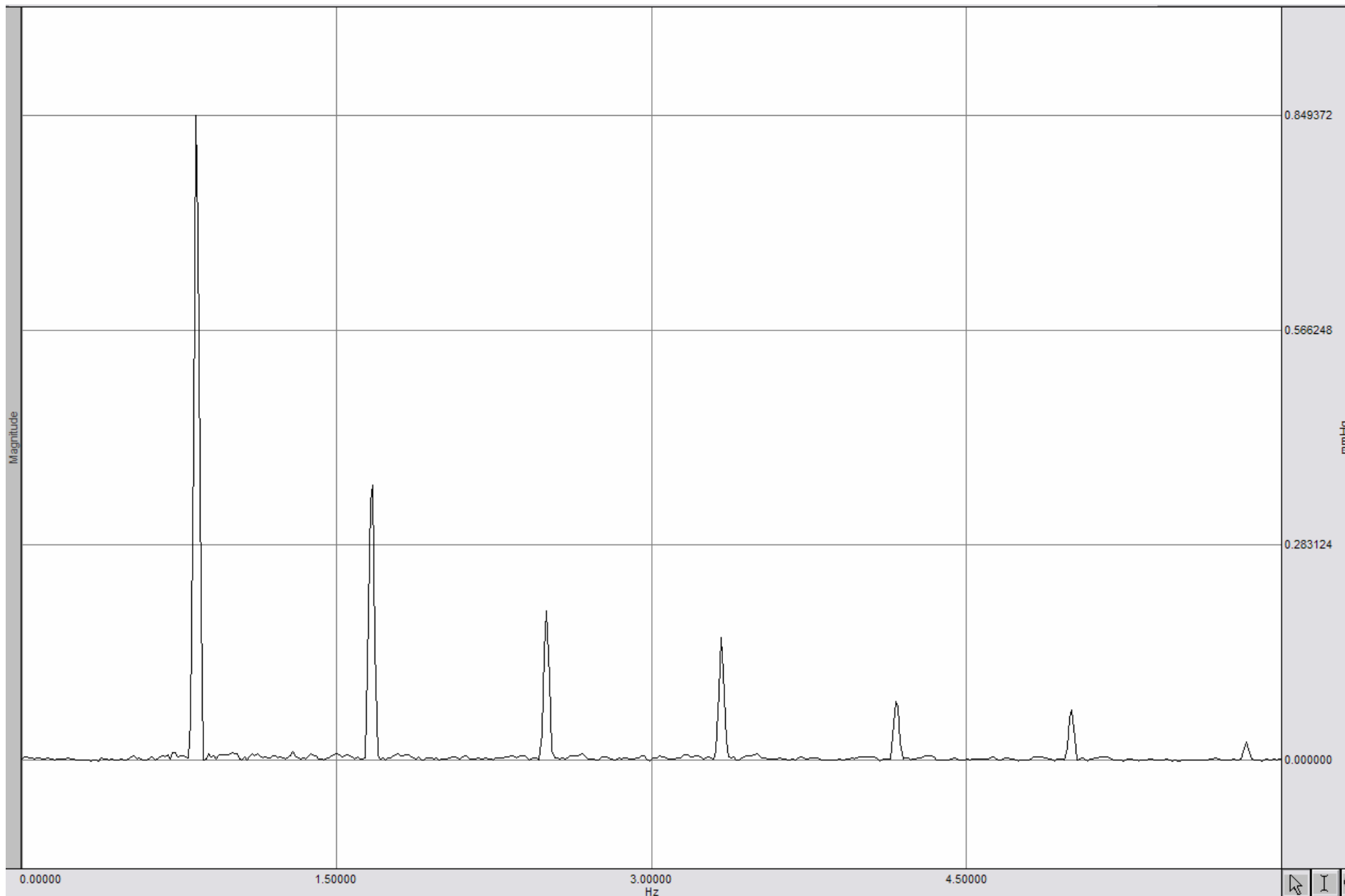


Arterial Model #6_8ths Double Occlusion

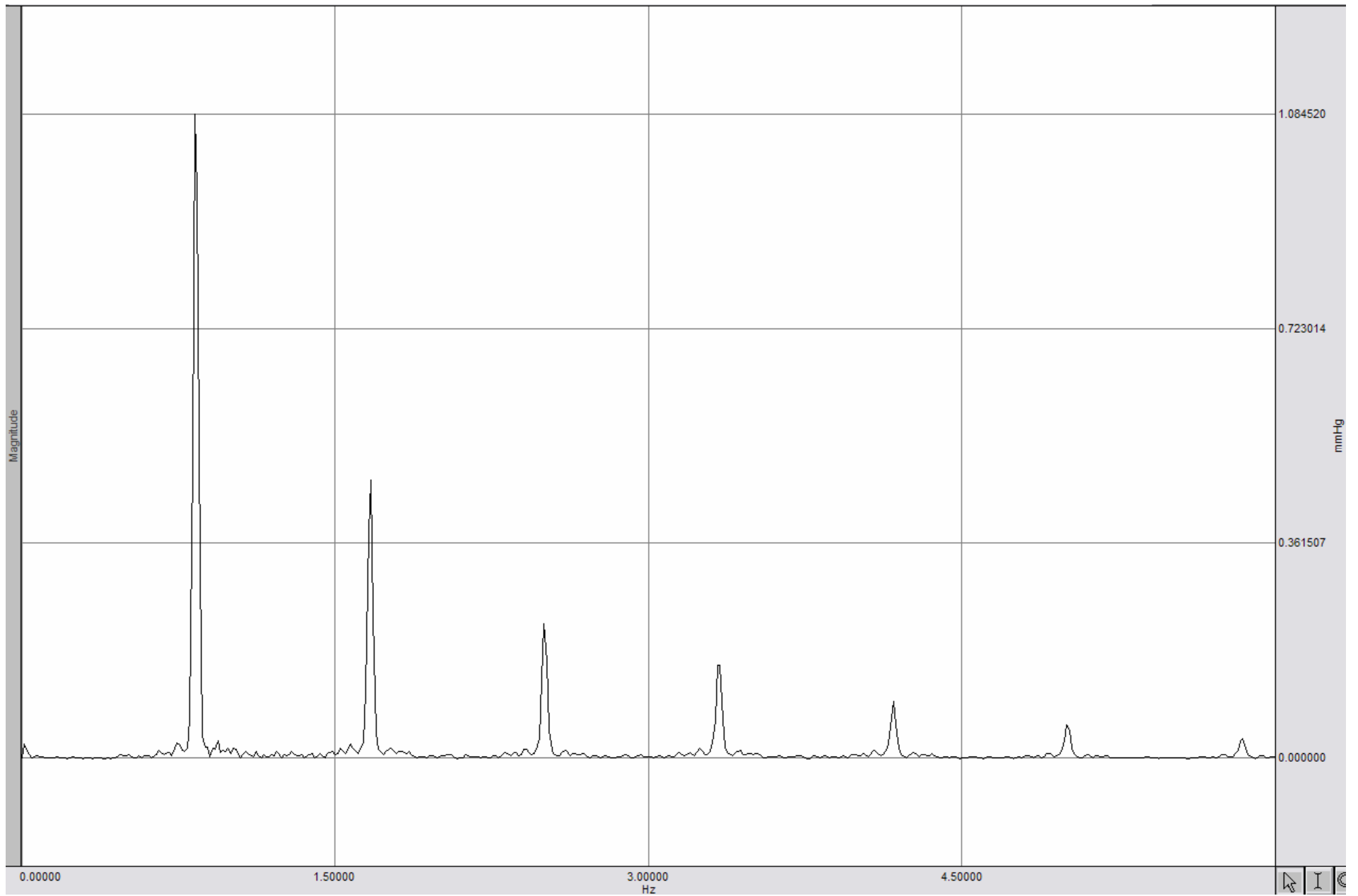
Appendix C: Pressure Waveform Fast Fourier Analysis



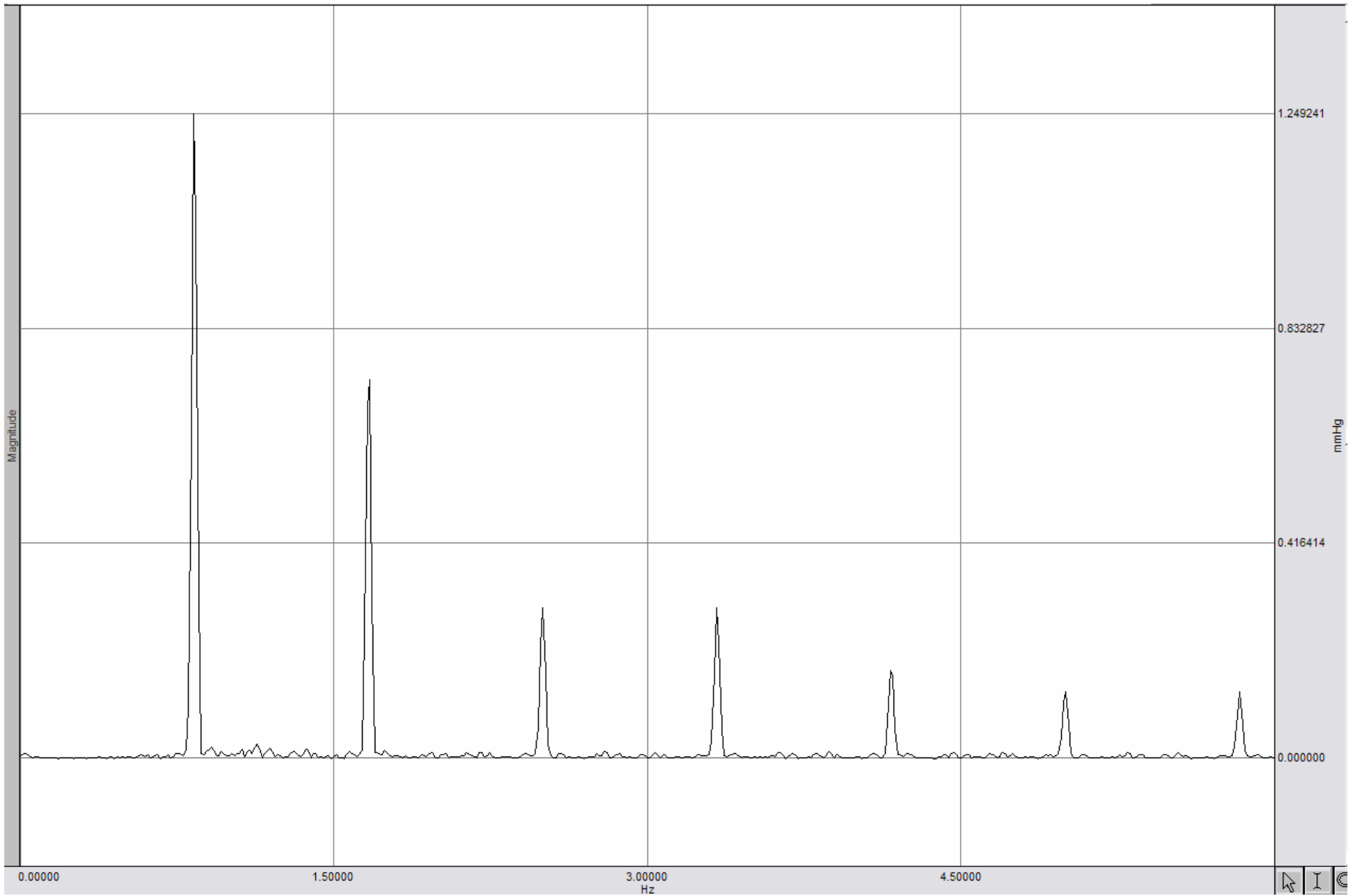
Arterial Model #8_2 - FFT



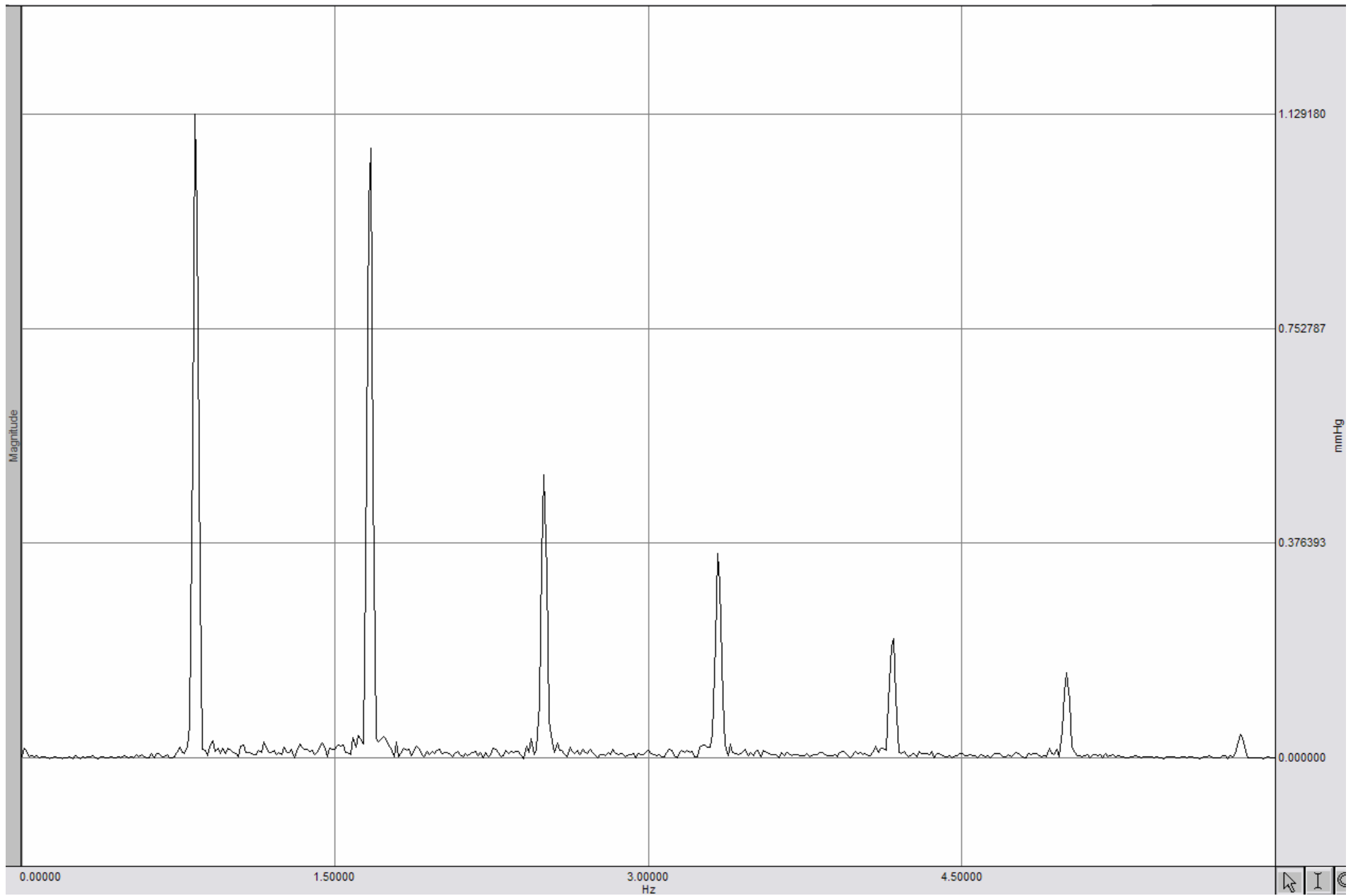
Arterial Model #8_3 – FFT



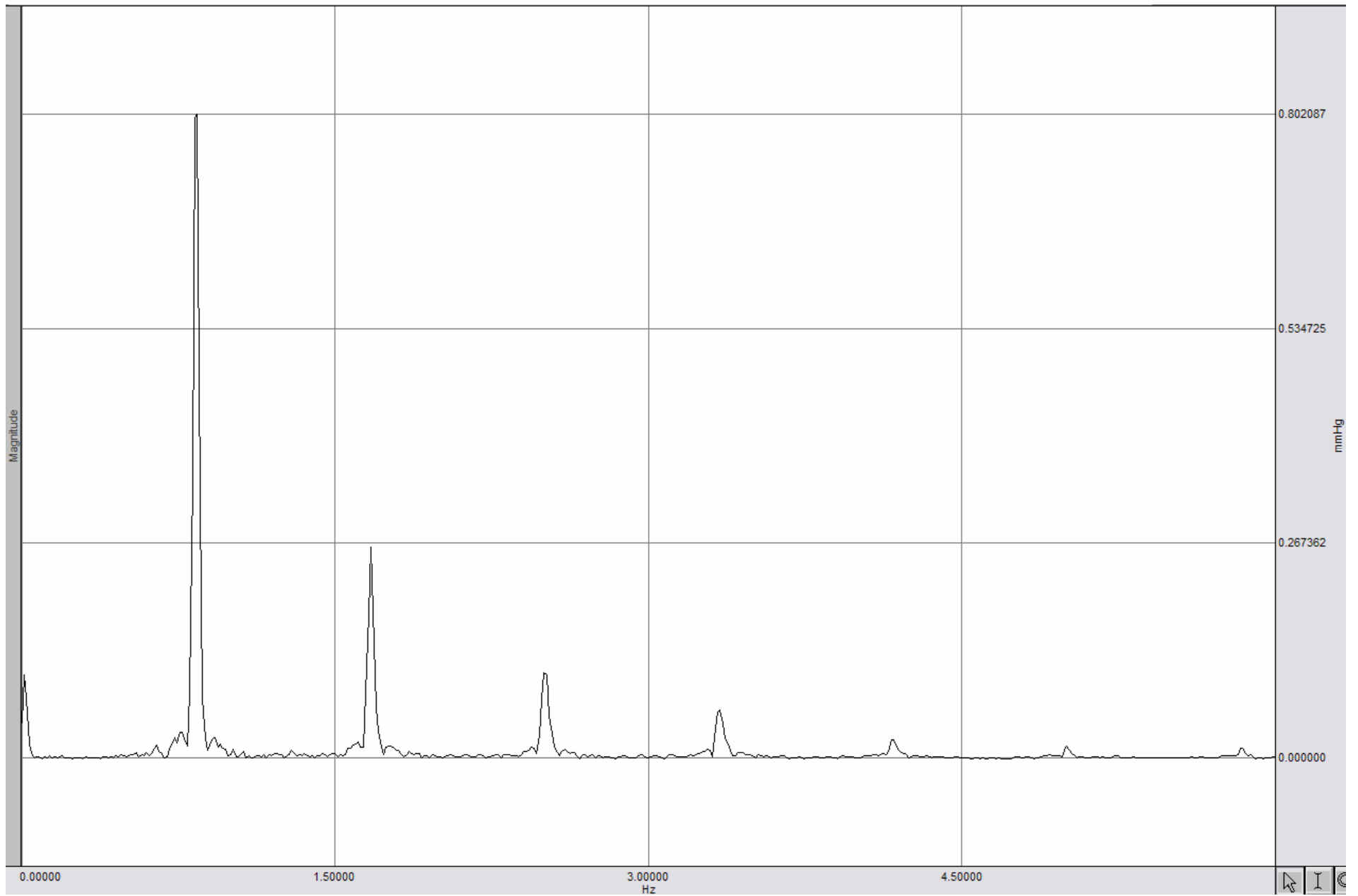
Arterial Model #10_2 – FFT



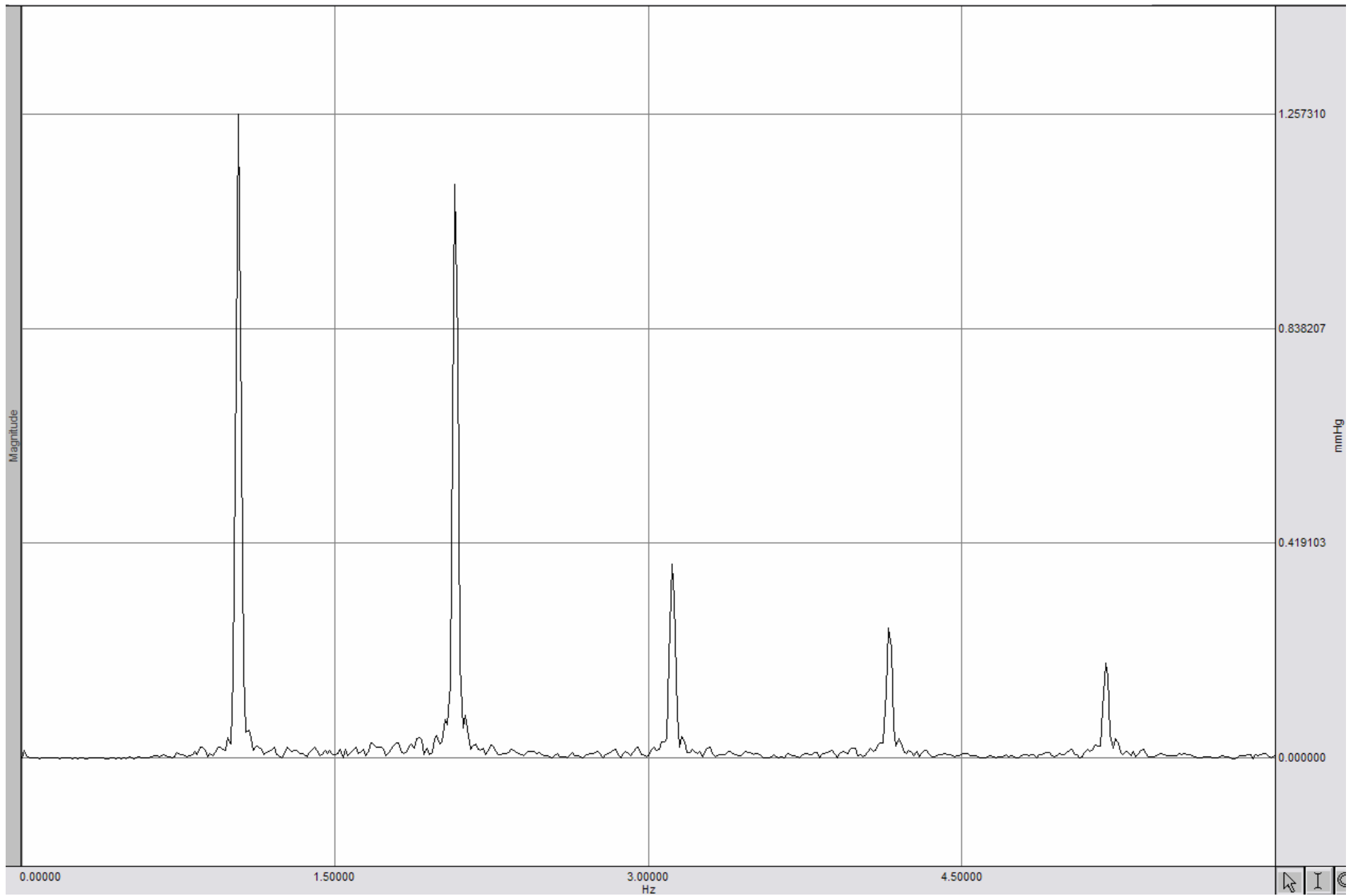
Arterial Model #10_3 – FFT



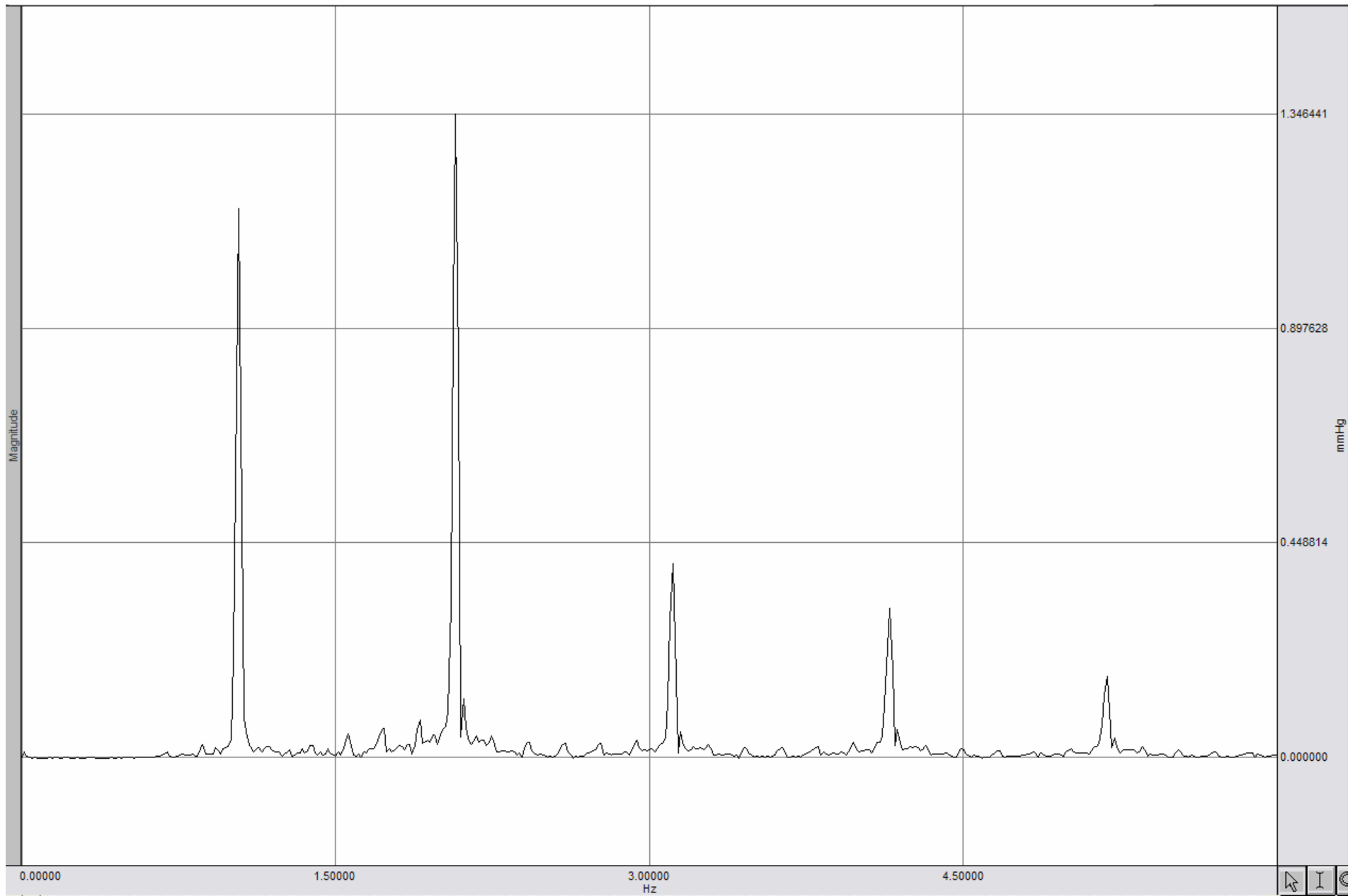
Arterial Model #12_1_1 – FFT



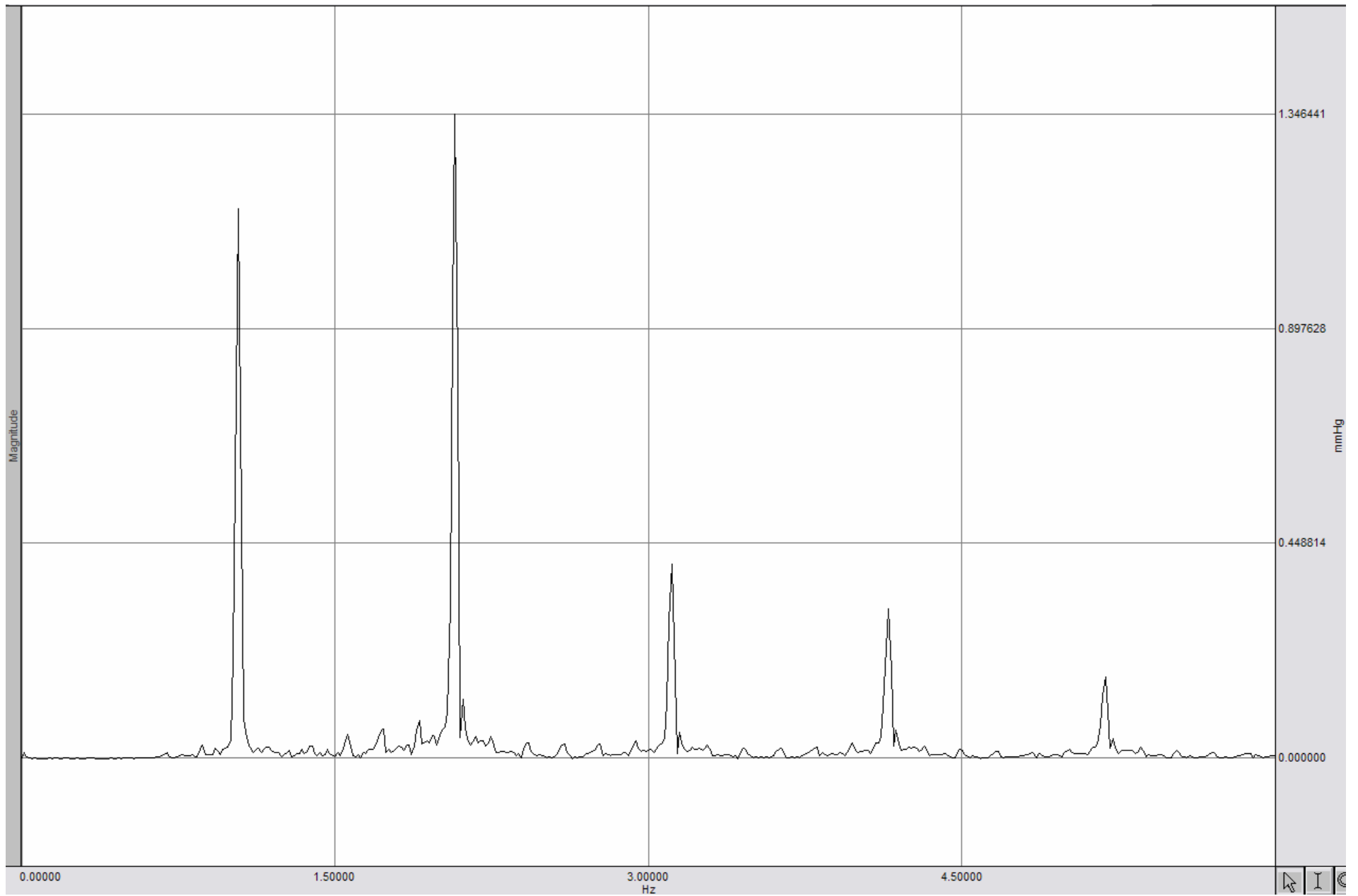
Arterial Model #12_1_2 – FFT



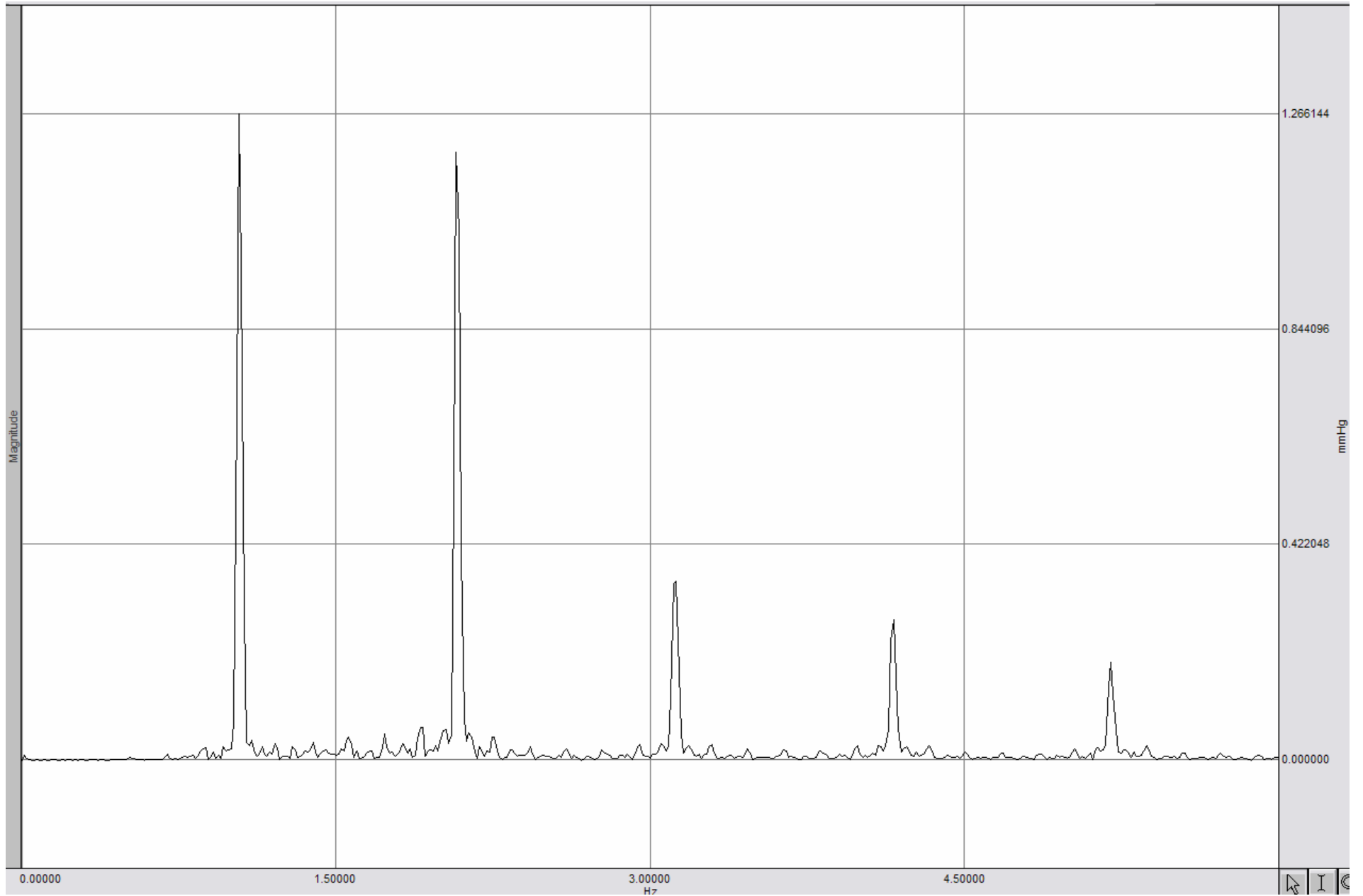
Arterial Model #2_8ths Occlusion FFT



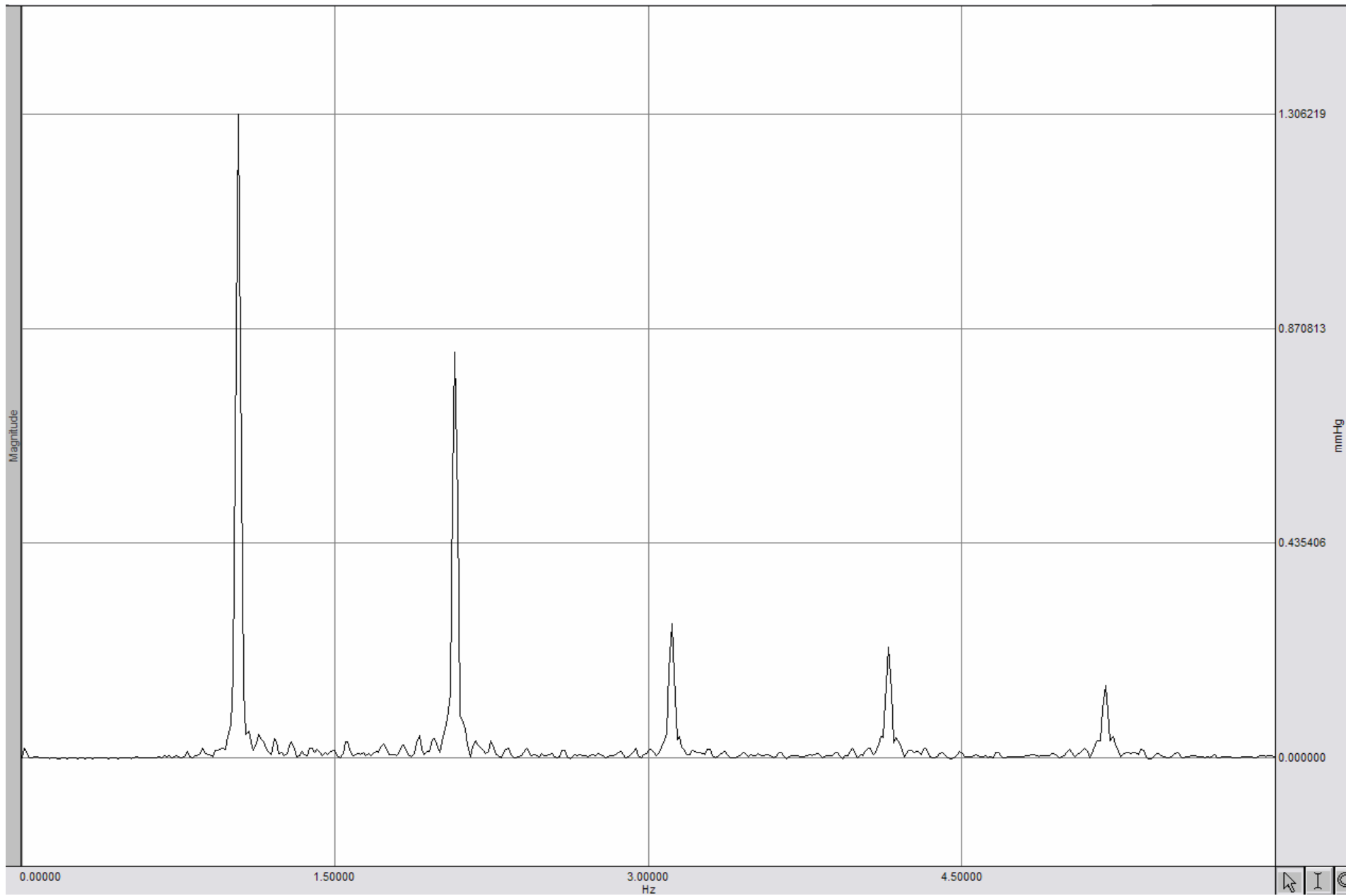
Arterial Model #3_8ths Occlusion FFT



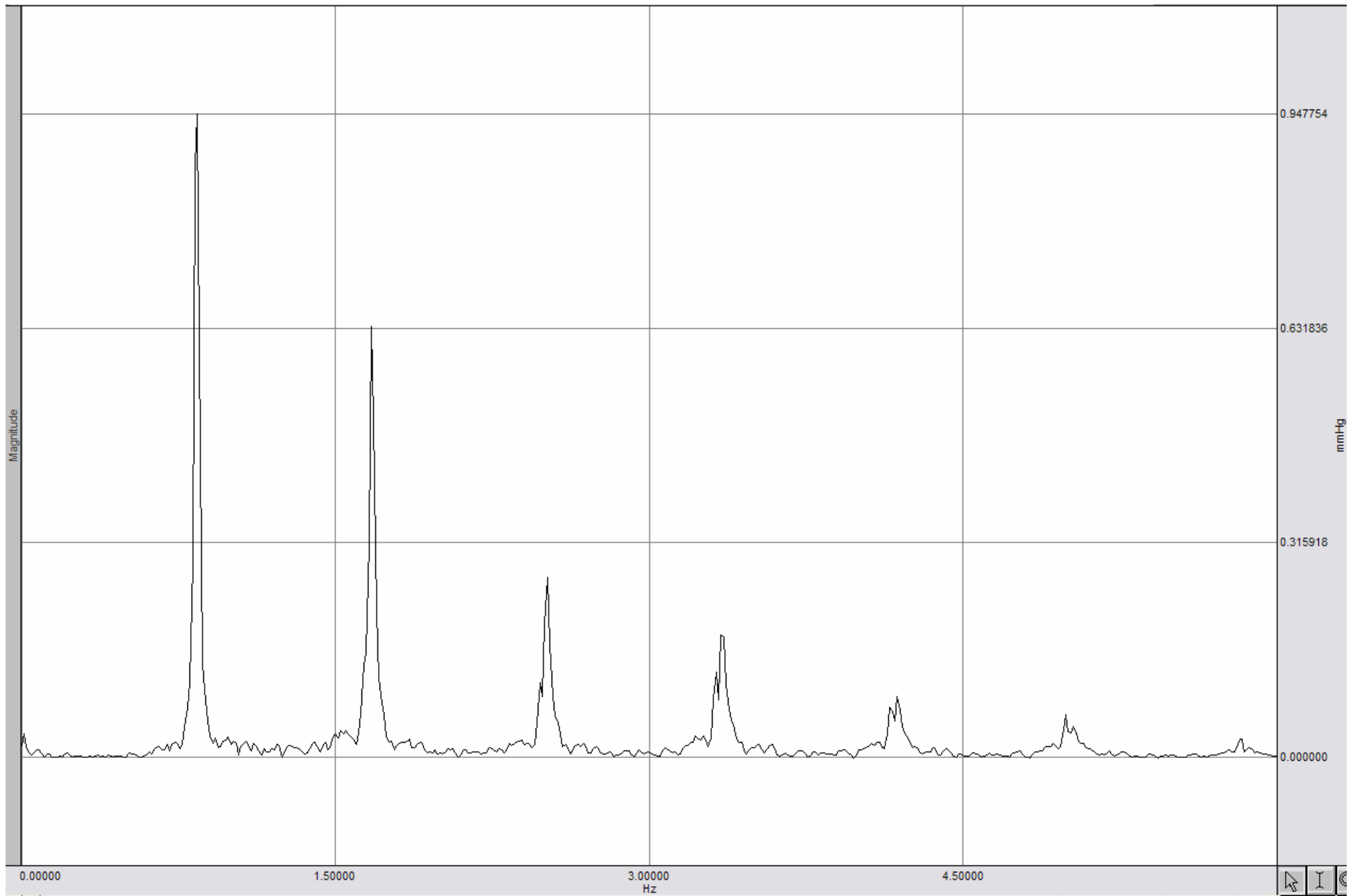
Arterial Model #4_8ths Occlusion FFT



Arterial Model #4_8ths Double Occlusion FFT



Arterial Model #6_8ths Double Occlusion FFT

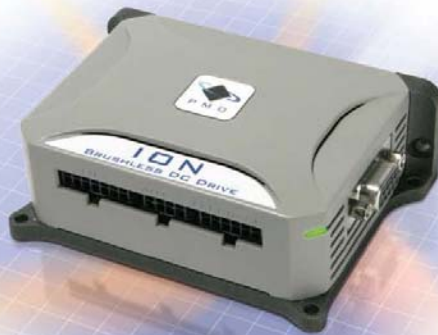


Arterial Model #6_3 – FFT

Appendix D: ION Digital Drive



The ION Digital Drive



The ION™ Digital Drive is a compact, fully enclosed module that provides high performance motion control, network connectivity and power amplification for DC brush, brushless DC or step motors. Using advanced MOSFETs and surface mount technology, ION provides very high power density in a rugged, flexible form factor. It performs profile generation, servo compensation, stall detection, field oriented control, digital torque control and many other motion control functions. The single axis ION drive is based on the Magellan Motion Processor, and provides CANBus or serial communications. It is ideal for medical, scientific, semiconductor, automation, industrial and robotic applications.

User selectable profiling modes include S-curve, trapezoidal, velocity contouring and electronic gearing. The ION Digital Drive accepts commands over the network

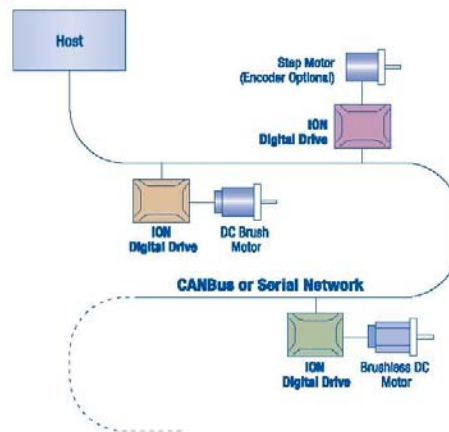
such as position, velocity, acceleration and jerk from the host and generates a corresponding trajectory on-the-fly. Servo loop compensation utilizes a full 32-bit position error, PID with velocity and acceleration feedforward, integration limit and dual biquad filters for sophisticated control of complex loads. Additional features include limit switches, breakpoints, secondary encoder input for master-slave and electronic gearing applications, as well as general purpose inputs and outputs.

The ION's Magellan Motion Processor provides a flexible and powerful instruction set to initialize and control the motion application, monitor performance, and synchronize overall drive behavior. Working with the ION Digital Drive, PMD's powerful Pro-Motion® GUI makes it easy to graph and analyze system performance, while C-Motion® and VB-Motion allow you to develop your own application using C/C++ or Visual BASIC.

> FEATURES

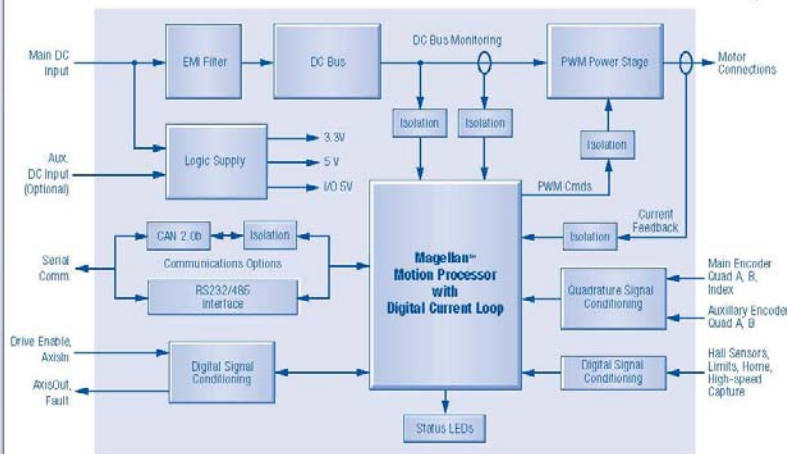
- Enhanced Magellan™ instruction set
- Complete single axis motion module
- All digital drive
- DC brush, brushless DC and step motor versions
- CANBus or serial communications
- S-curve, trapezoidal, velocity contouring and electronic gearing profiles
- Compact, powerful package
- 500 W capability
- 8 Amps continuous, 15 Amps peak current
- Optional heatsink for increased current capability
- 12 - 56 volt single power source
- High efficiency MOSFETs
- 40 kHz PWM frequency
- 102 µsec servo loop rate
- Auxiliary encoder input supports gearing & dual loop applications
- Position, velocity and current loops
- Field oriented control
- Sinusoidal commutation
- Stall detection & auto current reduction
- Includes Pro-Motion, C-Motion and VB-Motion software
- Separately programmable acceleration and deceleration value changes on-the-fly
- Advanced PID filter with velocity and acceleration feedforward
- Programmable dual biquad filters

> CONFIGURATION



Technical Overview

> POWER RATINGS

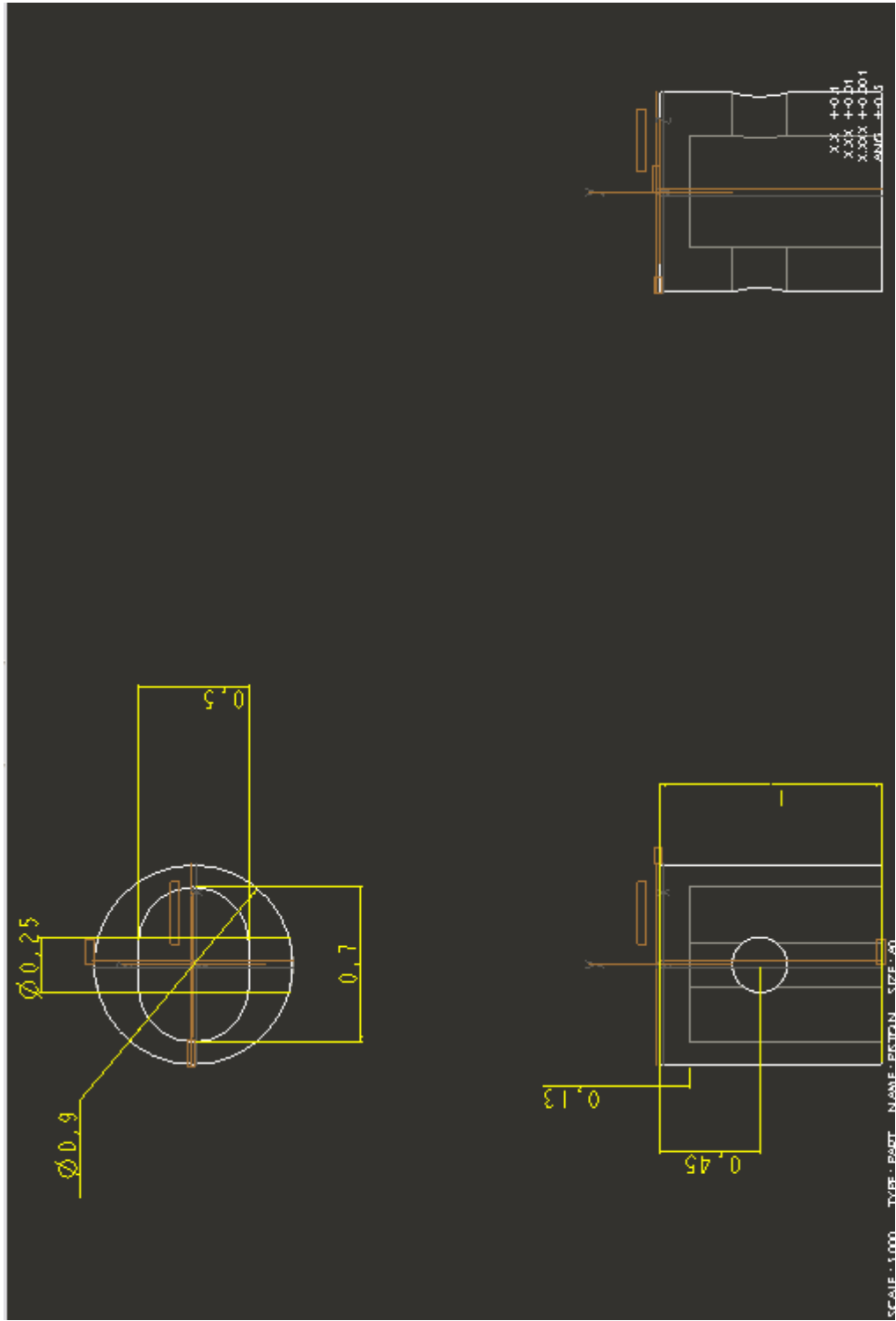


DC Brush	
Voltage input	12 – 56 VDC
Continuous current output	8 ADC (panel mount, T<50 C)
Peak current output (2 sec)	15 ADC
Continuous power output	400 W (panel mount, T<50 C)
Brushless DC	
Voltage input	12 – 56 VDC
Continuous current output	8 A rms (panel mount, T<50 C)
Peak current output (2 sec)	15 A rms
Continuous power output	500 W (panel mount, T<50 C)
Step	
Voltage input	12 – 56 VDC
Continuous current output	5 A rms (panel mount, T<50 C)
Peak current output (2 sec)	Not applicable
Continuous power output	350 W (panel mount, T<50 C)

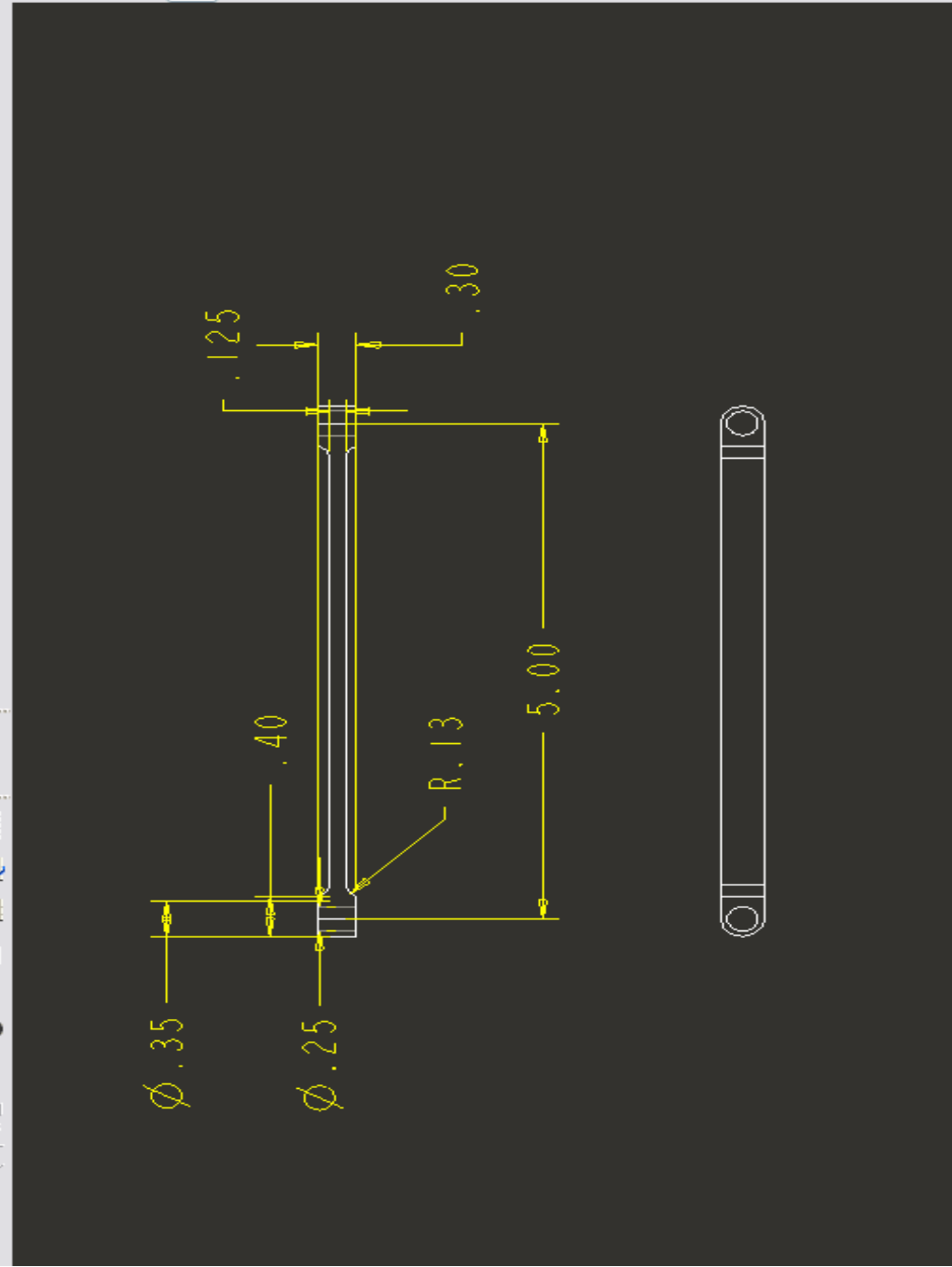
> SPECIFICATIONS

<p>Supported motor types DC brush, brushless DC, step motor</p> <p>Supported communications options RS232/485 and CANBus</p> <p>Profile modes S-curve point-to-point: Position, velocity, acceleration, deceleration, jerk Trapezoidal point-to-point: Position, velocity, acceleration, deceleration Velocity-contouring: Velocity, acceleration, deceleration Electronic gearing: Using auxiliary encoder</p> <p>Filter parameters Scalable PID with Vel + Acc feedforward, integration limit, offset bias, dual liquid filter and settable derivative sampling time</p> <p>Position error tracking Motion error window allows axis to be stopped upon exceeding programmable window. Tracking window allows flag to be set if axis exceeds a programmable position window.</p>	<p>Digital current loop Scalable PI with integration limit, torque control, PI current limiting</p> <p>Brushless DC commutation modes Sinusoidal, 6-step, field oriented control</p> <p>Microstepping resolution Up to 256 steps/step</p> <p>PWM frequency 20 kHz or 40 kHz (user selectable)</p> <p>Maximum encoder rate Up to 10 M counts/sec</p> <p>Loop rates Commutation & current loop: 51.2 µsec Position loop & trajectory generator: 102.4 µsec to 1.6 sec</p> <p>Signals Differential inputs: Encoder A, Encoder B, Index, Aux Encoder A, Aux Encoder B Digital inputs: Hall A, Hall B, Hall C, Home, +Limit, -Limit, Axial, High-speed capture Digital output: AxisOut</p>	<p>Power connectors Motor: 5-pin Molex MiniFit Jr. DC Bus: 3-pin Molex MiniFit Jr.</p> <p>Communications connector RS232/485 version: DB9 CAN version: Dual RJ45</p> <p>Signal connectors: Motor feedback: 12-pin Molex MicroFit 3.0 Auxiliary encoder: 8-pin Molex MicroFit 3.0 I/O: 14-pin Molex MicroFit 3.0</p> <p>Available encoder & I/O power 5V @ 300 mA Short circuit protected</p> <p>Safety and protection Short circuit protection: line-to-line, line-to-power supply and line-to-case Interlocks: Enable input and Fault output Overvoltage shutdown Overtemperature shutdown</p>	<p>Mechanical Dimensions: 4.3" (109 mm) x 2.9" (74 mm) x 1.5" (38 mm) Weight: 0.75 lb (0.34 kg) Enclosure protection: IP20</p> <p>Mechanical options Heatsink: 4.3" (109 mm) x 2.9" (74 mm) x 1" (25 mm) DIN Rail mounting adapter</p> <p>Environmental Operating temperature: 0 to 50 C Storage temperature: -20 to 85 C Humidity: 0 to 95% RH (non-condensing) Altitude: Up to 20000 meters without derating Contamination: Pollution Degree 2</p> <p>Compliance CE marked: EN62024-1, EN55011, EN61000-6-1, EN61000-6-3 RoHS Designed to UL508c</p>
----------------------------------------------------------------------------------------------------------------------------------------------------------------------------------------------------------------------------------------------------------------------------------------------------------------------------------------------------------------------------------------------------------------------------------------------------------------------------------------------------------------------------------------------------------------------------------------------------------------------------------------------------------------------------------------------------------------------------------------------------------------------------------------------------------------------------------------------------------	----------------------------------------------------------------------------------------------------------------------------------------------------------------------------------------------------------------------------------------------------------------------------------------------------------------------------------------------------------------------------------------------------------------------------------------------------------------------------------------------------------------------------------------------------------------------------------------------------------------------------------------------------------------------------------------------------------------------------------------------------------------------------------------	--------------------------------------------------------------------------------------------------------------------------------------------------------------------------------------------------------------------------------------------------------------------------------------------------------------------------------------------------------------------------------------------------------------------------------------------------------------------------------------------------------------------------------------------------------------------------------------------------------------------------------------------------------------------------------------------	--------------------------------------------------------------------------------------------------------------------------------------------------------------------------------------------------------------------------------------------------------------------------------------------------------------------------------------------------------------------------------------------------------------------------------------------------------------------------------------------------------------------------------------------------------------------------------------------------------------------------------------------

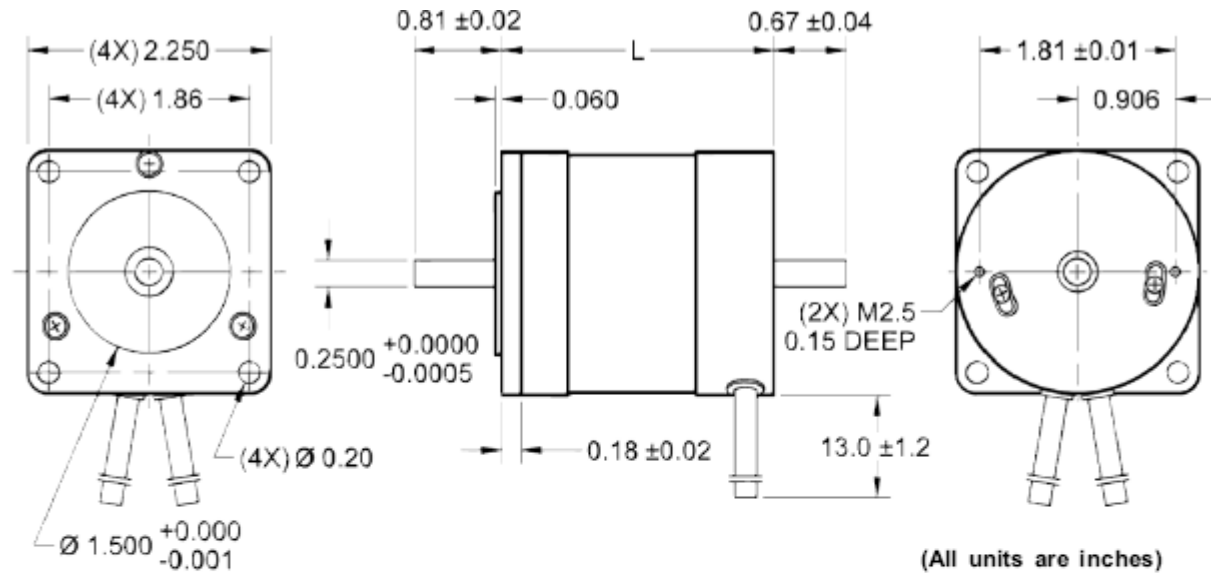
Appendix E: Piston CAD Drawing



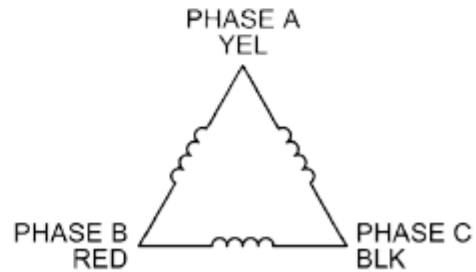
Appendix F: Connecting Rod CAD Drawing



Appendix G: DC Motor Specifications



Wire Color	Description
Red	Hall Supply
Blue	Hall A
Green	Hall B
White	Hall C
Black	Hall Ground
Yellow	Phase A
Red	Phase B
Black	Phase C



Step Angle Accuracy:	+/- 5% (Full Step, No Load)	Insulation Resistance:	100M Ohm Min, 500VDC
Resistance Accuracy:	+/- 10%	Dielectric Strength:	500VDC for one minute
Inductance Accuracy:	+/- 20%	Radial Play:	0.0001" at 1.0 lbs
Temperature Rise:	80° C Max (2 Phases On)	End Play:	0.0001" at 8.8 lbs
Ambient Temperature:	-20° to +50° C	Max Radial Force:	16.9 lbs (0.79" from flange)
Insulation Type:	Class B	Max Axial Force:	3.4 lbs-Force

Appendix H: Pressure Transducer Specifications





Figure 8: BIOPAC Pressure Transducer

BIOPAC SS13L Pressure Transducer	
Operational Pressure:	-50 mmHg to 300 mmHg
Overpressure:	-400 to + 4000 mmHg
Dynamic response:	100 Hz
Transducer Dimensions:	67mm long, 25mm wide
Weight:	11.5 grams
Unbalance:	50 mmHg max
Connection ports:	Male Luer (2)
Eight hour drift:	1 mmHg after 5 minute warm-up
Isolation:	$\leq 5 \mu\text{A}$ leakage at 120 VAC/60 Hz
Defibrillation:	Withstands 5 discharges of 400 joules in 5 minutes across a load
Operating Temperature:	+ 15 to + 40 °C
Storage Temperature:	-30 to + 60 °C
Combined effects of sensitivity linearity and hysteresis:	1 mmHg (nominal)
Output:	5 $\mu\text{V/mmHg}$ (normalized to 1Vexcitation)
Cable Length:	2 meters

Appendix I: Expense Report

<u>Biomedical Engineering Department</u>				
<u>Item Description</u>	<u>Item Quantity</u>	<u>Price</u>	<u>Purchase Date</u>	<u>Receipt/Purchase Order</u>
#17 O-Ring	1 Pack	\$1.97	11/18/2006	
#14 O-Ring	1 Pack	\$1.97	11/18/2006	
#18 O-Ring	1 Pack	\$1.97	11/18/2006	
T6511 3-1/2" Diameter, 1/4" Length Aluminum Rod	4	\$16.80	12/18/2006	
Brushless DC Motor 36VDC & 1000 Line Differential Encoder w/ Index	1	\$107.37	12/21/2007	
Tygon Tubing 1" ID	12.20FT	\$79.91	CH-01/30/2007	
Glycerine	7.50L	\$270.90	CH-01/30/2007	
1/2" ID Tygon Tubing	10FT	\$33.50	CH-02/01/2007	
1L Squeeze Bottle	1	\$5.78	CH-02/01/2007	
3/4" Tygon Tubing	1FT	\$3.35	CH-02/01/2007	
Nitrile Latex Gloves	1 Box	\$10.00	CH-02/01/2007	
5GAL Bucket Lid	1	\$1.38	2/9/2007	
330GPH Direct Drive Pump	1	\$49.97	2/9/2007	
Sliding Drawer	1	\$6.48	2/17/2007	
80" Upright Brackets	2	\$19.94	2/20/2007	
Sheet Metal	2	\$12.88	2/20/2007	
			TOTAL:	\$624.17

Mechanical Engineering Department

<u>Item Description</u>	<u>Item Quantity</u>	<u>Price</u>	<u>Purchase Date</u>	<u>Receipt/Purchase Order</u>
BSL Pressure Transducer	2	\$490.00	11/6/2006	
BK Precision Power Supply	1	\$229.00	11/22/2006	
1x12x4 No.2 Wood	1	\$10.50	1/16/2007	
2x4-96 Stud Wood	1	\$2.07	1/17/2007	
1" Corner Brace	1 Pack	\$1.89	1/17/2007	
Mold Builder	1 Pint	\$12.24	1/23/2007	
Mold Builder	1 Pint	\$12.99	1/25/2007	
Mold Builder	1 Pint	\$12.99	1/28/2007	
Polyurethane Glue	1	\$6.97	1/29/2007	
Vinyl Tubing	4FT	\$3.49	1/29/2007	
Teflon Tape	1 Roll	\$0.70	CH-02/01/2007	
Ethanol	1L	\$3.10	CH-02/01/2007	
1L Plastic Bottle	1	\$3.90	CH-02/01/2007	
Quick Plastic	1	\$2.97	2/5/2007	
5GAL Bucket Lid	1	\$1.99	2/5/2007	
3/4 F Adapter	1	\$0.64	2/5/2007	

3/4 M Adapter	1	\$0.50	2/5/2007	
1/2 M Adapter	1	\$0.21	2/5/2007	
PVC Bushing	1	\$0.45	2/5/2007	
PVC Ball Valve	1	\$5.41	2/5/2007	
1 1/4" PVC Ball Valve	1	\$5.93	2/9/2007	
1/4" Adapter	2	\$2.72	2/9/2007	
5GAL Bucket	1	\$4.98	2/9/2007	
1x6x6 Pine Wood	1	\$4.29	2/17/2007	
Aquamend	2	\$5.94	2/17/2007	
1-1/12 Angle Brackets	4	\$1.56	2/20/2007	
Screws	1 Bag	\$0.98	2/20/2007	
Screws	1 Bag	\$0.98	2/20/2007	
Contact Cement	30 OZ	\$3.19	2/20/2007	
Sheet Metal	1	\$6.66	2/21/2007	
1-1/2 Angle Bracket	2	\$0.78	2/21/2007	
1x1/2 Slip Joint	2	\$5.06	2/23/2007	
Nylon Barb	1	\$2.13	2/23/2007	
6', 1-1/4" Outer, 1" Inner	1	\$9.64	2/23/2007	
Aquamend	1	\$2.97	3/3/2007	
Aquamend	3	\$8.91	3/5/2007	

1x10 PVC	1	\$2.90	3/5/2007	
			TOTAL:	\$871.63